INVESTIGATION OF THE ATMOSPHERIC OZONE FORMATION POTENTIAL OF T-BUTYL ALCOHOL, N-METHYL PYRROLIDINONE AND PROPYLENE CARBONATE

Report to
ARCO Chemical Corporation

by
William P. L. Carter, Dongmin Luo, Irina L. Malkina,
Ernesto C. Tuazon, Sara M. Aschmann, and Roger Atkinson

July 8, 1996

Statewide Air Pollution Rsearch Center
and
College of Engineering
Center for Environmental Research and Technology
University of California
Riverside, California 92521

96:AP:034:F

ABSTRACT

A series of laboratory studies, environmental chamber experiments, and computer model calculations were carried out to asses the atmospheric ozone formation potential of t-butyl alcohol (TBA), N-methyl pyrrolidinone (NMP), and propylene carbonate (PC). The OH radical rate constants at 296-298°K were measured to be (1.43±0.36) x 10^{-12}, (2.15±0.36) x 10^{-11}, and (6.9±1.5) x 10^{-13} cm^3 $molec^{-1}$ s^{-1}, for TBA, NMP, and PC, respectively, and the NO_3 radical rate constant for NMP was measured to be (1.26±0.40) x 10^{-13} cm^3 $molec^{-1}$ s^{-1}. Photolysis and reaction with ozone were found not to be significant loss processes for NMP and PC under atmospheric conditions. NMP was observed to form N-methylsuccinimide and 1-formyl-2-pyrrolidinone with yields of 44% and 41%, respectively in the OH radical reaction, and of 59% and ~4% in the reaction with NO_3. The chamber data confirmed that the major products from TBA are formaldehyde and acetone, and ruled out mechanisms predicting that formaldehyde is a major product from PC.

The chamber experiments consisted of determining the effects on NO oxidation, ozone formation and integrated OH radical levels of adding these compounds to simulated model photochemical smog systems. Mechanisms were developed for TBA and PC which were consistent with the results of these experiments, though to obtain acceptable fits it was necessary to assume ~7% organic nitrate yields in the reactions of NO with the peroxy radicals formed from TBA, and ~8% for those formed from PC. NMP was found to inhibit NO oxidation during the initial stages of the experiments, then accelerate O_3 formation once O_3 formation began. This is attributed to the effect of its NO_3 reaction, and was well simulated by the estimated mechanism provided a ~15% nitrate yield in the NO + peroxy radical reactions was assumed. However, the estimated NMP mechanism overpredicted its effect on final ozone yields by up to 50%, and to obtain improved fits in this regard it was necessary to assume fewer NO to NO_2 conversions are involved in the photooxidation reactions than could be rationalized. This adjustment reduced NNP' predicted atmospheric reactivities by 15-20%.

The experimentally evaluated mechanisms were then used to predict the ozone reactivities of these compounds under various atmospheric conditions. TBA and PC were calculated to have ozone impacts very close to those of ethane, with reactivities relative to ethane varying from ~1.4 to 1.0±0.2 for TBA and ~1.4 to 0.9±0.2 for PC, depending on conditions and how O_3 impacts were quantified. NMP was calculated to form 5-6 times more ozone than ethane, though it was somewhat less reactive than the average of all emissions, and its Maximum Incremental Reactivity was less than half that of toluene.

ACKNOWLEDGEMENTS

The authors gratefully acknowledge Mr. Dennis Fitz for assistance in administering this program, Mr. Kurt Bumiller and Ms. Kathalena Smihula for assistance in carrying out the experiments. This work was funded by ARCO Chemical Co. However, the opinions and conclusions expressed in this report are entirely those of the primary author, Dr. William P. L. Carter. Mention of trade names or commercial products do not constitute endorsement or recommendation for use.

TABLE OF CONTENTS

LIST OF TABLES

LIST OF FIGURES

INTRODUCTION

Ozone in photochemical smog is formed from the gas-phase reactions of volatile organic compounds (VOCs) and oxides of nitrogen (NO_x) in sunlight. Although Los Angeles has the worst ozone problem in the United States, other areas of the country also have episodes where ozone exceeds the federal air quality standard of 0.12 ppm. Ozone control strategies in the past have focused primarily on VOC controls, though the importance of NO_x control has become recognized in recent years. VOC and NO_x controls have differing effects on ozone formation. NO_x is required for ozone formation, and if the levels of NO_x are low compared to the levels of reactive VOCs, then changing VOC emissions will have relatively little effect on ozone. Since NO_x is removed from the atmosphere more rapidly than VOCs, ozone in areas far downwind from the primary sources tend to be more NO_x limited, and thus less responsive to VOC controls. VOC controls tend to reduce the rate that O_3 is formed when NO_x is present, so VOC controls are the most beneficial in reducing O_3 in the urban source areas, where NO_x is relatively plentiful, and where O_3 are determined primarily by how rapidly it is being formed. Because of this, any comprehensive ozone control strategy must involve reduction of emissions of both NO_x and VOCs.

Many different types of VOC compounds are emitted into the atmosphere, each reacting at different rates and having different mechanisms for their reactions. Because of this, they can differ significantly in their effects on ozone formation, or their "reactivity". Some compounds, such as CFCs, do not react in the lower atmosphere at all, and thus make no contribution to ground-level ozone formation. Others, such as methane, react and contribute to ozone formation, but react so slowly that their practical effect on ozone formation in urban areas is negligible. Obviously, it does not make sense to regulate such compounds as ozone precursors. In recognition of this, the EPA has exempted certain compounds from such regulations on the basis of having "negligible" effects on ozone formation. Although the EPA has no formal policy on what constitutes "negligible" reactivity, in practice it has used the ozone formation potential of ethane as the standard in this regard. This is because ethane is the most reactive of the compounds the EPA has exempted to date. Therefore, the ozone formation potential of a compound relative to ethane is of particular interest when assessing whether it might be a likely candidate for exemption from regulation as an ozone precursor.

The EPA is now also proposing grouping non-exempt compounds into "reactive" and "highly reactive" groupings, which can serve as a basis for regulations for encouraging or requiring use of less reactive compounds in consumer and commercial products. Dimitriades (private communication, 1994) has proposed a classification scheme based on model calculations of ozone formation potentials of VOCs in the atmosphere, with the dividing line between reactive and highly reactive being a "maximum incremental reactivity" (MIR) of 4 grams O_3 per gram VOC (Carter, 1994a). This would put the dividing line somewhere between the MIR of toluene and acetaldehyde. Although the regulatory implications of

this classification has not yet been established, it is clear that producers of solvent VOCs will need to know how their VOCs will be classified under this system, and whether the classification presently proposed for them is appropriate.

This report describes the results of an experimental and computer modeling study investigating the atmospheric ozone formation potential of three solvent compounds of interest to ARCO chemical company. These are t-butyl alcohol (TBA), N-methyl pyrrolidinone (NMP), and propylene carbonate (PC). TBA is included because it is an important solvent which reacts with OH radicals relatively slowly, and is a possible candidate for exemption as negligibly reactive. Propylene carbonate and NMP are included because they are also of interest to ARCO and because prior to this study there was no information available concerning their atmospheric lifetimes or impacts. The approach involved making laboratory measurements necessary to determine the atmospheric reaction rates for those compounds for which no such data were available, conducting environmental chamber experiments to determine their effects on ozone formation and other measures of atmospheric reactivity, developing chemical mechanisms for the atmospheric reactions of these compounds which are consistent with these data, and then using these mechanisms in model calculations to estimate their ozone impacts under atmospheric conditions.

EXPERIMENTAL AND DATA ANALYSIS METHODS

Kinetic and Product Studies

The experimental methods employed in the kinetic and product studies were generally similar to those used in our previous study of the atmospheric chemistry of a series of carbamates and lactates (Kwok *et a*l., 1996). The majority of these experiments were carried out in a 7900 liter all-Teflon chamber, equipped with two parallel banks of Sylvania F40/350BL blacklamps for irradiation, at 296 ± 2 K and 740 Torr total pressure of purified air at ~5% relative humidity. Experiments to measure the rate constant for the gas-phase reaction of the OH radical with propylene carbonate were carried out in a 5800 liter Teflon-coated evacuable chamber equipped with an *in situ* multiple reflection optical system interfaced with a Nicolet 7199 Fourier transform infrared (FT-IR) spectrometer, and with irradiation provided by a 24 KW xenon arc. The chambers are fitted with Teflon-coated fans for rapid mixing of reactants during their introduction in the chamber. The organic reactants and products were monitored by GC-FID or FT-IR as described below, and the NO and initial NO_2 concentrations were measured using a Thermo Environmental Instruments, Inc., Model 42 chemiluminescent NO-NO_x analyzer. The specific experimental and data analysis procedures for the various types of kinetic and mechanistic studies are discussed in more detail in the following sections.

OH and NO_3 Radical Rate Constant Measurements. Rate constants for the OH radical and NO_3 radical reactions with the test compounds were determined using relative rate methods in which the relative disappearance rates of the organic compound and a reference compound, whose OH radical or NO_3 radical reaction rate constant is reliably known, were measured in the presence of OH radicals or NO_3 radicals. Providing that the organic and reference compounds reacted only with OH radicals or NO_3 radicals, then

$$\ln\left\{\frac{[organic]_{t_o}}{[organic]_t}\right\} - D_t = \frac{k_1}{k_2}\left[\ln\left\{\frac{[reference\ compound]_{t_o}}{[reference\ compound]_t}\right\} - D_t\right] \qquad \text{(I)}$$

where $[organic]_{t_o}$ and $[reference\ compound]_{t_o}$ are the concentrations of the organic compound and reference compound, respectively, at time t_o, $[organic]_t$ and $[reference\ compound]_t$ are the corresponding concentrations at time t, D_t is a factor to account for any dilution due to additions to the chamber, and k_1 and k_2 are the rate constants for reactions (1) and (2), respectively.

$$\left.\begin{matrix}OH\\NO_3\end{matrix}\right\} + \text{organic compound} \rightarrow \text{products} \qquad (1)$$

$$\left.\begin{matrix}OH\\NO_3\end{matrix}\right\} + \text{reference compound} \rightarrow \text{products} \qquad (2)$$

Hence plots of {ln([organic]$_{t_o}$/[organic]$_t$) - D_t} against {ln([reference compound]$_{to}$/[reference compound]$_t$) - D_t} should be straight lines with slope k_1/k_2 and zero intercept. Under conditions where wall losses of the organic and reference compounds were observed (the case with propylene carbonate for the OH radical reactions in the 5800 liter evacuable chamber), then

$$\frac{1}{(t-t_o)} \ln\left\{\frac{[organic]_{t_o}}{[organic]_t}\right\} = \frac{1}{(t-t_o)} \frac{k_1}{k_2} \ln\left\{\frac{[reference\ compound]_{t_o}}{[reference\ compound]_t}\right\} + k_3 - \frac{k_4\ k_1}{k_2} \qquad \text{(II)}$$

where k_3 and k_4 are the wall loss rates of the organic compound and reference compound, respectively.

Tertiary-Butyl Alcohol. Two experiments (run nos. EC-1647 and EC-1648) were carried out in the SAPRC 5800 liter, Teflon-coated evacuable chamber (EC), with analysis by long-path FT-IR spectroscopy. OH radicals were generated by the photolysis of methyl nitrite (CH_3ONO) in synthetic air (80% N_2 - 20% O_2) at wavelengths >300 nm (Atkinson *et a*l., 1981a), and NO was added to the reactant mixtures to suppress the formation of O_3, and hence of NO_3 radicals (Atkinson *et a*l., 1981a). Dimethyl ether was used as the reference compound, and the initial reactant concentrations (in molecule cm^{-3} units) were: CH_3ONO, 2.8 x 10^{14}; NO, 1.2 x 10^{14} (EC-1647) or 2.0 x 10^{14} (EC-1648); TBA, 3.1 x 10^{14}; and dimethyl ether, 1.6 x 10^{14}. Infrared spectra of the reaction mixtures were recorded at 4-5 min intervals for 30-40 min during the photolyses. The concentrations of both TBA alcohol and dimethyl ether were measured in the dark for 30-45 min prior to the addition of CH_3ONO and NO into the air mixture.

N-Methyl Pyrrolidinone. The experiments with NMP were carried out in a 7900 liter Teflon chamber. OH radicals were again generated by the photolysis of CH_3ONO in air, and in this case propene was used as the reference compound, and purified rather than synthetic air was employed. The initial reactant concentrations (in molecule cm^{-3} units) were: CH_3ONO, 2.4 x 10^{14}; NO, 2.4 x 10^{14}; NMP, (2.76-2.99) x 10^{13}; and propene, ~2.4 x 10^{13}. Irradiations were carried out at 20% of the maximum light intensity for 8-25 mins (with this light intensity corresponding to an NO_2 photolysis rate of ~2 x 10^{-3} s^{-1}). The factor D_t to take into account any dilution due to additions to the chamber was zero for these OH radical reaction rate constant determinations.

The concentrations of NMP and propene were measured by gas chromatography with flame ionization detection (GC-FID) during the experiments. For the analysis of NMP, 100 cm^3 volume gas samples were collected from the chamber onto Tenax-TA solid adsorbent, with subsequent thermal desorption at ~225 ^oC onto a DB-5.625 megabore column held at 0 ^oC and then temperature programmed to 250 ^oC at 8 ^oC min^{-1}. For the reference compound propene, gas samples were collected from the chamber in 100 cm^3 all-glass, gas-tight syringes and transferred via a 1 cm^3 stainless steel loop and gas sampling valve onto a 30 m DB-5 megabore column held at -25 ^oC and then temperature programmed at 8 ^oC min^{-1}. Based on replicate analyses in the dark, the GC-FID measurement uncertainties for NMP were 2-3%.

Propylene Carbonate. Experiments were carried out at 298 K and 740 Torr total pressure of synthetic air (80% N_2 - 20% O_2) in the SAPRC EC, with analysis by long-path FT-IR spectroscopy. One set of experiments (run nos. EC-1611, EC-1612, EC-1615, EC-1618, and EC-1619) was carried out with methanol as the reference compound, using the dark reaction of N_2H_4 with O_3 as the source of OH radicals (Tuazon *et a*l., 1983). This method of generating OH radicals has generally been carried out with O_3 being initially added in a large excess to the organic compound - reference compound - air mixture, followed by incremental additions of hydrazine, with each addition being made after the previous hydrazine aliquot had been consumed. The procedure followed in the present experiments consisted of adding, in succession, O_3 and N_2H_4 aliquots to the PC - methanol - air mixture, with O_3 being added in excess and prior to N_2H_4. Two FT-IR spectra of the reaction mixture were recorded after each addition, with the first spectrum being collected 5-10 minutes after the O_3 - N_2H_4 injection, with this time duration being sufficient for the O_3 + N_2H_4 reaction to be essentially complete. The interval of the succeeding O_3 - N_2H_4 injection was scheduled such that the first FT-IR spectrum was obtained generally within 15 min of the second FT-IR spectrum of the previous O_3 - N_2H_4 injection. Each experiment consisted of three to five O_3 - N_2H_4 additions. The decays of both PC and methanol were observed for 30-120 min prior to the addition of O_3 and N_2H_4 . The initial concentrations of propylene carbonate and CH_3OH were 6.4 x 10^{13} molecule cm^{-3} and 6.0 x 10^{13} molecule cm^{-3}, respectively. Injections of O_3 and N_2H_4 were in aliquots of 1.1 x 10^{14} molecule cm^{-3} and (0.8-1.1) x 10^{14} molecule cm^{-3}, respectively, with higher concentrations of N_2H_4 being introduced for later injections to react more of the accumulated, excess O_3.

A second set of experiments (run nos. EC-1640 and EC-1641) utilized the photolysis of CH_3ONO as the OH radical source (see above), and propane as the reference compound. The initial concentrations (in molecule cm^{-3} units) were: CH_3ONO, 2.9 x 10^{14}; NO, 1.2 x 10^{14}; PC, 1.0 x 10^{14}; and propane, (1.2-1.4) x 10^{14}. The reactant mixtures were irradiated for 1 hr by radiation from a 24-kw Xenon arc lamp which was filtered through a 6-mm thick Pyrex pane. The FT-IR spectra of the reaction mixtures were recorded every 6-8 min during the irradiations. The dark decays of the reactants were also monitored for 30 min prior to irradiation and for 60 min after the irradiation.

Photolysis of Propylene Carbonate and N-Methyl Pyrrolidinone. Photolysis of a PC (2.8 x 10^{13} molecule cm^{-3}) - NMP (2.5 x 10^{13} molecule cm^{-3}) - air mixture with added cyclohexane (3.5 x 10^{15} molecule cm^{-3}) to scavenge any OH radicals formed from the photolysis of organic or NO_x impurities in the chamber was also carried out at the maximum light intensity for up to 185 min to check that photolysis of PC or NMP was not occurring under blacklamp irradiation. The concentrations of NMP and PC were measured during this experiment by GC-FID, using the procedure described above for the GC-FID analysis of NMP.

Rate Constants for the Reactions of the NO_3 Radical with Propylene Carbonate and N-Methyl Pyrrolidinone. Measurements of the rate constants for the reactions of the NO_3 radical with PC and NMP were carried out in the dark in the 7900 liter Teflon chamber. NO_3 radicals were generated in the dark by the thermal decomposition of N_2O_5 (Atkinson *et a*l., 1984). 2,3-Dimethylbutane was used as the reference compound for the experiments with PC and for the initial experiment with NMP, with *trans*-2-butene being used as the reference compound for the remainder of the experiments with NMP. The initial reactant concentrations (in molecule cm^{-3} units) were: PC, 2.5 x 10^{13}, or NMP (2.7-2.9) x 10^{13}; 2,3-dimethylbutane or *trans*-2-butene, ~2.4 x 10^{13}; NO_2, (7.2-12) x 10^{13}, or (for the PC experiment to scavenge any OH radicals formed) ethane, 6.8 x 10^{15} molecule cm^{-3}. One to foour additions of N_2O_5 (each addition corresponding to an initial N_2O_5 concentration in the chamber of (0.50-20) x 10^{13} molecule cm^{-3}) were made to the chamber during an experiment. The factor D_t to take into account dilution was D_t = 0.0012 per N_2O_5 addition to the chamber.

The concentrations of PC, NMP, 2,3-dimethyl-butane and *trans*-2-butene during the experiments were measured by GC-FID, as described above (with the analyses of 2,3-dimethylbutane and *trans*-2-butene being carried out as described above for propene).

Rate Constants for the O_3 Reactions. Rate constants, or upper limits thereof, for the reactions of PC and NMP with O_3 were determined in the dark by measuring the decay rates of PC or NMP in the presence of known concentrations of O_3 (Atkinson *et a*l., 1981b). Excess concentrations of cyclohexane were added to the reactant mixtures to scavenge any OH radicals formed in the reaction systems. Providing that any measured loss of the PC or NMP was due only to reaction with O_3, then,

$$\ln([\text{organic}]_{t_o}/[\text{organic}]_t) = k_5[O_3](t - t_o) \qquad \text{(III)}$$

where k_5 is the rate constant for the reaction.

$$O_3 + \text{organic} \rightarrow \text{products} \qquad (3)$$

The initial concentrations of PC, NMP, cyclohexane and O_3 were 2.7 x 10^{13} molecule cm^{-3}, 3.2 x 10^{13} molecule cm^{-3}, 2.4 x 10^{14} molecule cm^{-3} (for the experiment with PC) or 1.1 x 10^{16} molecule cm^{-3} (for the experiment with NMP), and (2.44-4.87) x 10^{13} molecule cm^{-3}, respectively, and the reactions were monitored for up to 3.1-3.4 hr. The concentrations of PC and NMP were measured by GC-FID as described above. Ozone concentrations were measured by ultraviolet absorption using a Dasibi 1003-AH ozone analyzer.

Products of the OH and NO_3 Radical Reactions with N-Methyl Pyrrolidinone. In addition to the GC-FID analyses of the irradiated CH_3ONO - NO - NMP - propene - air and the NO_3 - N_2O_5 - NO_2 - NMP - *trans*-2-butene (or 2,3-dimethylbutane) - air mixtures carried out for the rate constant determinations, gas samples were also collected from the reacted NO_3 - N_2O_5 - NO_2 - NMP - 2,3-dimethylbutane - air mixture onto Tenax-TA solid adsorbent for subsequent thermal desorption with analysis by combined gas chromatography-mass spectrometry (GC-MS), using a 50 m HP-5 fused silica capillary column in a Hewlett Packard (HP) 5890 GC interfaced to a HP 5971 mass selective detector operating in the scanning mode.

Calibration of GC-FID Response Factors. The GC-FID response factors for PC and NMP were determined by introducing measured amounts of the chemicals into the 7900 liter chamber and conducting several replicate GC-FID analyses. The chamber volume was determined by introducing a measured volume of *trans*-2-butene and measuring the *trans*-2-butene concentration with an HP 5890 GC and loop/gas sampling valve injection. For PC, partial pressures of the gaseous compound were measured in a 2.03 liter Pyrex bulb using an MKS Baratron 0-100 Torr sensor, and the contents of the bulb were then flushed into the chamber with a stream of N_2 gas. For NMP, measured volumes of the liquid compound were introduced into a 1 liter Pyrex bulb and the contents of the bulb flushed into the chamber with a stream of N_2 gas. The relative GC-FID response factors of NMP and *N*-methylsuccinimide were determined by spiking a Tenax-TA solid adsorbent cartridge with a methanol solution containing known amounts of NMP and *N*-methylsuccinimide.

Chemicals. The chemicals used, and their stated purities, were: cyclohexane (high-purity solvent grade), American Burdick and Jackson; 2,3-dimethylbutane (99%), hydrazine (98%), NMP (95%), PC (99+%), and *N*-methylsuccinimide (99%), Aldrich Chemical Company; methanol (≥99.9%), Fisher Scientific; TBA, J.T. Baker Chemical Co; propane (≥99.0%), and propene (≥99.0%), Matheson Gas Products; and NO (≥99%) and *trans*-2-butene (C.P. grade), Liquid Carbonic. O_3 in O_2 diluent was generated from a Welsbach T-408 ozone generator at pre-calibrated voltage settings and flow of O_2 (99.995 % min., Liquid Carbonic). The diluent air for the experiments in the 5800 liter evacuable chamber was a synthetic mixture of 80% N_2 (head gas from liquid nitrogen, California Tool and Welding) and 20% O_2 (≥99.995%, Liquid Carbonic). Methyl nitrite and N_2O_5 were prepared and stored as described previously (Atkinson *et a*l., 1981a, 1984), and NO_2 was prepared just prior to use by reacting NO with an excess of O_2.

Environmental Chamber Experiments

Overall Approach. The environmental chamber experiments consisted primarily of measurements of "incremental reactivities" of TBA, NMP, and PC under various conditions. These involve two types of irradiations of model photochemical smog mixtures. The first is a "base case" experiment where a mixture of reactive organic gases (ROGs) representing those present in polluted atmospheres (the "ROG surrogate") is irradiated in the presence of oxides of nitrogen (NO_x) in air. The second is the "test"

experiment which consists of repeating the base case irradiation except that the VOC whose reactivity is being assessed is added. The differences between the results of these experiments provide a measure of the atmospheric impact of the test compound, and the difference relative to the amount added is a measure of its reactivity.

To provide data concerning the reactivities of the test compound under varying atmospheric conditions, three types of base case experiments were carried out:

1. Mini-Surrogate Experiments. This base case employed a simplified ROG surrogate and relatively low ROG/NO_x ratios. Low ROG/NO_x ratios represent "maximum incremental reactivity" (MIR) conditions, which are most sensitive to VOC effects. This is useful because it provides a sensitive test for the model, and also because it is most important that the model correctly predict a VOC's reactivity under conditions where the atmosphere is most sensitive to the VOCs. The ROG mini-surrogate mixture employed consisted of ethene, n-hexane, and m-xylene. This same surrogate was employed in our previous studies (Carter *et al.*, 1993a,b; 1995a), and was found to provide a more sensitive test to the mechanism than the more complex surrogates which more closely represent atmospheric conditions (Carter *et al.*, 1995a). This high sensitivity to mechanism differences made this type of experiment most useful for mechanism evaluation.

2. Full Surrogate Experiments. This base case employing a more complex ROG surrogate under somewhat higher, though still relatively low, ROG/NO_x conditions. While less sensitive to the mechanism employed, experiments with a more representative ROG surrogate are needed to evaluate the mechanism under conditions more closely resembling the atmosphere. The ROG surrogate employed was the same as the 8-component "lumped molecule" surrogate as employed in our previous study (Carter *et al.*, 1995a), and consists of n-butane, n-octane, ethene, propene, trans-2-butene, toluene, m-xylene, and formaldehyde. Calculations have indicated that use of this 8-component mixture will give essentially the same results in incremental reactivity experiments as use of actual ambient mixtures (Carter *et al.*, 1995a).

3. Full Surrogate, low NO_x Experiments. This base case employing the same 8-component lumped molecule surrogate as the above set, except that lower NO_x levels (higher ROG/NO_x ratios) were employed to represent NO_x-limited conditions. Such experiments are necessary to assess the ability of the model to properly simulate reactivities under conditions where NO_x is low. The conditions employed were comparable to those employed in our previous studies (Carter *et al.* 1995a).

An appropriate set of control and characterization experiments necessary for assuring data quality and characterizing the conditions of the runs for mechanism evaluation were also carried out. These are discussed where relevant in the results or modeling methods sections.

Environmental Chamber. The environmental chamber system employed in this study was the CE-CERT "Dividable Teflon Chamber" (DTC) with a blacklight light source. This consists of two ~5000-liter 2-mil heat-sealed FEP Teflon reaction bags located adjacent to each other and fitted inside an 8' cubic framework, and which uses two diametrically opposed banks of 32 Sylvania 40-W BL black lights as the light source. The lighting system in the DTC was found to provide so much intensity that only half the lights were used for irradiation. The unused black lights were covered with aluminum sheet as well, and were used to bring the chamber up to the temperature it will encounter during the irradiation before the uncovered lights are turned on. The air conditioner for the chamber room was turned on before and during the experiments. Four air blowers which are located in the bottom of the chamber were used to help cooling the chamber as well as mixing the contents of the chamber. The CE-CERT DTC is very similar to the SAPRC DTC which is described in detail elsewhere (Carter *et al.*, 1995a,b).

The DTC is designed to allow simultaneous irradiations of the base case and the test experiments under the same reaction conditions. As indicated above, the chamber is actually two adjacent FEP Teflon reaction bags which can be simultaneously irradiated using the same light source and with the same temperature control system. These are referred to as the two "sides" of the chamber (Side A and Side B) in the subsequent discussion. The sides are interconnected with two ports, each with a box fan, which rapidly exchange their contents to assure that reactants which are desired to have equal concentrations in each are equalized. In addition, a fan is located in each of the reaction bags to rapidly mix the reactants within each chamber. The ports connecting the two reactors can then be closed to allow separate injections on each side, and separate monitoring of each. This design is optimized for carrying out incremental reactivity experiments such as those for this program.

Experimental Procedures. The reaction bags were flushed with dry purified air for 14 hours (6pm-8am) on the nights before experiments. An AADCO air purification system was employed. The continuous monitors were connected prior to reactant injection and the data system began logging data from the continuous monitoring systems. The reactants were injected as described below (see also Carter *et al.*, 1993b,, 1995b). The common reactants were injected in both sides simultaneously using a three-way (one inlet and two outlets connected to side A and B respectively) bulb of 2 liters in the injection line and were well mixed before the chamber was divided. The contents of each side were blown into the other using two box fans located between them. Mixing fans were used to mix the reactants in the chamber during the injection period, but these were turned off prior to the irradiation. The sides were then separated by closing the ports which connected them, after turning all the fans off to allow their pressures to equalize. After that, reactants for specific sides (the test compound in the case of reactivity experiments) were injected and mixed. The irradiation began by turning on the lights and proceeded for 6 hours. After the run, the contents of the chamber were emptied by allowing the bag to collapse, and then was flushed with purified air. The contents of the reactors were vented into a fume hood.

The procedures for injecting the various types of reactants were as follows. The NO and NO_2 were prepared for injection using a high vacuum rack. Known pressure of NO, measured with MKS Baratron capacitance manometers, were expanded into Pyrex bulbs with known volumes, which were then filled with nitrogen (for NO) or oxygen (for NO2). The contents of the bulbs were then flushed into the chamber with AADCO air. The other gas reactants were prepared for injection either using a high vacuum rack or a gas-tight syringes whose amounts were calculated. The gas reactants in a gas-tight syringe was usually diluted to 100-ml with nitrogen in a syringe. The volatile liquid reactants (including TBA) were injected, using a micro syringe, into a 1-liter Pyrex bulb equipped with stopcocks on each end and a port for the injection of the liquid. The port was then closed and one end of the bulb was attached to the injection port of the chamber and the other to a dry air source. The stopcocks were then opened, and the contents of the bulb were flushed into the chamber with a combination of dry air and heat gun for approximately 5 minutes. Formaldehyde was prepared in a vacuum rack system by heating paraformaldehyde in an evacuated bulb until the pressure corresponded to the desired amount of formaldehyde. The bulb was then closed and detached from the vacuum system and its contents were flushed into the chamber with dry air through the injection port.

Since PC and NMP have high boiling points (202°C and 242°C, respectively), a special injection system was employed, which was a three-way glass tube (one port for liquid injection) surrounded with heat tape. The tape temperature was controlled with a variable transformer. After the tape was heated for 5 minutes and its temperature reached the desired value (200C), PC or NMP was injected into tube through the injection port. One end of the tube port was attached to AADCO purified air whose flow was set at 2 liter per minute and the other was connected to the chamber. The flush time was approximately 10 minutes and heat gun was used as well. This injection system can avoid any loss of high boiling point reactants during the injection due to condensation on cold spots. TBA was injected using a microliter syringe as described above for volatile liquid compounds.

Analytical Methods. Ozone and nitrogen oxides (NO_x) were monitored using commercially available continuous analyzers with Teflon sample lines inserted directly into the chambers. The sampling lines from each side of the chamber were connected to solenoids which switched from side to side every 10 minutes, so the instruments alternately collected data from each side. Ozone was monitored using a Dasibi 1003AH UV photometric ozone analyzer and NO and total oxides of nitrogen (including HNO_3 and organic nitrates) were monitored using a Teco Model 14B chemiluminescent NO/NO_x monitor. The output of these instruments, along with that from the temperature sensors and the and formaldehyde instrument, were attached to a computer data acquisition system, which recorded the data at 10 minutes intervals for ozone, NO and temperature (and at 15 minutes for formaldehyde), using 30 second averaging times. This yielded a sampling interval of 20 minutes for taking data from each side.

The Teco instrument and Dasibi CO analyzer were calibrated with a certified NO and CO source and CSI gas-phase dilution system. It was done prior to chamber experiment for each run. The NO_2

converter efficiency check was carried out in regular intervals. Dasibi ozone analyzer was calibrated against SAPRC transfer standard ozone analyzer using transfer standard method in a interval of three months and was check with CSI ozone generator (set to 400 ppb) for each experiment to assure that the instrument worked properly. The details were discussed elsewhere (Carter *et al.*, 1995b)

Organic reactants other than formaldehyde were measured by gas chromatography with FID and ECD detections as described elsewhere (Carter *et al.*, 1993b; 1995b). GC samples were taken for analysis at intervals from 20 minutes to 30 minutes either using 100 ml gas-tight glass syringes or by collecting the 100 ml sample from the chamber onto Tenax-GC solid adsorbent cartridge. These samples were taken from ports directly connected to the chamber after injection and before irradiation and at regular intervals after irradiation. Two sampling methods were employed for injecting the sample onto the GC column, depending on the volatility or "stickiness" of the compound. For analysis of the more volatile species (which includes all the components of the base case surrogates employed in this study), the contents of the syringe were flushed through a 2 ml or 3 ml stainless steel or 1/8 in. Teflon tube loop and subsequently injected onto the column by turning a gas sample valve. TBA, PC and NMP were measured with loop method and Tenax method, respectively, using GC-FID.

The calibrations for the GC analyses for most compounds were carried out by sampling from chambers into which known amounts of the reactants were injected, as described previously (Carter *et al.*, 1995b). The chamber volume was determined by measuring the CO concentration in chamber into which known amount of CO was injected using vacuum rack system.

Two different injection methods, vacuum rack system and micro syringe, were employed for calibration of TBA in order to check the purity in TBA solution. The results showed that the GC area response using vacuum rack system is slightly higher than those using micro syringe injection, indicating that the impurity in TBA solution existed and the TBA GC factor we obtained using vacuum injection should be recommended in use of TBA concentration calculation. The same injection procedure of PC and NMP was used for calibrations and chamber experiments.

Characterization Methods. Three temperature thermocouple for each chamber were used to monitor the chamber temperature, two of which were located in the sampling line of continuous analyzers to monitor the temperature in each side. The third one was located in the chamber to monitor chamber temperature. The temperature in these experiment were typically 21-25°C

The light intensity in the DTC chamber was monitored by periodic NO_2 actinometry experiments utilizing the quartz tube method of Zafonte *et al.* (1977), with the data analysis method modified as discussed by Carter *et al.* (1995b). The results of these experiments were tracked over time in this chamber since it was first constructed in early 1994, and were fit by a curve where the NO_2 photolysis rate decayed relatively rapidly from its initial values of ~0.31 min^{-1} when the chamber and lights were

new, then declining only slowly during the time of these experiments. A curve through the full set of actinometry results predicted NO_2 photolysis rates in the range of 0.221 - 0.219 min^{-1} during the time of these experiments (decreasing very slowly with time), and the results of the actinometry experiments associated with the runs in this study are consistent with this. The spectrum of the blacklight light source was measured using a LiCor LI-1200 spectra radiometer, and found to be essentially the same as the general blacklight spectrum recommended by Carter *et al.* (1995b) for use in modeling blacklight chamber experiments.

The dilution of the DTC chamber due to sampling is expected to be small because the flexible reactions bags can collapse as sample is withdrawn for analysis. However, some dilution occurs with the age of reaction bags because of small leaks. Information concerning dilution in an experiment can be obtained from relative rates of decay of added VOCs which react with OH radicals with differing rate constants (Carter *et al.*, 1993b; 1995b). All experiments has a more reactive compounds such as m-xylene and n-octane present either as a reactant or added in trace amounts to monitor OH radical levels. Trace amounts (~0.1 ppm) of n-butane was added to experiments if needed to provide a less reactive compound for the purposes of the monitoring dilution. In addition, specific dilution check experiments such as CO-NO were carried out and based on the results, the dilution rate was found to be 0.3% per hour in side A, which is slightly higher than dilution rate 0.1% in side B.

Reactivity Data Analysis Methods. As indicated above, most of the experiments for this program consisted of simultaneous irradiation of a "base case" reactive organic gas (ROG) surrogate - NO_x mixture in one of the dual reaction chambers, together with an irradiation, in the other reactor, of the same mixture with a n-C_{12+} n-alkane added. The results are analyzed to yield two measures of VOC reactivity: the effect of the added VOC on the amount of NO reacted plus the amount of ozone formed, and integrated OH radical levels. These are discussed in more detail below.

The first measure of reactivity is the effect of the VOC on the change in the quantity $[O_3]$-[NO], or $([O_3]_t$-$[NO]_t)$-$([O_3]_0$-$[NO]_0)$, which is abbreviated as $d(O_3$-NO) in the subsequent discussion. As discussed elsewhere (e.g., Johnson, 1983; Carter and Atkinson, 1987; Carter and Lurmann, 1990, 1991, Carter *et al.*, 1993b, 1995b,c), this gives a direct measure of the amount of conversion of NO to NO_2 by peroxy radicals formed in the photooxidation reactions, which is the process that is directly responsible for ozone formation in the atmosphere. (Johnson calls it "smog produces" or "SP".) The incremental reactivity of the VOC relative to this quantity, which is calculated for each hour of the experiment, is given by

$$IR[d(O_3\text{-}NO)]_t^{VOC} = \frac{d(O_3\text{-}NO)_t^{test} - d(O_3\text{-}NO)_t^{base}}{[VOC]_0} \qquad \text{(IV)}$$

where $d(O_3\text{-}NO)_t^{test}$ is the $d(O_3$-NO) measured at time t from the experiment where the test VOC was added, $d(O_3\text{-}NO)_t^{base}$ is the corresponding value from the corresponding base case run, and $[VOC]_0$ is the

amount of test VOC added. An estimated uncertainty for IR[d(O_3-NO)] is derived based on assuming an ~3% uncertainty or imprecision in the measured d(O_3-NO) values. This is consistent with the results of the side equivalency test, where equivalent base case mixtures are irradiated on each side of the chamber.

Note that reactivity relative to d(O_3-NO) is essentially the same as reactivity relative to O_3 in experiments where O_3 levels are high, because under such conditions $[NO]_t^{base} \approx [NO]_t^{test} \approx 0$, so a change d($O_3$-NO) caused by the test compound is due to the change in O_3 alone. However, d(O_3-NO) reactivity has the advantage that it provides a useful measure of the effect of the VOC the processes responsible for O_3 formation even in experiments where O_3 formation is suppressed by relatively high NO levels.

The second measure of reactivity is the effect of the VOC on integrated hydroxyl (OH) radical concentrations in the experiment, which is abbreviated as "IntOH" in the subsequent discussion. This is an important factor affecting reactivity because radical levels affect how rapidly all VOCs present, including the base ROG components, react to form ozone. If a compound is present in the experiment which reacts primarily with OH radicals, then the IntOH at time t can be estimated from

$$IntOH_t = \int_0^t [OH]_\tau d\tau = \frac{ln\left(\frac{[tracer]_0}{[tracer]_t}\right) - Dt}{kOH^{tracer}}, \qquad \text{(V)}$$

where $[tracer]_0$ and $[tracer]_t$ are the initial and time=t concentrations of the tracer compound, KOH^{tracer} its OH rate constant, and D is the dilution rate in the experiments. The latter was found to be small and was neglected in our analysis. The concentration of tracer at each hourly interval was determined by linear interpolation of the experimentally measured values. M-xylene was used as the OH tracer in these experiments because it is a surrogate component present in all experiments, its OH rate constant is known (the value used was 2.36×10^{-11} cm^3 $molec^{-1}$ s^{-1} [Atkinson, 1989]), and it reacts relatively rapidly.

The effect of the VOC on OH radicals can thus be measured by its IntOH incremental reactivity, which is defined as

$$IR[IntOH]_t^{VOC} = \frac{IntOH_t^{test} - IntOH_t^{base}}{[VOC]_0} \qquad \text{(VI)}$$

where $IntOH_t^{test}$ and $IntOH_t^{base}$ are the IntOH values measured at time t in the added VOC and the base case experiment, respectively. The results are reported in units of 10^6 min. The uncertainties in IntOH and IR[IntOH] are estimated based on assuming an ~2% imprecision in the measurements of the m-xylene concentrations. This is consistent with the observed precision of results of replicate analyses of this compound.

RESULTS OF RATE CONSTANT AND PRODUCT STUDIES

Rate Constants for OH Radical Reactions

T-Butyl Alcohol. As indicated above, two experiments (run nos. EC-1647 and EC-1648) were carried out in the 5800 liter evacuable chamber in which CH_3ONO - NO - TBA - dimethyl ether (the reference compound) - air mixtures were irradiated. There was no measurable dark decay of dimethyl ether in the chamber, and the dark decay rate of TBA was negligible, being ~1 x 10^{-4} min^{-1}. The data obtained from both experiments are plotted in accordance with Equation (I) in Figure 1 (no dilution terms are involved when a rigid chamber is used). A least-squares analysis of these data leads to a rate constant ratio of k(TBA + OH)/k(dimethyl ether + OH) = 0.481 ± 0.017 and an intercept within one standard deviation of zero, where the indicated error in the rate constant ratio is two least-squares standard deviations. This rate constant ratio is placed on an absolute basis by use of a rate constant for the reaction of the OH radical with dimethyl ether of 2.98 x 10^{-12} cm^3 $molecule^{-1}$ s^{-1} (±25%) at 298 K (Atkinson, 1989, 1994), resulting in

$$k(TBA + OH) = (1.43 \pm 0.36) \times 10^{-12} \text{ cm}^3 \text{ molecule}^{-1} \text{ s}^{-1} \text{ at 298 K,}$$

where the indicated error is two least-squares standard deviations combined with the estimated overall uncertainty in the rate constant k_2.

The present rate constant is somewhat higher than the previously measured absolute rate constants of (1.07 ± 0.08) x 10^{-12} cm^3 $molecule^{-1}$ s^{-1} at 298 K (Wallington *et a*l., 1988), (8.1 ± 1.7) x 10^{-13} cm^3 $molecule^{-1}$ s^{-1} at 298 K (Saunders *et a*l., 1994), and (1.08±0.10 x 10^{-12} cm^3 $molecule^{-1}$ s^{-1} (Teton *et al.*, 1996), and the relative rate measurement of Cox and Goldstone (1982) of 1.08 x 10^{-12} cm^3 $molecule^{-1}$ s^{-1} at 295 ± 2 K. This is discussed further below in conjunction with the discussion of the development and evaluation of the TBA atmospheric photooxidation mechanism.

N-Methyl Pyrrolidinone. The data obtained from the CH_3ONO - NO - NMP - propene - air irradiations are plotted in accordance with Equation (I) in Figure 2. A good straight line plot is observed, and a least-squares analysis of these data leads to a rate constant ratio of k(NMP + OH)/k(propene + OH) = 0.810 ± 0.054, where the indicated error is two least-squares standard deviations. This rate constant ratio is placed on an absolute basis by use of a rate constant for the OH + propene reaction at 296 K of 2.66 x 10^{-11} cm^3 $molecule^{-1}$ s^{-1} (±15%) (Atkinson, 1989, 1994), resulting in a rate constant of

$$k(NMP + OH) = (2.15 \pm 0.36) \times 10^{-11} \text{ cm}^3 \text{ molecule}^{-1} \text{ s}^{-1} \text{ at 296 ± 2 K,}$$

Figure 1. Plot of Equation (I) for the gas-phase reaction of the OH radical with *t*-butyl alcohol, with dimethyl ether as the reference organic. The two symbols denote data from the two experiments.

Figure 2. Plot of Equation (I) for the gas-phase reaction of the OH radical with N-methyl pyrrolidinone, with propene as the reference organic.

where the indicated error is two least-squares standard deviations combined with the estimated overall uncertainties in the rate constant k_2. This is the only available determination of this rate constant.

Propylene Carbonate. As indicated above, two sets of experiments were carried out to determine the OH + PC rate constant. The first set of experiments (runs EC-1611, EC-1612, EC-1615, EC-1618, and EC-1619) used the dark reaction of N_2H_4 with O_3 as the source of OH radicals, with methanol as the reference compound. The second set of experiments runs EC-1640 and EC-1641) utilized the photolysis of CH_3ONO as the OH radical source, with propane as the reference compound. The results of these two sets of experiments are discussed separately below.

In the $N_2H_4 + O_3$ experiments, the decay rates of both propylene carbonate and methanol were found to be variable and significant relative to their total consumptions. The range of decay constants observed were (4-8) x 10^{-4} min^{-1} for propylene carbonate and (2-8) x 10^{-4} min^{-1} for methanol. Thus, for example, the wall losses amounted to 15-20% of the total amount of propylene carbonate consumed during a 1 hr reaction with five injections of O_3 and N_2H_4. The mixing which accompanied the injections of O_3 and N_2H_4 most likely contributed additional perturbations to the decay rates of propylene carbonate and methanol.

The plots of $(t-t_o)^{-1} \ln \{[S]_{to}/[S]_t\}$ vs $(t-t_o)^{-1} \ln \{[R]_{to}/[R]_t\}$ for the propylene carbonate - methanol - ozone - hydrazine system showed poor linearity, which was probably a consequence of the dark decay rates not being adequately determined by the intermittent nature of the reaction with OH radicals during the experiments. For this reason, and as described above, the experiments were conducted with the purpose of treating each set of O_3 and N_2H_4 injections as a separate experiment. Due to the relatively slow reactions of both propylene carbonate and methanol with OH radicals, the wall losses are calculated to be still significant within the short time durations (generally 10-15 min) but the variability in the rates of wall losses are minimized. The plot of equation (II) for the combined "mini-experiments" from five runs (nos. EC-1611, EC-1612, EC-1615, EC-1618, and EC-1619) is shown in Figure 3. The linear regression results (the indicated errors being two standard deviations) are: slope = k(OH + PC)/k(OH + methanol) = 0.722 ± 0.168; intercept = (3.1 ± 12.2) x 10^{-4} min^{-1}; r^2 = 0.80. The OH + PC rate constant is placed on an absolute basis using k(OH + methanol) = (9.44 ± 2.36) x 10^{-13} cm^3 $molecule^{-1}$ s^{-1} (Atkinson, 1994), yielding k(OH + PC) = (6.8 ± 2.3) x 10^{-13} cm^3 $molecule^{-1}$ s^{-1} at 298 K.

In the CH_3ONO photolysis experiments (runs EC-1640 and EC-1641), the average dark decay rates of PC were 1.1 x 10^{-3} min^{-1} and 5.2 x 10^{-4} min^{-1}, respectively, before and after the irradiations. The slower loss rates after the irradiation period was presumably due to the slightly higher temperature of the chamber walls. No parallel decay was detected for the reference compound propane before or after photolysis of the air mixtures. The plot of equation (II) for the combined data of the two experiments is shown in Figure 4, with the linear regression statistics (the indicated errors being two standard deviations): slope = k(OH + PC)/k(OH + propane) = 0.612 ± 0.104; intercept = (6.2 ± 4.7) x 10^{-4}

Figure 3. Plot of Equation (II) for the reaction of the OH radical with propylene carbonate, using the N_2H_4 reaction as the OH radical source and methanol as the reference compound. Different symbols denote data from different experiments.

Figure 4. Plot of Equation (II) for the reaction of the OH radical with propylene carbonate, in the experiments using photolysis of CH_3ONO as the OH radical source and propane as the reference compound. Different symbols denote data from different experiments.

min^{-1}; $r^2 = 0.91$. Since propane exhibited no measurable dark decay, $k_4 = 0$ and hence, the value of the intercept is equal to k_3, which is seen to be in good agreement with the range of the measured dark decayrates for propylene carbonate. On the basis of the recommended rate constant for the OH radical reaction with propane of $(1.15 \pm 0.23) \times 10^{-12}$ cm^3 $molecule^{-1}$ s^{-1} (Atkinson, 1994), this yields k_1(OH + propylene carbonate) = $(7.0 \pm 1.8) \times 10^{-13}$ cm^3 $molecule^{-1}$ s^{-1}, in excellent agreement with the results of the experiments using $N_2H_4 + O_3$ as the OH radical source.

The combined value from the two sets of experiments yields a rate constant for the reaction of the OH radical with propylene carbonate of

$$k(OH + PC) = (6.9 \pm 1.5) \times 10^{-13} \text{ cm}^3 \text{ molecule}^{-1} \text{ s}^{-1} \text{ at } 298 \text{ K}.$$

This is the only known measurement of this rate constant.

NO_3 Radical Reaction Rate Constants

Propylene Carbonate. No losses of PC (<5%) were observed in reacting NO_3 - N_2O_5 - NO_2 - PC - 2,3-dimethylbutane - air mixtures, while up to 30% reaction of the 2,3-dimethylbutane reference compound was observed. These data lead to an upper limit to the rate constant ratio of k(PC + NO_3)/k(2,3-dimethylbutane + NO_3) <0.14. This rate constant ratio can be placed on an absolute basis by use of a rate constant of k(2,3-dimetlylbutene + NO_3) = 4.08×10^{-16} cm^3 $molecule^{-1}$ s^{-1} (uncertain to a factor of 1.5) at 296 K (Atkinson, 1991), resulting in

$$k(PC + NO_3) < 9 \times 10^{-17} \text{ cm}^3 \text{ molecule}^{-1} \text{ s}^{-1} \text{ at } 296 \pm 2 \text{ K}.$$

Based on these results, we conclude that reaction of PC with NO_3 radicals is negligible under atmospheric conditions.

N-Methyl Pyrrolidinone. In contrast to the case with PC, rapid reaction of NMP was observed in an initial NO_3 - N_2O_5 - NO_2 - NMP - 2,3-dimethylbutane - air mixture, and further experiments utilized *trans*-2-butene as the reference compound. The experimental data obtained from reacting NO_3 - N_2O_5 - NO_2 - NMP - *trans*-2-butene - air mixtures are plotted in accordance with Equation (I) in Figure 5. Least-squares analyses of these data lead to the rate constant ratio of k(NMP + NO_3)/k(*trans*-2-butene + NO_3) = 0.323 ± 0.028, where the indicated error is two least-squares standard deviations. This rate constant ratio can be placed on an absolute basis by use of a rate constant of k(*trans*-2-butene+NO_3) = 3.89×10^{-13} cm^3 $molecule^{-1}$ s^{-1} (±30%) at 296 K (Atkinson, 1991), resulting in

$$k(NMP + NO_3) = (1.26 \pm 0.40) \times 10^{-13} \text{ cm}^3 \text{ molecule}^{-1} \text{ s}^{-1} \text{ at } 296 \pm 2 \text{ K},$$

Figure 5. Plot of Equation (I) for the gas-phase reaction of the NO_3 radical with n-methyl pyrrolidinone, with *trans*-2-butene as the reference organic.

where the indicated error is two least-squares standard deviations combined with the estimated overall uncertainties in the rate constant. This result was incorporated in the model (see below).

Photolysis by Blacklamps

Irradiation of a propylene carbonate (PC) - N-methyl pyrrolidinone (NMP) - cyclohexane (in excess) - air mixture at the maximum light intensity for 3.1 hr resulted in <5% loss of either PC or NMP. This corresponds to upper limits to the photolysis rate of k_{phot} <4.5 x 10^{-6} s^{-1} for this light intensity and spectral distribution condition. Based on this, it is concluded that loss of these compounds by photolyses is negligible under atmospheric conditions.

O_3 Reaction Rate Constants

For both PC and NMP, <5% losses were observed in the presence of (2.44-4.87) x 10^{13} molecule cm^{-3} of O_3 over periods of 3.1-3.4 hr. Combining these maximum losses with the reaction times and the O_3 concentrations measured during the experiments leads to upper limits to the rate constants at 296 ± 2 K of

$$k(PC + O_3) < 2 \times 10^{-19} \text{ cm}^3 \text{ molecule}^{-1} \text{ s}^{-1}$$

and

$$k(NMP + O_3) < 1 \times 10^{-19} \text{ cm}^3 \text{ molecule}^{-1} \text{ s}^{-1}$$

Based on this, it is concluded that losses of these compounds by reaction with O_3 is negligible under atmospheric conditions.

Observation of N-Methyl Pyrrolidinone Reaction Products

NO_3 Radical Reaction. GC-FID and GC-MS analyses of the reacted NO_3 - N_2O_5 - NO_2 - NMP - 2,3-dimethylbutane - air mixture, in which 97% of the initially present NMP had reacted, showed the presence of one major and one minor product. The mass spectrum of the major product showed strong ion peaks at 113 and 56 amu, together with much weaker ion peaks at 85, 84, 58, 57, 55, 43 and 42 amu. The mass spectrum of the minor product showed strong peaks at 85 amu (the base peak), 57, 56, 42 and 41 amu, together with somewhat weaker peaks at 113, 84, 58, 55, 44 and 43 amu. Both products are taken to be of molecular weight 113. Based on matching the GC retention times and mass spectrum with those of an authentic standard, the major product of this NO_3 radical reaction was identified as *N*-methylsuccinimide. The minor product is tentatively identified as 1-formyl-2-pyrrolidinone, based on the mass spectrum and the expectation that formation of this product is analogous to the formation of *N*-methylsuccinimide. A plot of the amounts of *N*-methylsuccinimide formed against the amounts of NMP reacted with the NO_3 radical in reacting NO_3 - N_2O_5 - NO_2 - NMP - *trans*-2-butene - air mixtures is shown in Figure 6. A good straight line plot is observed, with an intercept which is within one standard deviation of zero. The lack of curvature in the plot shown in Figure 6, together with the fact that the reacted NO_3 - N_2O_5 - NO_2 - NMP - 2,3-dimethylbutane - air mixture, in which 97% of the initially

Figure 6. Plot of the amount of *N*-methylsuccinimide formed against the amount of n-methyl pyrrolidinone reacted with the NO_3 radical.

present NMP had reacted, gave a similar yield of *N*-methylsuccinimide, indicates that *N*-methylsuccinimide reacts much slower with the NO_3 than does NMP [with k(NO_3 + *N*-methylsuccinimide)/k(NO_3 + NMP) <0.1]. A least-squares analysis of the data shown in Figure 6 leads to a formation yield of *N*-methylsuccinimide from the reaction of the NO_3 radical with NMP of 0.59 ± 0.16, where the indicated error is two least-squares standard deviations of the slope of the line shown in Figure 2 combined with an estimated overall uncertainty of ±25% in the relative GC-FID response factors for *N*-methylsuccinimide and NMP. The formation yield of the minor product (1-formyl-2-pyrrolidinone) is estimated to be ~0.04 based on the data point from the reacted NO_3 - N_2O_5 - NO_2 - NMP - 2,3-dimethylbutane - air mixture and assuming the same GC-FID response for 1-formyl-2-pyrrolidinone as for *N*-methylsuccinimide.

OH Radical Reaction. GC-FID analyses of irradiated CH_3ONO - NO - NMP - propene - air mixtures showed the formation of the same two reaction products as observed in the reaction of the NO_3 radical with NMP. The measured amounts of these two products, *N*-methylsuccinimide and (tentatively) 1-formyl-2-pyrrolidinone formed are plotted against the amounts of NMP reacted with the OH radical in Figure 7, and it can be seen that the measured yields, defined as {([product] measured)/([NMP] reacted)} decrease with the amount (and fraction) of NMP reacted. This indicates that the products are also reacting with the OH radical, more so for 1-formyl-2-pyrrolidinone, as expected. As described by Atkinson *et a*l. (1982), the measured product concentrations were corrected for reaction with the OH radical, using various rate constants for the reactions of the OH radical with the products and our measured rate constant for the reaction of the OH radical with NMP, until the plots of {($[product]_{corr}$)/([NMP] reacted)} were linear (Figure 7).

The rate constants derived for the reactions of the OH radical with *N*-methylsuccinimide and 1-formyl-2-pyrrolidinone are 0.5 (± 0.15) and 1.0 (± 0.2) of that for the OH radical reaction with NMP, with

$$k(OH + N\text{-methylsuccinimide}) = (1.1 \pm 0.4) \times 10^{-11} \text{ cm}^3 \text{ molecule}^{-1} \text{ s}^{-1}$$

and

$$k(OH + \text{1-formyl-2-pyrrolidinone}) = (2.15 \pm 0.6) \times 10^{-11} \text{ cm}^3 \text{ molecule}^{-1} \text{ s}^{-1}$$

at 296 ± 2 K, where the indicated errors are the estimated overall uncertainties.

The product formation yields, corrected for reaction with the OH radical, are then 0.44 for *N*-methylsuccinimide and 0.41 for 1-formyl-2-pyrrolidinone, accounting for the majority of the reaction pathways and products for the OH radical reaction. The mechanistic implications of these results are discussed in the following section.

Figure 7. Plot of the amounts of *N*-methylsuccinimide and 1-formyl-2-pyrrolidinone formed against the amount of N-methyl pyrrolidinone reacted with the OH radical.
○, Δ - measured concentrations of *N*-methylsuccinimide and 1-formyl-2-pyrrolidinone; •, ▲ - concentrations of *N*-methylsuccinimide and 1-formyl-2-pyrrolidinone corrected for reaction with the OH radical (see text).

CHEMICAL MECHANISMS AND MODELING METHODS

General Atmospheric Photooxidation Mechanism

The chemical mechanism used in the environmental chamber and atmospheric model simulations this study is given in Tables 1-3. Table 1 lists the species used in the mechanism, Table 2 gives the reactions and rate constants, and Table 3 gives the parameters used to calculate the rates of the photolysis reactions. This mechanism is based on that documented by Carter (1990), with a number of updates as discussed below. It can explicitly represent a large number of different types of organic compounds, but it lumps together species reacting with similar rate constants and mechanisms in atmospheric simulations, and it uses a condensed representation for many of the reactive organic products. The reactions of inorganics, CO, formaldehyde, acetaldehyde, peroxyacetyl nitrate, propionaldehyde, peroxypropionyl nitrate, glyoxal and its PAN analog, methylglyoxal and several other product compounds are represented explicitly. In addition, the reactions of unknown photoreactive products formed in the reactions of aromatic hydrocarbons are represented by a model species "AFG2", whose yields and photolysis rate are adjusted based on fits of model simulations to environmental chamber experiments. A chemical operator approach is used to represent peroxy radical reactions, as indicated on Table 1 and discussed in detail by Carter (1990). Generalized reactions with variable rate constants and product yields are used to represent the primary emitted alkane, alkene, aromatic and other VOCs (with rate constants and product yields appropriate for the individual compounds being represented in each simulation); Tables 1 and 2 list only those VOCs (or groups of VOCs) used in the simulations in this work. Most of the higher molecular weight oxygenated product species are represented using the "surrogate species" approach, where simpler molecules such as propionaldehyde or 2-butanone are used to represent the reactions of higher molecular weight analogues that are assumed to react similarly.

Several aspects of the Carter (1990) mechanism was updated prior to this work to account for new kinetic and mechanistic information for certain classes of compounds as described by Carter et. al. (1993a) and Carter (1995). In addition, further modifications were made to the uncertain portions of the mechanisms for the aromatic hydrocarbons to satisfactorily simulate results of experiments carried out using the chamber and light source employed in this study. The previously optimized aromatic mechanisms tended to underpredict the rates of NO oxidation and O_3 formation in the aromatic - NO_x experiments carried out in the chamber employed in this study (Carter *et al.*, 1995d), so the aromatic mechanisms were re-optimized, with MGLY yields being adjusted as well as the AFG2 yields and photolysis rate, to satisfactorily fit data from this chamber as well those used in the previous optimizations (unpublished results from this laboratory). Note that while in the previous mechanisms the model species MGLY represented methylglyoxal alone, in the re-optimized mechanism it is being used to represent uncharacterized products as well. The re-optimized MGLY and AFG2 yields were for toluene were changed from respectively 0.13 and 0.49 to 0.85 and 0.27, and those for m-xylene were changed from

Table 1. List of species in the chemical mechanism used in the model simulations for this study.

Name	Description
Constant Species.	
O2	Oxygen
M	Air
H2O	Water
Active Inorganic Species.	
O3	Ozone
NO	Nitric Oxide
NO2	Nitrogen Dioxide
NO3	Nitrate Radical
N2O5	Nitrogen Pentoxide
HONO	Nitrous Acid
HNO3	Nitric Acid
HNO4	Peroxynitric Acid
HO2H	Hydrogen Peroxide
Active Radical Species and Operators.	
HO2.	Hydroperoxide Radicals
RO2.	Operator to Calculate Total Organic Peroxy Radicals
RCO3.	Operator to Calculate Total Acetyl Peroxy Radicals
Active Reactive Organic Product Species.	
CO	Carbon Monoxide
HCHO	Formaldehyde
CCHO	Acetaldehyde
RCHO	Lumped C3+ Aldehydes
ACET	Acetone
MEK	Lumped Ketones
PHEN	Phenol
CRES	Cresols
BALD	Aromatic aldehydes (e.g., benzaldehyde)
GLY	Glyoxal
MGLY	Methyl Glyoxal
AFG1	Reactive Aromatic Fragmentation Products from benzene and naphthalene
AFG2	Other Reactive Aromatic Fragmentation Products
AFG3	Aromatic Fragmentation Products used in adjusted m-xylene mechanism
RNO3	Organic Nitrates
NPHE	Nitrophenols
ISOPROD	Lumped isoprene product species
PAN	Peroxy Acetyl Nitrate
PPN	Peroxy Propionyl Nitrate
GPAN	PAN Analogue formed from Glyoxal
PBZN	PAN Analogues formed from Aromatic Aldehydes
-OOH	Operator Representing Hydroperoxy Groups
Non-Reacting Species	
CO2	Carbon Dioxide
-C	"Lost Carbon"
-N	"Lost Nitrogen"
H2	Hydrogen

Table 1, (continued)

Name	Description
Steady State Species and Operators.	
HO.	Hydroxyl Radicals
O	Ground State Oxygen Atoms
O*1D2	Excited Oxygen Atoms
RO2-R.	Peroxy Radical Operator representing NO to NO_2 conversion with HO_2 formation.
RO2-N.	Peroxy Radical Operator representing NO consumption with organic nitrate formation.
RO2-NP.	Peroxy Radical Operator representing NO consumption with nitrophenol formation
R2O2.	Peroxy Radical Operator representing NO to NO_2 conversion.
CCO-O2.	Peroxy Acetyl Radicals
C2CO-O2.	Peroxy Propionyl Radicals
HCOCO-O2.	Peroxyacyl Radical formed from Glyoxal
BZ-CO-O2.	Peroxyacyl Radical formed from Aromatic Aldehydes
HOCOO.	Intermediate formed in Formaldehyde + HO_2 reaction
C2(C)-O.	T-Butoxy Radicals.
BZ-O.	Phenoxy Radicals
BZ(NO2)-O.	Nitratophenoxy Radicals
HOCOO.	Radical Intermediate formed in the HO_2 + Formaldehyde system.
(HCHO2)	Excited Criegee biradicals formed from $=CH_2$ groups
(CCHO2)	Excited Criegee biradicals formed from $=CHCH_3$ groups
(RCHO2)	Excited Criegee biradicals formed from =CHR groups, where R not CH_3
(C(C)CO2)	Excited Criegee biradicals formed from $=C(CH_3)_2$ groups
(C(R)CO2)	Excited Criegee biradicals formed from $=C(CH_3)R$ or CR_2 groups
(BZCHO2)	Excited Criegee biradicals formed from styrenes
Hydrocarbon species represented explicitly	
CH4	Methane (EKMA simulations only)
ETHANE	Ethane (Ethane reactivity simulations only)
N-C4	n-Butane (Chamber simulations only)
N-C6	n-Hexane (Chamber simulations only)
N-C8	n-Octane (Chamber simulations only)
ETHE	Ethene
ISOP	Isoprene (EKMA Simulations only)
APIN	α-Pinene (EKMA Simulations only)
UNKN	Unknown biogenics. (EKMA Simulations only)
PROPENE	Propene (Chamber simulations only)
T-2-BUTE	trans-2-Butene (Chamber simulations only)
TOLUENE	Toluene (Chamber simulations only)
M-XYLENE	m-Xylene (Chamber simulations only)
T-C4-OH	T-Butyl Alcohol
NMP	N-Methyl Pyrrolidinone
NMS	N-Methyl Succinimide
1FP	1-Formyl-2-Pyrrolidinone
PC	Propylene Carbonate
Lumped species used to represent the Base ROG mixture in the EKMA model simulations.	
ALK1	Alkanes and other saturated compounds with $k_{OH} < 10^4$ ppm^{-1} min^{-1}.
ALK2	Alkanes and other saturated compounds with $k_{OH} \geq 10^4$ ppm^{-1} min^{-1}.
ARO1	Aromatics with $k_{OH} < 2x10^4$ ppm^{-1} min^{-1}.
ARO2	Aromatics with $k_{OH} \geq 2x10^4$ ppm^{-1} min^{-1}.
OLE2	Alkenes (other than ethene) with $k_{OH} < 7x10^4$ ppm^{-1} min^{-1}.
OLE3	Alkenes with $k_{OH} \geq 7x10^4$ ppm^{-1} min^{-1}.

Table 2. List of reactions in the chemical mechanism used in the model simulations for this study.

Rxn. Label	Kinetic Parameters [a] k(300)	A	Ea	B	Reactions [b]
Inorganic Reactions					
1	(Phot. Set = NO2)				NO2 + HV = NO + O
2	6.00E-34	6.00E-34	0.00	-2.30	O + O2 + M = O3 + M
3A	9.69E-12	6.50E-12	-0.24	0.00	O + NO2 = NO + O2
3B	1.55E-12	(Falloff Kinetics)			O + NO2 = NO3 + M
	k0 =	9.00E-32	0.00	-2.00	
	kINF =	2.20E-11	0.00	0.00	
		F= 0.60	n= 1.00		
4	1.88E-14	2.00E-12	2.78	0.00	O3 + NO = NO2 + O2
5	3.36E-17	1.40E-13	4.97	0.00	O3 + NO2 = O2 + NO3
6	2.80E-11	1.70E-11	-0.30	0.00	NO + NO3 = 2 NO2
7	1.92E-38	3.30E-39	-1.05	0.00	NO + NO + O2 = 2 NO2
8	1.26E-12	(Falloff Kinetics)			NO2 + NO3 = N2O5
	k0 =	2.20E-30	0.00	-4.30	
	kINF =	1.50E-12	0.00	-0.50	
		F= 0.60	n= 1.00		
9	5.53E+10	9.09E+26	22.26	0.00	N2O5 + #RCON8 = NO2 + NO3
10	1.00E-21	(No T Dependence)			N2O5 + H2O = 2 HNO3
11	4.17E-16	2.50E-14	2.44	0.00	NO2 + NO3 = NO + NO2 + O2
12A	(Phot. Set = NO3NO)				NO3 + HV = NO + O2
12B	(Phot. Set = NO3NO2)				NO3 + HV = NO2 + O
13A	(Phot. Set = O3O3P)				O3 + HV = O + O2
13B	(Phot. Set = O3O1D)				O3 + HV = O*1D2 + O2
14	2.20E-10	(No T Dependence)			O*1D2 + H2O = 2 HO.
15	2.92E-11	1.92E-11	-0.25	0.00	O*1D2 + M = O + M
16	4.81E-12	(Falloff Kinetics)			HO. + NO = HONO
	k0 =	7.00E-31	0.00	-2.60	
	kINF =	1.50E-11	0.00	-0.50	
		F= 0.60	n= 1.00		
17	(Phot. Set = HONO)				HONO + HV = HO. + NO
18	1.13E-11	(Falloff Kinetics)			HO. + NO2 = HNO3
	k0 =	2.60E-30	0.00	-3.20	
	kINF =	2.40E-11	0.00	-1.30	
		F= 0.60	n= 1.00		
19	1.03E-13	6.45E-15	-1.65	0.00	HO. + HNO3 = H2O + NO3
21	2.40E-13	(No T Dependence)			HO. + CO = HO2. + CO2
22	6.95E-14	1.60E-12	1.87	0.00	HO. + O3 = HO2. + O2
23	8.28E-12	3.70E-12	-0.48	0.00	HO2. + NO = HO. + NO2
24	1.37E-12	(Falloff Kinetics)			HO2. + NO2 = HNO4
	k0 =	1.80E-31	0.00	-3.20	
	kINF =	4.70E-12	0.00	-1.40	
		F= 0.60	n= 1.00		
25	7.92E+10	4.76E+26	21.66	0.00	HNO4 + #RCON24 = HO2. + NO2
27	4.61E-12	1.30E-12	-0.75	0.00	HNO4 + HO. = H2O + NO2 + O2
28	2.08E-15	1.10E-14	0.99	0.00	HO2. + O3 = HO. + 2 O2
29A	1.73E-12	2.20E-13	-1.23	0.00	HO2. + HO2. = HO2H + O2
29B	5.00E-32	1.90E-33	-1.95	0.00	HO2. + HO2. + M = HO2H + O2
29C	3.72E-30	3.10E-34	-5.60	0.00	HO2. + HO2. + H2O = HO2H + O2 + H2O
29D	2.65E-30	6.60E-35	-6.32	0.00	HO2. + HO2. + H2O = HO2H + O2 + H2O
30A	1.73E-12	2.20E-13	-1.23	0.00	NO3 + HO2. = HNO3 + O2
30B	5.00E-32	1.90E-33	-1.95	0.00	NO3 + HO2. + M = HNO3 + O2
30C	3.72E-30	3.10E-34	-5.60	0.00	NO3 + HO2. + H2O = HNO3 + O2 + H2O
30D	2.65E-30	6.60E-35	-6.32	0.00	NO3 + HO2. + H2O = HNO3 + O2 + H2O
31	(Phot. Set = H2O2)				HO2H + HV = 2 HO.
32	1.70E-12	3.30E-12	0.40	0.00	HO2H + HO. = HO2. + H2O
33	9.90E-11	4.60E-11	-0.46	0.00	HO. + HO2. = H2O + O2
Peroxy Radical Operators					
B1	7.68E-12	4.20E-12	-0.36	0.00	RO2. + NO = NO
B2	2.25E-11	(Falloff Kinetics)			RCO3. + NO = NO
	k0 =	5.65E-28	0.00	-7.10	
	kINF =	2.64E-11	0.00	-0.90	
		F= 0.27	n= 1.00		
B4	1.04E-11	(Falloff Kinetics)			RCO3. + NO2 = NO2
	k0 =	2.57E-28	0.00	-7.10	
	kINF =	1.20E-11	0.00	-0.90	
		F= 0.30	n= 1.00		
B5	4.90E-12	3.40E-13	-1.59	0.00	RO2. + HO2. = HO2. + RO2-HO2-PROD
B6	4.90E-12	3.40E-13	-1.59	0.00	RCO3. + HO2. = HO2. + RO2-HO2-PROD
B8	1.00E-15	(No T Dependence)			RO2. + RO2. = RO2-RO2-PROD
B9	1.09E-11	1.86E-12	-1.05	0.00	RO2. + RCO3. = RO2-RO2-PROD
B10	1.64E-11	2.80E-12	-1.05	0.00	RCO3. + RCO3. = RO2-RO2-PROD

Table 2 (continued)

Rxn. Label	Kinetic Parameters [a] k(300)	A	Ea	B	Reactions [b]
B11	(Same k as for RO2.)				RO2-R. + NO = NO2 + HO2.
B12	(Same k as for RO2.)				RO2-R. + HO2. = -OOH
B13	(Same k as for RO2.)				RO2-R. + RO2. = RO2. + 0.5 HO2.
B14	(Same k as for RO2.)				RO2-R. + RCO3. = RCO3. + 0.5 HO2.
B19	(Same k as for RO2.)				RO2-N. + NO = RNO3
B20	(Same k as for RO2.)				RO2-N. + HO2. = -OOH + MEK + 1.5 -C
B21	(Same k as for RO2.)				RO2-N. + RO2. = RO2. + 0.5 HO2. + MEK + 1.5 -C
B22	(Same k as for RO2.)				RO2-N. + RCO3. = RCO3. + 0.5 HO2. + MEK + 1.5 -C
B15	(Same k as for RO2.)				R2O2. + NO = NO2
B16	(Same k as for RO2.)				R2O2. + HO2. =
B17	(Same k as for RO2.)				R2O2. + RO2. = RO2.
B18	(Same k as for RO2.)				R2O2. + RCO3. = RCO3.
B23	(Same k as for RO2.)				RO2-XN. + NO = -N
B24	(Same k as for RO2.)				RO2-XN. + HO2. = -OOH
B25	(Same k as for RO2.)				RO2-XN. + RO2. = RO2. + 0.5 HO2.
B26	(Same k as for RO2.)				RO2-XN. + RCO3. = RCO3. + HO2.
G2	(Same k as for RO2.)				RO2-NP. + NO = NPHE
G3	(Same k as for RO2.)				RO2-NP. + HO2. = -OOH + 6 -C
G4	(Same k as for RO2.)				RO2-NP. + RO2. = RO2. + 0.5 HO2. + 6 -C
G5	(Same k as for RO2.)				RO2-NP. + RCO3. = RCO3. + HO2. + 6 -C
Excited Criegee Biradicals					
RZ1	(fast)				(HCHO2) = 0.7 HCOOH + 0.12 "HO. + HO2. + CO" + 0.18 "H2 + CO2"
RZ2	(fast)				(CCHO2) = 0.25 CCOOH + 0.15 "CH4 + CO2" + 0.6 HO. + 0.3 "CCO-O2. + RCO3." + 0.3 "RO2-R. + HCHO + CO + RO2."
RZ3	(fast)				(RCHO2) = 0.25 CCOOH + 0.15 CO2 + 0.6 HO. + 0.3 "C2CO-O2. + RCO3." + 0.3 "RO2-R. + CCHO + CO + RO2." + 0.55 -C
RZ4	(fast)				(C(C)CO2) = HO. + R2O2. + HCHO + CCO-O2. + RCO3. + RO2.
RZ5	(fast)				(C(R)CO2) = HO. + CCO-O2. + CCHO + R2O2. + RCO3. + RO2.
RZ6	(fast)				(CYCCO2) = 0.3 "HO. + C2CO-O2. + R2O2. + RCO3. + RO2." + 0.3 RCHO + 4.2 -C
RZ8	(fast)				(BZCHO2) = 0.5 "BZ-O. + R2O2. + CO + HO."
ISZ1	(fast)				(C:CC(C)O2) = HO. + R2O2. + HCHO + C2CO-O2. + RO2. + RCO3.
ISZ2	(fast)				(C:C(C)CHO2) = 0.75 RCHO + 0.25 ISOPROD + 0.5 -C
MAZ1	(fast)				(C2(O2)CHO) = HO. + R2O2. + HCHO + HCOCO-O2. + RO2. + RCO3.
M1Z1	(fast)				(HOCCHO2) = 0.6 HO. + 0.3 "CCO-O2. + RCO3." + 0.3 "RO2-R. + HCHO + CO + RO2." + 0.8 -C
M2Z1	(fast)				(HCOCHO2) = 0.12 "HO2. + 2 CO + HO." + 0.74 -C + 0.51 "CO2 + HCHO"
M2Z2	(fast)				(C2(O2)COH) = HO. + MGLY + HO2. + R2O2. + RO2.
Organic Product Species					
B7	(Phot. Set = CO2H)				-OOH + HV = HO2. + HO.
B7A	1.81E-12	1.18E-12	-0.25	0.00	HO. + -OOH = HO.
B7B	3.71E-12	1.79E-12	-0.44	0.00	HO. + -OOH = RO2-R. + RO2.
C1	(Phot. Set = HCHONEWR)				HCHO + HV = 2 HO2. + CO
C2	(Phot. Set = HCHONEWM)				HCHO + HV = H2 + CO
C3	9.76E-12	1.13E-12	-1.29	2.00	HCHO + HO. = HO2. + CO + H2O
C4	7.79E-14	9.70E-15	-1.24	0.00	HCHO + HO2. = HOCOO.
C4A	1.77E+02	2.40E+12	13.91	0.00	HOCOO. = HO2. + HCHO
C4B	(Same k as for RO2.)				HOCOO. + NO = -C + NO2 + HO2.
C9	6.38E-16	2.80E-12	5.00	0.00	HCHO + NO3 = HNO3 + HO2. + CO
C10	1.57E-11	5.55E-12	-0.62	0.00	CCHO + HO. = CCO-O2. + H2O + RCO3.
C11A	(Phot. Set = CCHOR)				CCHO + HV = CO + HO2. + HCHO + RO2-R. + RO2.
C12	2.84E-15	1.40E-12	3.70	0.00	CCHO + NO3 = HNO3 + CCO-O2. + RCO3.
C25	1.97E-11	8.50E-12	-0.50	0.00	RCHO + HO. = C2CO-O2. + RCO3.
C26	(Phot. Set = RCHO)				RCHO + HV = CCHO + RO2-R. + RO2. + CO + HO2.
C27	2.84E-15	1.40E-12	3.70	0.00	NO3 + RCHO = HNO3 + C2CO-O2. + RCO3.
C38	2.23E-13	4.81E-13	0.46	2.00	ACET + HO. = R2O2. + HCHO + CCO-O2. + RCO3. + RO2.
C39	(Phot. Set = ACET-93C)				ACET + HV = CCO-O2. + HCHO + RO2-R. + RCO3. + RO2.
C44	1.16E-12	2.92E-13	-0.82	2.00	MEK + HO. = H2O + 0.5 "CCHO + HCHO + CCO-O2. + C2CO-O2." + RCO3. + 1.5 "R2O2. + RO2."

Table 2 (continued)

Rxn.	Kinetic Parameters [a]				Reactions [b]
Label	k(300)	A	Ea	B	
C57	(Phot. Set = KETONE) (Overall q.y = 0.1)				MEK + HV = CCO-O2. + CCHO + RO2-R. + RCO3. + RO2.
C95	2.07E-12	2.19E-11	1.41	0.00	RNO3 + HO. = NO2 + 0.155 MEK + 1.05 RCHO + 0.48 CCHO + 0.16 HCHO + 0.11 -C + 1.39 "R2O2. + RO2."
C58A	(Phot. Set = GLYOXAL1)				GLY + HV = 0.8 HO2. + 0.45 HCHO + 1.55 CO
C58B	(Phot. Set = GLYOXAL2) (Overall q.y = 0.029)				GLY + HV = 0.13 HCHO + 1.87 CO
C59	1.14E-11	(No T Dependence)			GLY + HO. = 0.6 HO2. + 1.2 CO + 0.4 "HCOCO-O2. + RCO3."
C60	(Same k as for CCHO)				GLY + NO3 = HNO3 + 0.6 HO2. + 1.2 CO + 0.4 "HCOCO-O2. + RCO3."
C68A	(Phot. Set = MEGLYOX1)				MGLY + HV = HO2. + CO + CCO-O2. + RCO3.
C68B	(Phot. Set = MEGLYOX2)				MGLY + HV + 0.107 = HO2. + CO + CCO-O2. + RCO3.
C69	1.72E-11	(No T Dependence)			MGLY + HO. = CO + CCO-O2. + RCO3.
C70	(Same k as for CCHO)				MGLY + NO3 = HNO3 + CO + CCO-O2. + RCO3.
G7	1.14E-11	(No T Dependence)			HO. + AFG1 = HCOCO-O2. + RCO3.
G8	(Phot. Set = ACROLEIN) (Overall q.y = 0.029)				AFG1 + HV = HO2. + HCOCO-O2. + RCO3.
U2OH	1.72E-11	(No T Dependence)			HO. + AFG2 = C2CO-O2. + RCO3.
U2HV	(Phot. Set = ACROLEIN)				AFG2 + HV = HO2. + CO + CCO-O2. + RCO3.
G46	2.63E-11	(No T Dependence)			HO. + PHEN = 0.15 RO2-NP. + 0.85 RO2-R. + 0.2 GLY + 4.7 -C + RO2.
G51	3.60E-12	(No T Dependence)			NO3 + PHEN = HNO3 + BZ-O.
G52	4.20E-11	(No T Dependence)			HO. + CRES = 0.15 RO2-NP. + 0.85 RO2-R. + 0.2 MGLY + 5.5 -C + RO2.
G57	2.10E-11	(No T Dependence)			NO3 + CRES = HNO3 + BZ-O. + -C
G30	1.29E-11	(No T Dependence)			BALD + HO. = BZ-CO-O2. + RCO3.
G31	(Phot. Set = BZCHO) (Overall q.y = 0.05)				BALD + HV = 7 -C
G32	2.61E-15	1.40E-12	3.75	0.00	BALD + NO3 = HNO3 + BZ-CO-O2.
G58	3.60E-12	(No T Dependence)			NPHE + NO3 = HNO3 + BZ(NO2)-O.
G59	(Same k as for BZ-O.)				BZ(NO2)-O. + NO2 = 2 -N + 6 -C
G60	(Same k as for RO2.)				BZ(NO2)-O. + HO2. = NPHE
G61	(Same k as for BZ-O.)				BZ(NO2)-O. = NPHE
C13	(Same k as for RCO3.)				CCO-O2. + NO = CO2 + NO2 + HCHO + RO2-R. + RO2.
C14	(Same k as for RCO3.)				CCO-O2. + NO2 = PAN
C15	(Same k as for RCO3.)				CCO-O2. + HO2. = -OOH + CO2 + HCHO
C16	(Same k as for RCO3.)				CCO-O2. + RO2. = RO2. + 0.5 HO2. + CO2 + HCHO
C17	(Same k as for RCO3.)				CCO-O2. + RCO3. = RCO3. + HO2. + CO2 + HCHO
C18	6.50E-04	(Falloff Kinetics)			PAN = CCO-O2. + NO2 + RCO3.
	k0 =	4.90E-03	23.97	0.00	
	kINF =	4.00E+16	27.08	0.00	
		F= 0.30	n= 1.00		
C28	(Same k as for RCO3.)				C2CO-O2. + NO = CCHO + RO2-R. + CO2 + NO2 + RO2.
C29	8.40E-12	(No T Dependence)			C2CO-O2. + NO2 = PPN
C30	(Same k as for RCO3.)				C2CO-O2. + HO2. = -OOH + CCHO + CO2
C31	(Same k as for RCO3.)				C2CO-O2. + RO2. = RO2. + 0.5 HO2. + CCHO + CO2
C32	(Same k as for RCO3.)				C2CO-O2. + RCO3. = RCO3. + HO2. + CCHO + CO2
C33	6.78E-04	1.60E+17	27.97	0.00	PPN = C2CO-O2. + NO2 + RCO3.
C62	(Same k as for RCO3.)				HCOCO-O2. + NO = NO2 + CO2 + CO + HO2.
C63	(Same k as for RCO3.)				HCOCO-O2. + NO2 = GPAN
C65	(Same k as for RCO3.)				HCOCO-O2. + HO2. = -OOH + CO2 + CO
C66	(Same k as for RCO3.)				HCOCO-O2. + RO2. = RO2. + 0.5 HO2. + CO2 + CO
C67	(Same k as for RCO3.)				HCOCO-O2. + RCO3. = RCO3. + HO2. + CO2 + CO
C64	(Same k as for PAN)				GPAN = HCOCO-O2. + NO2 + RCO3.
G33	(Same k as for RCO3.)				BZ-CO-O2. + NO = BZ-O. + CO2 + NO2 + R2O2. + RO2.
G43	3.53E-11	1.30E-11	-0.60	0.00	BZ-O. + NO2 = NPHE
G44	(Same k as for RO2.)				BZ-O. + HO2. = PHEN
G45	1.00E-03	(No T Dependence)			BZ-O. = PHEN
G34	8.40E-12	(No T Dependence)			BZ-CO-O2. + NO2 = PBZN
G36	(Same k as for RCO3.)				BZ-CO-O2. + HO2. = -OOH + CO2 + PHEN
G37	(Same k as for RCO3.)				BZ-CO-O2. + RO2. = RO2. + 0.5 HO2. + CO2 + PHEN
G38	(Same k as for RCO3.)				BZ-CO-O2. + RCO3. = RCO3. + HO2. + CO2 + PHEN
G35	2.17E-04	1.60E+15	25.90	0.00	PBZN = BZ-CO-O2. + NO2 + RCO3.

Table 2 (continued)

Rxn. Label	Kinetic Parameters [a] k(300)	A	Ea	B	Reactions [b]
IPOH	3.36E-11	(No T Dependence)			ISOPROD + HO. = 0.293 CO + 0.252 CCHO + 0.126 HCHO + 0.041 GLY + 0.021 RCHO + 0.168 MGLY + 0.314 MEK + 0.503 RO2-R. + 0.21 CCO-O2. + 0.288 C2CO-O2. + 0.21 R2O2. + 0.713 RO2. + 0.498 RCO3. + -0.112 -C
IPO3	7.11E-18	(No T Dependence)			ISOPROD + O3 = 0.02 CCHO + 0.04 HCHO + 0.01 GLY + 0.84 MGLY + 0.09 MEK + 0.66 (HCHO2) + 0.09 (HCOCHO2) + 0.18 (HOCCHO2) + 0.06 (C2(O2)CHO) + 0.01 (C2(O2)COH) + -0.39 -C
IPHV	(Phot. Set = ACROLEIN)				ISOPROD + HV + 0.0036 = 0.333 CO + 0.067 CCHO + 0.9 HCHO + 0.033 MEK + 0.333 HO2. + 0.7 RO2-R. + 0.267 CCO-O2. + 0.7 C2CO-O2. + 0.7 RO2. + 0.967 RCO3. + -0.133 -C
IPN3	1.00E-15	(No T Dependence)			ISOPROD + NO3 = 0.643 CO + 0.282 HCHO + 0.85 RNO3 + 0.357 RCHO + 0.925 HO2. + 0.075 C2CO-O2. + 0.075 R2O2. + 0.925 RO2. + 0.075 RCO3. + 0.075 HNO3 + -2.471 -C
Hydrocarbon Species Represented Explicitly					
	2.56E-12	1.36E-12	-0.38	2.00	N-C4 + HO. = 0.076 RO2-N. + 0.924 RO2-R. + 0.397 R2O2. + 0.001 HCHO + 0.571 CCHO + 0.14 RCHO + 0.533 MEK + -0.076 -C + 1.397 RO2.
	5.63E-12	1.35E-11	0.52	0.00	N-C6 + HO. = 0.185 RO2-N. + 0.815 RO2-R. + 0.738 R2O2. + 0.02 CCHO + 0.105 RCHO + 1.134 MEK + 0.186 -C + 1.738 RO2.
	8.76E-12	3.15E-11	0.76	0.00	N-C8 + HO. = 0.333 RO2-N. + 0.667 RO2-R. + 0.706 R2O2. + 0.002 RCHO + 1.333 MEK + 0.998 -C + 1.706 RO2.
	8.43E-12	1.96E-12	-0.87	0.00	ETHENE + HO. = RO2-R. + RO2. + 1.56 HCHO + 0.22 CCHO
	1.68E-18	9.14E-15	5.13	0.00	ETHENE + O3 = HCHO + (HCHO2)
	2.18E-16	4.39E-13	4.53	2.00	ETHENE + NO3 = R2O2. + RO2. + 2 HCHO + NO2
	7.42E-13	1.04E-11	1.57	0.00	ETHENE + O = RO2-R. + HO2. + RO2. + HCHO + CO
	2.60E-11	4.85E-12	-1.00	0.00	PROPENE + HO. = RO2-R. + RO2. + HCHO + CCHO
	1.05E-17	5.51E-15	3.73	0.00	PROPENE + O3 = 0.6 HCHO + 0.4 CCHO + 0.4 (HCHO2) + 0.6 (CCHO2)
	9.74E-15	4.59E-13	2.30	0.00	PROPENE + NO3 = R2O2. + RO2. + HCHO + CCHO + NO2
	4.01E-12	1.18E-11	0.64	0.00	PROPENE + O = 0.4 HO2. + 0.5 RCHO + 0.5 MEK + -0.5 -C
	6.30E-11	1.01E-11	-1.09	0.00	T-2-BUTE + HO. = RO2-R. + RO2. + 2 CCHO
	1.95E-16	6.64E-15	2.10	0.00	T-2-BUTE + O3 = CCHO + (CCHO2)
	3.92E-13	1.10E-13	-0.76	2.00	T-2-BUTE + NO3 = R2O2. + RO2. + 2 CCHO + NO2
	2.34E-11	2.26E-11	-0.02	0.00	T-2-BUTE + O = 0.4 HO2. + 0.5 RCHO + 0.5 MEK + 0.5 -C
	9.88E-11	2.54E-11	-0.81	0.00	ISOP + HO. = 0.088 RO2-N. + 0.912 RO2-R. + 0.629 HCHO + 0.912 ISOPROD + 0.079 R2O2. + 1.079 RO2. + 0.283 -C
	1.34E-17	7.86E-15	3.80	0.00	ISOP + O3 = 0.4 HCHO + 0.6 ISOPROD + 0.55 (HCHO2) + 0.2 (C:CC(C)O2) + 0.2 (C:C(C)CHO2) + 0.05 -C
	3.60E-11	(No T Dependence)			ISOP + O = 0.75 "ISOPROD + -C "+ 0.25 "C2CO-O2. + RCO3. + 2 HCHO + RO2-R. + RO2."
	6.81E-13	3.03E-12	0.89	0.00	ISOP + NO3 = 0.8 "RCHO + RNO3 + RO2-R." + 0.2 "ISOPROD + R2O2. + NO2" + RO2. + -2.2 -C
	1.50E-19	(No T Dependence)			ISOP + NO2 = 0.8 "RCHO + RNO3 + RO2-R." + 0.2 "ISOPROD + R2O2. + NO" + RO2. + -2.2 -C
	5.31E-11	1.21E-11	-0.88	0.00	APIN + HO. = RO2-R. + RCHO + RO2. + 7 -C
	1.00E-16	9.90E-16	1.37	0.00	APIN + O3 = 0.05 HCHO + 0.2 CCHO + 0.5 RCHO + 0.61 MEK + 0.075 CO + 0.05 CCO-O2. + 0.05 C2CO-O2. + 0.1 RCO3. + 0.105 HO2. + 0.16 HO. + 0.135 RO2-R. + 0.15 R2O2. + 0.285 RO2. + 5.285 -C
	6.10E-12	1.19E-12	-0.97	0.00	APIN + NO3 = NO2 + R2O2. + RCHO + RO2. + 7 -C
	3.00E-11	(No T Dependence)			APIN + O = 0.4 HO2. + 0.5 MEK + 0.5 RCHO + 6.5 -C
	6.57E-11	(No T Dependence)			UNKN + HO. = RO2-R. + RO2. + 0.5 HCHO + RCHO + 6.5 -C
	5.85E-17	(No T Dependence)			UNKN + O3 = 0.135 RO2-R. + 0.135 HO2. + 0.075 R2O2. + 0.21 RO2. + 0.025 CCO-O2. + 0.025 C2CO-O2. + 0.05 RCO3. + 0.275 HCHO + 0.175 CCHO + 0.5 RCHO + 0.41 MEK + 0.185 CO + 5.925 -C + 0.11 HO.
	4.30E-12	(No T Dependence)			UNKN + NO3 = R2O2. + RO2. + 0.5 HCHO + RCHO + 6.5 -C + NO2
	2.90E-11	(No T Dependence)			UNKN + O = 0.4 HO2. + 0.5 RCHO + 0.5 MEK + 6.5 -C
	5.91E-12	1.81E-12	-0.70	0.00	TOLUENE + HO. = 0.085 BALD + 0.26 CRES + 0.118 GLY + 0.847 MGLY + 0.276 AFG2 + 0.74 RO2-R. + 0.26 HO2. + 0.981 -C + 0.74 RO2.

Table 2 (continued)

Rxn. Label	Kinetic Parameters [a] k(300)	A	Ea	B	Reactions [b]
	2.36E-11	(No T Dependence)			M-XYLENE + HO. = 0.04 BALD + 0.18 CRES + 0.108 GLY + 1.554 MGLY + 0.505 AFG2 + 0.82 RO2-R. + 0.18 HO2. + 0.068 -C + 0.82 RO2.
Lumped Species used in EKMA Simulations [c]					
A1OH	3.46E-12	2.56E-12	-0.18	0.00	ALK1 + HO. = 0.911 RO2-R. + 0.074 RO2-N. + 0.005 RO2-XN. + 0.011 HO2. + 0.575 R2O2. + 1.564 RO2. + 0.065 HCHO + 0.339 CCHO + 0.196 RCHO + 0.322 ACET + 0.448 MEK + 0.024 CO + 0.025 GLY + 0.051 -C
A2OH	9.14E-12	5.12E-12	-0.35	0.00	ALK2 + HO. = 0.749 RO2-R. + 0.249 RO2-N. + 0.002 RO2-XN. + 0.891 R2O2. + 1.891 RO2. + 0.029 HCHO + 0.048 CCHO + 0.288 RCHO + 0.028 ACET + 1.105 MEK + 0.043 CO + 0.018 CO2 + 1.268 -C
B1OH	5.87E-12	(No T Dependence)			ARO1 + HO. = 0.742 RO2-R. + 0.258 HO2. + 0.742 RO2. + 0.015 PHEN + 0.244 CRES + 0.08 BALD + 0.124 GLY + 0.681 MGLY + 0.11 AFG1 + 0.244 AFG2 + 1.857 -C
B2OH	3.22E-11	1.20E-11	-0.59	0.00	ARO2 + HO. = 0.82 RO2-R. + 0.18 HO2. + 0.82 RO2. + 0.18 CRES + 0.036 BALD + 0.068 GLY + 1.02 MGLY + 0.532 AFG2 + 2.588 -C
O2OH	3.17E-11	2.22E-12	-1.59	0.00	OLE2 + HO. = 0.858 RO2-R. + 0.142 RO2-N. + RO2. + 0.858 HCHO + 0.252 CCHO + 0.606 RCHO + 1.267 -C
O2O3	1.08E-17	1.42E-15	2.91	0.00	OLE2 + O3 = 0.6 HCHO + 0.635 RCHO + 0.981 -C + 0.4 (HCHO2) + 0.529 (CCHO2) + 0.071 (RCHO2)
O2N3	1.16E-14	1.99E-13	1.69	0.00	OLE2 + NO3 = R2O2. + RO2. + HCHO + 0.294 CCHO + 0.706 RCHO + 1.451 -C + NO2
O2OA	4.11E-12	4.51E-12	0.06	0.00	OLE2 + O = 0.4 HO2. + 0.5 RCHO + 0.5 MEK + 1.657 -C
O3OH	6.23E-11	4.54E-12	-1.56	0.00	OLE3 + HO. = 0.861 RO2-R. + 0.139 RO2-N. + RO2. + 0.24 HCHO + 0.661 CCHO + 0.506 RCHO + 0.113 ACET + 0.086 MEK + 0.057 BALD + 0.848 -C
O3O3	1.70E-16	1.77E-15	1.40	0.00	OLE3 + O3 = 0.203 HCHO + 0.358 CCHO + 0.309 RCHO + 0.061 MEK + 0.027 BALD + 0.976 -C + 0.076 (HCHO2) + 0.409 (CCHO2) + 0.279 (RCHO2) + 0.158 (C(C)CO2 + 0.039 (C(R)CO2 + 0.04 (BZCHO2)
O3N3	1.07E-12	3.19E-13	-0.72	0.00	OLE3 + NO3 = R2O2. + RO2. + 0.278 HCHO + 0.767 CCHO + 0.588 RCHO + 0.131 ACET + 0.1 MEK + 0.066 BALD + 0.871 -C + NO2
O3OA	2.52E-11	8.66E-12	-0.64	0.00	OLE3 + O = 0.4 HO2. + 0.5 RCHO + 0.5 MEK + 2.205 -C
T-Butyl Alcohol					
TBOH	1.08E-12	(No T Dependence)			T-C4-OH + HO. = 0.07 RO2-N. + 0.83 RO2-R. + 0.83 HCHO + 0.83 ACET + -0.07 -C + 0.9 RO2. + 0.1 C2(C)-O.
TBON	2.40E-11	(No T Dependence)			C2(C)-O. + NO2 = RNO3 + -2 -C
TBOD	1.18E+03	7.50E+14	16.20	0.00	C2(C)-O. = ACET + HCHO + RO2-R. + RO2.
N-Methyl Pyrrolidone (Standard Mechanism)					
NMOH	2.15E-11	(No T Dependence)			NMP + HO. = 0.85 "RO2-R. + 0.5 1FP + 0.5 NMS" + 0.15 RO2-N. + RO2.
NMN3	1.26E-13	(No T Dependence)			NMP + NO3 = 0.85 "RO2-R. + NMS" + 0.15 RO2-N. + RO2. + HNO3
MSOH	1.10E-11	(No T Dependence)			NMS + HO. = 0.85 "RO2-R. + RCHO + 2 -C" + 0.15 RO2-N. + RO2.
FPOH	2.15E-11	(No T Dependence)			1FP + HO. = 0.5 "C2CO-O2. + RCO3. + 2 -C + RO2." + 0.425 "RO2-R. + RCHO + 2 -C" + 0.075 RO2-N.
FPN3	1.26E-13	(No T Dependence)			1FP + NO3 = 0.85 "RO2-R. + RCHO + 2 -C" + 0.15 RO2-N. + RO2. + HNO3
N-Methyl Pyrrolidone (Adjusted Mechanism)					
NMOH	2.15E-11	(No T Dependence)			NMP + HO. = 0.93 "HO2. + 0.5 1FP + 0.5 NMS" + 0.07 "RO2-N. + RO2."
NMN3	1.26E-13	(No T Dependence)			NMP + NO3 = 0.93 "HO2. + NMS" + 0.07 "RO2-N. + RO2." + HNO3
MSOH	1.10E-11	(No T Dependence)			NMS + HO. = 0.93 "HO2. + RCHO + 2 -C" + 0.07 "RO2-N. + RO2."
FPOH	2.15E-11	(No T Dependence)			1FP + HO. = 0.5 "C2CO-O2. + RCO3. + 2 -C" + 0.465 "HO2. + RCHO + 2 -C" + 0.035 "RO2-N. + RO2."

Table 2 (continued)

Rxn. Label	Kinetic Parameters [a] k(300)	A	Ea	B	Reactions [b]
FPN3	1.26E-13	(No T Dependence)			1FP + NO3 = 0.93 "HO2. + RCHO + 2 -C" + 0.07 "RO2-N. + RO2." + HNO3
Propylene Carbonate					
PCOH	6.90E-13	(No T Dependence)			PC + HO. = 0.08 RO2-N. + 0.92 RO2-R. + 0.24 R2O2. + 0.24 HCHO + 0.92 CO2 + -0.11 -C + 0.24 GLY + 0.69 MGLY + 1.24 RO2.
Reactions used to Represent Chamber-Dependent Processes [d]					
O3W	(varied)	(No T Dependence)			O3 =
N25I	(varied)	(No T Dependence)			N2O5 = 2 NOX-WALL
N25S	(varied)	(No T Dependence)			N2O5 + H2O = 2 NOX-WALL
NO2W	(varied)	(No T Dependence)			NO2 = (yHONO) HONO + (1-yHONO) NOX-WALL
XSHC	(varied)	(No T Dependence)			HO. = HO2.
RSI	(Phot. Set = NO2)				HV + #RS/K1 = HO.
ONO2	(Phot. Set = NO2)				HV + #E-NO2/K1 = NO2 + #-1 NOX-WALL

[a] Except as noted, expression for rate constant is k = A $e^{Ea/RT}$ $(T/300)^B$. Rate constants and A factor are in cm, molecule, sec. units. Units of Ea is kcal $mole^{-1}$. "Phot Set" means this is a photolysis reaction, with the absorption coefficients and quantum yields given in Table 3. If "(overall qy) is given on the following line, then the photolysis data given in Table 3 are only for the absorption cross sections, and the quantum yield given is assumed for all wavelengths. In addition, if "#(number)" or "#(parameter)" is given as a reactant, then the value of that number or parameter is multiplied by the result in the "rate constant expression" columns to obtain the rate constant used. Furthermore, "#RCONnn" as a reactant means that the rate constant for the reaction is obtained by multiplying the rate constant given by that for reaction "nn". Thus, the rate constant given is actually an equilibrium constant.
[b] Format of reaction listing same as used in documentation of the detailed mechanism (Carter 1990).
[c] Rate constants and product yield parameters based on the mixture of species in the base ROG mixture which are being represented.
[d] See Table 4 for the values of the parameters used for the specific chambers modeled in this study.

Table 3. Absorption cross sections and quantum yields for photolysis reactions.

WL (nm)	Abs (cm^2)	QY	WL (nm)	Abs (cm^2)	QY	WL (nm)	Abs (cm^2)	QY	WL (nm)	Abs (cm^2)	QY	WL (nm)	Abs (cm^2)	QY
Photolysis File = NO2														
250.0	2.83E-20	1.000	255.0	1.45E-20	1.000	260.0	1.90E-20	1.000	265.0	2.05E-20	1.000	270.0	3.13E-20	1.000
275.0	4.02E-20	1.000	280.0	5.54E-20	1.000	285.0	6.99E-20	1.000	290.0	8.18E-20	0.999	295.0	9.67E-20	0.998
300.0	1.17E-19	0.997	305.0	1.66E-19	0.996	310.0	1.76E-19	0.995	315.0	2.25E-19	0.994	320.0	2.54E-19	0.993
325.0	2.79E-19	0.992	330.0	2.99E-19	0.991	335.0	3.45E-19	0.990	340.0	3.88E-19	0.989	345.0	4.07E-19	0.988
350.0	4.10E-19	0.987	355.0	5.13E-19	0.986	360.0	4.51E-19	0.984	365.0	5.78E-19	0.983	370.0	5.42E-19	0.981
375.0	5.35E-19	0.979	380.0	5.99E-19	0.975	381.0	5.98E-19	0.974	382.0	5.97E-19	0.973	383.0	5.96E-19	0.972
384.0	5.95E-19	0.971	385.0	5.94E-19	0.969	386.0	5.95E-19	0.967	387.0	5.96E-19	0.966	388.0	5.98E-19	0.964
389.0	5.99E-19	0.962	390.0	6.00E-19	0.960	391.0	5.98E-19	0.959	392.0	5.96E-19	0.957	393.0	5.93E-19	0.953
394.0	5.91E-19	0.950	395.0	5.89E-19	0.942	396.0	6.06E-19	0.922	397.0	6.24E-19	0.870	398.0	6.41E-19	0.820
399.0	6.59E-19	0.760	400.0	6.76E-19	0.695	401.0	6.67E-19	0.635	402.0	6.58E-19	0.560	403.0	6.50E-19	0.485
404.0	6.41E-19	0.425	405.0	6.32E-19	0.350	406.0	6.21E-19	0.290	407.0	6.10E-19	0.225	408.0	5.99E-19	0.185
409.0	5.88E-19	0.153	410.0	5.77E-19	0.130	411.0	5.88E-19	0.110	412.0	5.98E-19	0.094	413.0	6.09E-19	0.083
414.0	6.19E-19	0.070	415.0	6.30E-19	0.059	416.0	6.29E-19	0.048	417.0	6.27E-19	0.039	418.0	6.26E-19	0.030
419.0	6.24E-19	0.023	420.0	6.23E-19	0.018	421.0	6.18E-19	0.012	422.0	6.14E-19	0.008	423.0	6.09E-19	0.004
424.0	6.05E-19	0.000	425.0	6.00E-19	0.000									
Photolysis File = NO3NO														
585.0	2.77E-18	0.000	590.0	5.14E-18	0.250	595.0	4.08E-18	0.400	600.0	2.83E-18	0.250	605.0	3.45E-18	0.200
610.0	1.48E-18	0.200	615.0	1.96E-18	0.100	620.0	3.58E-18	0.100	625.0	9.25E-18	0.050	630.0	5.66E-18	0.050
635.0	1.45E-18	0.030	640.0	1.11E-18	0.000									
Photolysis File = NO3NO2														
400.0	0.00E+00	1.000	405.0	3.00E-20	1.000	410.0	4.00E-20	1.000	415.0	5.00E-20	1.000	420.0	8.00E-20	1.000
425.0	1.00E-19	1.000	430.0	1.30E-19	1.000	435.0	1.80E-19	1.000	440.0	1.90E-19	1.000	445.0	2.20E-19	1.000
450.0	2.80E-19	1.000	455.0	3.30E-19	1.000	460.0	3.70E-19	1.000	465.0	4.30E-19	1.000	470.0	5.10E-19	1.000
475.0	6.00E-19	1.000	480.0	6.40E-19	1.000	485.0	6.90E-19	1.000	490.0	8.80E-19	1.000	495.0	9.50E-19	1.000
500.0	1.01E-18	1.000	505.0	1.10E-18	1.000	510.0	1.32E-18	1.000	515.0	1.40E-18	1.000	520.0	1.45E-18	1.000
525.0	1.48E-18	1.000	530.0	1.94E-18	1.000	535.0	2.04E-18	1.000	540.0	1.81E-18	1.000	545.0	1.81E-18	1.000
550.0	2.36E-18	1.000	555.0	2.68E-18	1.000	560.0	3.07E-18	1.000	565.0	2.53E-18	1.000	570.0	2.54E-18	1.000
575.0	2.74E-18	1.000	580.0	3.05E-18	1.000	585.0	2.77E-18	1.000	590.0	5.14E-18	0.750	595.0	4.08E-18	0.600
600.0	2.83E-18	0.550	605.0	3.45E-18	0.400	610.0	1.45E-18	0.300	615.0	1.96E-18	0.250	620.0	3.58E-18	0.200
625.0	9.25E-18	0.150	630.0	5.66E-18	0.050	635.0	1.45E-18	0.000						

Table 3. (continued)

WL (nm)	Abs (cm^2)	QY	WL (nm)	Abs (cm^2)	QY	WL (nm)	Abs (cm^2)	QY	WL (nm)	Abs (cm^2)	QY	WL (nm)	Abs (cm^2)	QY
Photolysis File = O3O3P														
280.0	3.97E-18	0.100	281.0	3.60E-18	0.100	282.0	3.24E-18	0.100	283.0	3.01E-18	0.100	284.0	2.73E-18	0.100
285.0	2.44E-18	0.100	286.0	2.21E-18	0.100	287.0	2.01E-18	0.100	288.0	1.76E-18	0.100	289.0	1.58E-18	0.100
290.0	1.41E-18	0.100	291.0	1.26E-18	0.100	292.0	1.10E-18	0.100	293.0	9.89E-19	0.100	294.0	8.59E-19	0.100
295.0	7.70E-19	0.100	296.0	6.67E-19	0.100	297.0	5.84E-19	0.100	298.0	5.07E-19	0.100	299.0	4.52E-19	0.100
300.0	3.92E-19	0.100	301.0	3.42E-19	0.100	302.0	3.06E-19	0.100	303.0	2.60E-19	0.100	304.0	2.37E-19	0.100
305.0	2.01E-19	0.112	306.0	1.79E-19	0.149	307.0	1.56E-19	0.197	308.0	1.38E-19	0.259	309.0	1.25E-19	0.339
310.0	1.02E-19	0.437	311.0	9.17E-20	0.546	312.0	7.88E-20	0.652	313.0	6.77E-20	0.743	314.0	6.35E-20	0.816
315.0	5.10E-20	0.872	316.0	4.61E-20	0.916	317.0	4.17E-20	0.949	318.0	3.72E-20	0.976	319.0	2.69E-20	0.997
320.0	3.23E-20	1.000	330.0	6.70E-21	1.000	340.0	1.70E-21	1.000	350.0	4.00E-22	1.000	355.0	0.00E+00	1.000
400.0	0.00E+00	1.000	450.0	1.60E-22	1.000	500.0	1.34E-21	1.000	550.0	3.32E-21	1.000	600.0	5.06E-21	1.000
650.0	2.45E-21	1.000	700.0	8.70E-22	1.000	750.0	3.20E-22	1.000	800.0	1.60E-22	1.000	900.0	0.00E+00	1.000
Photolysis File = O3O1D														
280.0	3.97E-18	0.900	281.0	3.60E-18	0.900	282.0	3.24E-18	0.900	283.0	3.01E-18	0.900	284.0	2.73E-18	0.900
285.0	2.44E-18	0.900	286.0	2.21E-18	0.900	287.0	2.01E-18	0.900	288.0	1.76E-18	0.900	289.0	1.58E-18	0.900
290.0	1.41E-18	0.900	291.0	1.26E-18	0.900	292.0	1.10E-18	0.900	293.0	9.89E-19	0.900	294.0	8.59E-19	0.900
295.0	7.70E-19	0.900	296.0	6.67E-19	0.900	297.0	5.84E-19	0.900	298.0	5.07E-19	0.900	299.0	4.52E-19	0.900
300.0	3.92E-19	0.900	301.0	3.42E-19	0.900	302.0	3.06E-19	0.900	303.0	2.60E-19	0.900	304.0	2.37E-19	0.900
305.0	2.01E-19	0.888	306.0	1.79E-19	0.851	307.0	1.56E-19	0.803	308.0	1.38E-19	0.741	309.0	1.25E-19	0.661
310.0	1.02E-19	0.563	311.0	9.17E-20	0.454	312.0	7.88E-20	0.348	313.0	6.77E-20	0.257	314.0	6.35E-20	0.184
315.0	5.10E-20	0.128	316.0	4.61E-20	0.084	317.0	4.17E-20	0.051	318.0	3.72E-20	0.024	319.0	2.69E-20	0.003
320.0	3.23E-20	0.000												
Photolysis File = HONO														
311.0	0.00E+00	1.000	312.0	2.00E-21	1.000	313.0	4.20E-21	1.000	314.0	4.60E-21	1.000	315.0	4.20E-21	1.000
316.0	3.00E-21	1.000	317.0	4.60E-21	1.000	318.0	3.60E-20	1.000	319.0	6.10E-20	1.000	320.0	2.10E-20	1.000
321.0	4.27E-20	1.000	322.0	4.01E-20	1.000	323.0	3.93E-20	1.000	324.0	4.01E-20	1.000	325.0	4.04E-20	1.000
326.0	3.13E-20	1.000	327.0	4.12E-20	1.000	328.0	7.55E-20	1.000	329.0	6.64E-20	1.000	330.0	7.29E-20	1.000
331.0	8.70E-20	1.000	332.0	1.38E-19	1.000	333.0	5.91E-20	1.000	334.0	5.91E-20	1.000	335.0	6.45E-20	1.000
336.0	5.91E-20	1.000	337.0	4.58E-20	1.000	338.0	1.91E-19	1.000	339.0	1.63E-19	1.000	340.0	1.05E-19	1.000
341.0	8.70E-20	1.000	342.0	3.35E-19	1.000	343.0	2.01E-19	1.000	344.0	1.02E-19	1.000	345.0	8.54E-20	1.000
346.0	8.32E-20	1.000	347.0	8.20E-20	1.000	348.0	7.49E-20	1.000	349.0	7.13E-20	1.000	350.0	6.83E-20	1.000
351.0	1.74E-19	1.000	352.0	1.14E-19	1.000	353.0	3.71E-19	1.000	354.0	4.96E-19	1.000	355.0	2.46E-19	1.000
356.0	1.19E-19	1.000	357.0	9.35E-20	1.000	358.0	7.78E-20	1.000	359.0	7.29E-20	1.000	360.0	6.83E-20	1.000
361.0	6.90E-20	1.000	362.0	7.32E-20	1.000	363.0	9.00E-20	1.000	364.0	1.21E-19	1.000	365.0	1.33E-19	1.000
366.0	2.13E-19	1.000	367.0	3.52E-19	1.000	368.0	4.50E-19	1.000	369.0	2.93E-19	1.000	370.0	1.19E-19	1.000
371.0	9.46E-20	1.000	372.0	8.85E-20	1.000	373.0	7.44E-20	1.000	374.0	4.77E-20	1.000	375.0	2.70E-20	1.000
376.0	1.90E-20	1.000	377.0	1.50E-20	1.000	378.0	1.90E-20	1.000	379.0	5.80E-20	1.000	380.0	7.78E-20	1.000
381.0	1.14E-19	1.000	382.0	1.40E-19	1.000	383.0	1.72E-19	1.000	384.0	1.99E-19	1.000	385.0	1.90E-19	1.000
386.0	1.19E-19	1.000	387.0	5.65E-20	1.000	388.0	3.20E-20	1.000	389.0	1.90E-20	1.000	390.0	1.20E-20	1.000
391.0	5.00E-21	1.000	392.0	0.00E+00	1.000									
Photolysis File = H2O2														
250.0	8.30E-20	1.000	255.0	6.70E-20	1.000	260.0	5.20E-20	1.000	265.0	4.20E-20	1.000	270.0	3.20E-20	1.000
275.0	2.50E-20	1.000	280.0	2.00E-20	1.000	285.0	1.50E-20	1.000	290.0	1.13E-20	1.000	295.0	8.70E-21	1.000
300.0	6.60E-21	1.000	305.0	4.90E-21	1.000	310.0	3.70E-21	1.000	315.0	2.80E-21	1.000	320.0	2.00E-21	1.000
325.0	1.50E-21	1.000	330.0	1.20E-21	1.000	335.0	9.00E-22	1.000	340.0	7.00E-22	1.000	345.0	5.00E-22	1.000
350.0	3.00E-22	1.000	355.0	0.00E+00	1.000									
Photolysis File = CO2H														
210.0	3.75E-19	1.000	220.0	2.20E-19	1.000	230.0	1.38E-19	1.000	240.0	8.80E-20	1.000	250.0	5.80E-20	1.000
260.0	3.80E-20	1.000	270.0	2.50E-20	1.000	280.0	1.50E-20	1.000	290.0	9.00E-21	1.000	300.0	5.80E-21	1.000
310.0	3.40E-21	1.000	320.0	1.90E-21	1.000	330.0	1.10E-21	1.000	340.0	6.00E-22	1.000	350.0	4.00E-22	1.000
360.0	0.00E+00	1.000												
Photolysis File = HCHONEWR														
280.0	2.49E-20	0.590	280.5	1.42E-20	0.596	281.0	1.51E-20	0.602	281.5	1.32E-20	0.608	282.0	9.73E-21	0.614
282.5	6.76E-21	0.620	283.0	5.82E-21	0.626	283.5	9.10E-21	0.632	284.0	3.71E-20	0.638	284.5	4.81E-20	0.644
285.0	3.95E-20	0.650	285.5	2.87E-20	0.656	286.0	2.24E-20	0.662	286.5	1.74E-20	0.668	287.0	1.13E-20	0.674
287.5	1.10E-20	0.680	288.0	2.62E-20	0.686	288.5	4.00E-20	0.692	289.0	3.55E-20	0.698	289.5	2.12E-20	0.704
290.0	1.07E-20	0.710	290.5	1.35E-20	0.713	291.0	1.99E-20	0.717	291.5	1.56E-20	0.721	292.0	8.65E-21	0.724
292.5	5.90E-21	0.727	293.0	1.11E-20	0.731	293.5	6.26E-20	0.735	294.0	7.40E-20	0.738	294.5	5.36E-20	0.741
295.0	4.17E-20	0.745	295.5	3.51E-20	0.749	296.0	2.70E-20	0.752	296.5	1.75E-20	0.755	297.0	1.16E-20	0.759
297.5	1.51E-20	0.763	298.0	3.69E-20	0.766	298.5	4.40E-20	0.769	299.0	3.44E-20	0.773	299.5	2.02E-20	0.776
300.0	1.06E-20	0.780	300.4	7.01E-21	0.780	300.6	8.63E-21	0.779	300.8	1.47E-20	0.779	301.0	2.01E-20	0.779
301.2	2.17E-20	0.779	301.4	1.96E-20	0.779	301.6	1.54E-20	0.778	301.8	1.26E-20	0.778	302.0	1.03E-20	0.778
302.2	8.53E-21	0.778	302.4	7.13E-21	0.778	302.6	6.61E-21	0.777	302.8	1.44E-20	0.777	303.0	3.18E-20	0.777
303.2	3.81E-20	0.777	303.4	5.57E-20	0.777	303.6	6.91E-20	0.776	303.8	6.58E-20	0.776	304.0	6.96E-20	0.776
304.2	5.79E-20	0.776	304.4	5.24E-20	0.776	304.6	4.30E-20	0.775	304.8	3.28E-20	0.775	305.0	3.60E-20	0.775
305.2	5.12E-20	0.775	305.4	4.77E-20	0.775	305.6	4.43E-20	0.774	305.8	4.60E-20	0.774	306.0	4.01E-20	0.774
306.2	3.28E-20	0.774	306.4	2.66E-20	0.774	306.6	2.42E-20	0.773	306.8	1.95E-20	0.773	307.0	1.58E-20	0.773
307.2	1.37E-20	0.773	307.4	1.19E-20	0.773	307.6	1.01E-20	0.772	307.8	9.01E-21	0.772	308.0	8.84E-21	0.772
308.2	2.08E-20	0.772	308.4	2.39E-20	0.772	308.6	3.08E-20	0.771	308.8	3.39E-20	0.771	309.0	3.18E-20	0.771
309.2	3.06E-20	0.771	309.4	2.84E-20	0.771	309.6	2.46E-20	0.770	309.8	1.95E-20	0.770	310.0	1.57E-20	0.770
310.2	1.26E-20	0.767	310.4	9.26E-21	0.764	310.6	7.71E-21	0.761	310.8	6.05E-21	0.758	311.0	5.13E-21	0.755
311.2	4.82E-21	0.752	311.4	4.54E-21	0.749	311.6	6.81E-21	0.746	311.8	1.04E-20	0.743	312.0	1.43E-20	0.740
312.2	1.47E-20	0.737	312.4	1.35E-20	0.734	312.6	1.13E-20	0.731	312.8	9.86E-21	0.728	313.0	7.82E-21	0.725
313.2	6.48E-21	0.722	313.4	1.07E-20	0.719	313.6	2.39E-20	0.716	313.8	3.80E-20	0.713	314.0	5.76E-20	0.710
314.2	6.14E-20	0.707	314.4	7.45E-20	0.704	314.6	5.78E-20	0.701	314.8	5.59E-20	0.698	315.0	4.91E-20	0.695
315.2	4.37E-20	0.692	315.4	3.92E-20	0.689	315.6	2.89E-20	0.686	315.8	2.82E-20	0.683	316.0	2.10E-20	0.680
316.2	1.66E-20	0.677	316.4	2.05E-20	0.674	316.6	4.38E-20	0.671	316.8	5.86E-20	0.668	317.0	6.28E-20	0.665
317.2	5.07E-20	0.662	317.4	4.33E-20	0.659	317.6	4.17E-20	0.656	317.8	3.11E-20	0.653	318.0	2.64E-20	0.650
318.2	2.24E-20	0.647	318.4	1.70E-20	0.644	318.6	1.24E-20	0.641	318.8	1.11E-20	0.638	319.0	7.70E-21	0.635
319.2	6.36E-21	0.632	319.4	5.36E-21	0.629	319.6	4.79E-21	0.626	319.8	6.48E-21	0.623	320.0	1.48E-20	0.620
320.2	1.47E-20	0.614	320.4	1.36E-20	0.608	320.6	1.69E-20	0.601	320.8	1.32E-20	0.595	321.0	1.49E-20	0.589
321.2	1.17E-20	0.583	321.4	1.15E-20	0.577	321.6	9.64E-21	0.570	321.8	7.26E-21	0.564	322.0	5.94E-21	0.558

Table 3. (continued)

WL (nm)	Abs (cm^2)	QY	WL (nm)	Abs (cm^2)	QY	WL (nm)	Abs (cm^2)	QY	WL (nm)	Abs (cm^2)	QY	WL (nm)	Abs (cm^2)	QY
322.2	4.13E-21	0.552	322.4	3.36E-21	0.546	322.6	2.39E-21	0.539	322.8	2.01E-21	0.533	323.0	1.76E-21	0.527
323.2	2.82E-21	0.521	323.4	4.65E-21	0.515	323.6	7.00E-21	0.508	323.8	7.80E-21	0.502	324.0	7.87E-21	0.496
324.2	6.59E-21	0.490	324.4	5.60E-21	0.484	324.6	4.66E-21	0.477	324.8	4.21E-21	0.471	325.0	7.77E-21	0.465
325.2	2.15E-20	0.459	325.4	3.75E-20	0.453	325.6	4.10E-20	0.446	325.8	6.47E-20	0.440	326.0	7.59E-20	0.434
326.2	6.51E-20	0.428	326.4	5.53E-20	0.422	326.6	5.76E-20	0.415	326.8	4.43E-20	0.409	327.0	3.44E-20	0.403
327.2	3.22E-20	0.397	327.4	2.13E-20	0.391	327.6	1.91E-20	0.384	327.8	1.42E-20	0.378	328.0	9.15E-21	0.372
328.2	6.79E-21	0.366	328.4	4.99E-21	0.360	328.6	4.77E-21	0.353	328.8	1.75E-20	0.347	329.0	3.27E-20	0.341
329.2	3.99E-20	0.335	329.4	5.13E-20	0.329	329.6	4.00E-20	0.322	329.8	3.61E-20	0.316	330.0	3.38E-20	0.310
330.2	3.08E-20	0.304	330.4	2.16E-20	0.298	330.6	2.09E-20	0.291	330.8	1.41E-20	0.285	331.0	9.95E-21	0.279
331.2	7.76E-21	0.273	331.4	6.16E-21	0.267	331.6	4.06E-21	0.260	331.8	3.03E-21	0.254	332.0	2.41E-21	0.248
332.2	1.74E-21	0.242	332.4	1.33E-21	0.236	332.6	2.70E-21	0.229	332.8	1.65E-21	0.223	333.0	1.17E-21	0.217
333.2	9.84E-22	0.211	333.4	8.52E-22	0.205	333.6	6.32E-22	0.198	333.8	5.21E-22	0.192	334.0	1.46E-21	0.186
334.2	1.80E-21	0.180	334.4	1.43E-21	0.174	334.6	1.03E-21	0.167	334.8	7.19E-22	0.161	335.0	4.84E-22	0.155
335.2	2.73E-22	0.149	335.4	1.34E-22	0.143	335.6	-1.62E-22	0.136	335.8	1.25E-22	0.130	336.0	4.47E-22	0.124
336.2	1.23E-21	0.118	336.4	2.02E-21	0.112	336.6	3.00E-21	0.105	336.8	2.40E-21	0.099	337.0	3.07E-21	0.093
337.2	2.29E-21	0.087	337.4	2.46E-21	0.081	337.6	2.92E-21	0.074	337.8	8.10E-21	0.068	338.0	1.82E-20	0.062
338.2	3.10E-20	0.056	338.4	3.24E-20	0.050	338.6	4.79E-20	0.043	338.8	5.25E-20	0.037	339.0	5.85E-20	0.031
339.2	4.33E-20	0.025	339.4	4.20E-20	0.019	339.6	3.99E-20	0.012	339.8	3.11E-20	0.006	340.0	2.72E-20	0.000
Photolysis File = HCHONEWM														
280.0	2.49E-20	0.350	280.5	1.42E-20	0.346	281.0	1.51E-20	0.341	281.5	1.32E-20	0.336	282.0	9.73E-21	0.332
282.5	6.76E-21	0.327	283.0	5.82E-21	0.323	283.5	9.10E-21	0.319	284.0	3.71E-20	0.314	284.5	4.81E-20	0.309
285.0	3.95E-20	0.305	285.5	2.87E-20	0.301	286.0	2.24E-20	0.296	286.5	1.74E-20	0.291	287.0	1.13E-20	0.287
287.5	1.10E-20	0.282	288.0	2.62E-20	0.278	288.5	4.00E-20	0.273	289.0	3.55E-20	0.269	289.5	2.12E-20	0.264
290.0	1.07E-20	0.260	290.5	1.35E-20	0.258	291.0	1.99E-20	0.256	291.5	1.56E-20	0.254	292.0	8.65E-21	0.252
292.5	5.90E-21	0.250	293.0	1.11E-20	0.248	293.5	6.26E-20	0.246	294.0	7.40E-20	0.244	294.5	5.36E-20	0.242
295.0	4.17E-20	0.240	295.5	3.51E-20	0.238	296.0	2.70E-20	0.236	296.5	1.75E-20	0.234	297.0	1.16E-20	0.232
297.5	1.51E-20	0.230	298.0	3.69E-20	0.228	298.5	4.40E-20	0.226	299.0	3.44E-20	0.224	299.5	2.02E-20	0.222
300.0	1.06E-20	0.220	300.4	7.01E-21	0.220	300.6	8.63E-21	0.221	300.8	1.47E-20	0.221	301.0	2.01E-20	0.221
301.2	2.17E-20	0.221	301.4	1.96E-20	0.221	301.6	1.54E-20	0.222	301.8	1.26E-20	0.222	302.0	1.03E-20	0.222
302.2	8.53E-21	0.222	302.4	7.13E-21	0.222	302.6	6.61E-21	0.223	302.8	1.44E-20	0.223	303.0	3.18E-20	0.223
303.2	3.81E-20	0.223	303.4	5.57E-20	0.223	303.6	6.91E-20	0.224	303.8	6.58E-20	0.224	304.0	6.96E-20	0.224
304.2	5.79E-20	0.224	304.4	5.24E-20	0.224	304.6	4.30E-20	0.225	304.8	3.28E-20	0.225	305.0	3.60E-20	0.225
305.2	5.12E-20	0.225	305.4	4.77E-20	0.225	305.6	4.43E-20	0.226	305.8	4.60E-20	0.226	306.0	4.01E-20	0.226
306.2	3.28E-20	0.226	306.4	2.66E-20	0.226	306.6	2.42E-20	0.227	306.8	1.95E-20	0.227	307.0	1.58E-20	0.227
307.2	1.37E-20	0.227	307.4	1.19E-20	0.227	307.6	1.01E-20	0.228	307.8	9.01E-21	0.228	308.0	8.84E-21	0.228
308.2	2.08E-20	0.228	308.4	2.39E-20	0.228	308.6	3.08E-20	0.229	308.8	3.39E-20	0.229	309.0	3.18E-20	0.229
309.2	3.06E-20	0.229	309.4	2.84E-20	0.229	309.6	2.46E-20	0.230	309.8	1.95E-20	0.230	310.0	1.57E-20	0.230
310.2	1.26E-20	0.233	310.4	9.26E-21	0.236	310.6	7.71E-21	0.239	310.8	6.05E-21	0.242	311.0	5.13E-21	0.245
311.2	4.82E-21	0.248	311.4	4.54E-21	0.251	311.6	6.81E-21	0.254	311.8	1.04E-20	0.257	312.0	1.43E-20	0.260
312.2	1.47E-20	0.263	312.4	1.35E-20	0.266	312.6	1.13E-20	0.269	312.8	9.86E-21	0.272	313.0	7.82E-21	0.275
313.2	6.48E-21	0.278	313.4	1.07E-20	0.281	313.6	2.39E-20	0.284	313.8	3.80E-20	0.287	314.0	5.76E-20	0.290
314.2	6.14E-20	0.293	314.4	7.45E-20	0.296	314.6	5.78E-20	0.299	314.8	5.59E-20	0.302	315.0	4.91E-20	0.305
315.2	4.37E-20	0.308	315.4	3.92E-20	0.311	315.6	2.89E-20	0.314	315.8	2.82E-20	0.317	316.0	2.10E-20	0.320
316.2	1.66E-20	0.323	316.4	2.05E-20	0.326	316.6	4.38E-20	0.329	316.8	5.86E-20	0.332	317.0	6.28E-20	0.335
317.2	5.07E-20	0.338	317.4	4.33E-20	0.341	317.6	4.17E-20	0.344	317.8	3.11E-20	0.347	318.0	2.64E-20	0.350
318.2	2.24E-20	0.353	318.4	1.70E-20	0.356	318.6	1.24E-20	0.359	318.8	1.11E-20	0.362	319.0	7.70E-21	0.365
319.2	6.36E-21	0.368	319.4	5.36E-21	0.371	319.6	4.79E-21	0.374	319.8	6.48E-21	0.377	320.0	1.48E-20	0.380
320.2	1.47E-20	0.386	320.4	1.36E-20	0.392	320.6	1.69E-20	0.399	320.8	1.32E-20	0.405	321.0	1.49E-20	0.411
321.2	1.17E-20	0.417	321.4	1.15E-20	0.423	321.6	9.64E-21	0.430	321.8	7.26E-21	0.436	322.0	5.94E-21	0.442
322.2	4.13E-21	0.448	322.4	3.36E-21	0.454	322.6	2.39E-21	0.461	322.8	2.01E-21	0.467	323.0	1.76E-21	0.473
323.2	2.82E-21	0.479	323.4	4.65E-21	0.485	323.6	7.00E-21	0.492	323.8	7.80E-21	0.498	324.0	7.87E-21	0.504
324.2	6.59E-21	0.510	324.4	5.60E-21	0.516	324.6	4.66E-21	0.523	324.8	4.21E-21	0.529	325.0	7.77E-21	0.535
325.2	2.15E-20	0.541	325.4	3.75E-20	0.547	325.6	4.10E-20	0.554	325.8	6.47E-20	0.560	326.0	7.59E-20	0.566
326.2	6.51E-20	0.572	326.4	5.53E-20	0.578	326.6	5.76E-20	0.585	326.8	4.43E-20	0.591	327.0	3.44E-20	0.597
327.2	3.22E-20	0.603	327.4	2.13E-20	0.609	327.6	1.91E-20	0.616	327.8	1.42E-20	0.622	328.0	9.15E-21	0.628
328.2	6.79E-21	0.634	328.4	4.99E-21	0.640	328.6	4.77E-21	0.647	328.8	1.75E-20	0.653	329.0	3.27E-20	0.659
329.2	3.99E-20	0.665	329.4	5.13E-20	0.671	329.6	4.00E-20	0.678	329.8	3.61E-20	0.684	330.0	3.38E-20	0.690
330.2	3.08E-20	0.694	330.4	2.16E-20	0.699	330.6	2.09E-20	0.703	330.8	1.41E-20	0.708	331.0	9.95E-21	0.712
331.2	7.76E-21	0.717	331.4	6.16E-21	0.721	331.6	4.06E-21	0.726	331.8	3.03E-21	0.730	332.0	2.41E-21	0.735
332.2	1.74E-21	0.739	332.4	1.33E-21	0.744	332.6	2.70E-21	0.748	332.8	1.65E-21	0.753	333.0	1.17E-21	0.757
333.2	9.84E-22	0.762	333.4	8.52E-22	0.766	333.6	6.32E-22	0.771	333.8	5.21E-22	0.775	334.0	1.46E-21	0.780
334.2	1.80E-21	0.784	334.4	1.43E-21	0.789	334.6	1.03E-21	0.793	334.8	7.19E-22	0.798	335.0	4.84E-22	0.802
335.2	2.73E-22	0.798	335.4	1.34E-22	0.794	335.6	0.00E+00	0.790	335.8	1.25E-22	0.786	336.0	4.47E-22	0.782
336.2	1.23E-21	0.778	336.4	2.02E-21	0.773	336.6	3.00E-21	0.769	336.8	2.40E-21	0.764	337.0	3.07E-21	0.759
337.2	2.29E-21	0.754	337.4	2.46E-21	0.749	337.6	2.92E-21	0.745	337.8	8.10E-21	0.740	338.0	1.82E-20	0.734
338.2	3.10E-20	0.729	338.4	3.24E-20	0.724	338.6	4.79E-20	0.719	338.8	5.25E-20	0.714	339.0	5.85E-20	0.709
339.2	4.33E-20	0.703	339.4	4.20E-20	0.698	339.6	3.99E-20	0.693	339.8	3.11E-20	0.687	340.0	2.72E-20	0.682
340.2	1.99E-20	0.676	340.4	1.76E-20	0.671	340.6	1.39E-20	0.666	340.8	1.01E-20	0.660	341.0	6.57E-21	0.655
341.2	4.83E-21	0.649	341.4	3.47E-21	0.643	341.6	2.23E-21	0.638	341.8	1.55E-21	0.632	342.0	3.70E-21	0.627
342.2	4.64E-21	0.621	342.4	1.08E-20	0.616	342.6	1.14E-20	0.610	342.8	1.79E-20	0.604	343.0	2.33E-20	0.599
343.2	1.72E-20	0.593	343.4	1.55E-20	0.588	343.6	1.46E-20	0.582	343.8	1.38E-20	0.576	344.0	1.00E-20	0.571
344.2	8.26E-21	0.565	344.4	6.32E-21	0.559	344.6	4.28E-21	0.554	344.8	3.22E-21	0.548	345.0	2.54E-21	0.542
345.2	1.60E-21	0.537	345.4	1.15E-21	0.531	345.6	8.90E-22	0.525	345.8	6.50E-22	0.520	346.0	5.09E-22	0.514
346.2	5.15E-22	0.508	346.4	3.45E-22	0.503	346.6	3.18E-22	0.497	346.8	3.56E-22	0.491	347.0	3.24E-22	0.485
347.2	3.34E-22	0.480	347.4	2.88E-22	0.474	347.6	2.84E-22	0.468	347.8	9.37E-22	0.463	348.0	9.70E-22	0.457
348.2	7.60E-22	0.451	348.4	6.24E-22	0.446	348.6	4.99E-22	0.440	348.8	4.08E-22	0.434	349.0	3.39E-22	0.428
349.2	1.64E-22	0.423	349.4	1.49E-22	0.417	349.6	8.30E-23	0.411	349.8	2.52E-23	0.406	350.0	2.57E-23	0.400
350.2	0.00E+00	0.394	350.4	5.16E-23	0.389	350.6	0.00E+00	0.383	350.8	2.16E-23	0.377	351.0	7.07E-23	0.371
351.2	3.45E-23	0.366	351.4	1.97E-22	0.360	351.6	4.80E-22	0.354	351.8	3.13E-21	0.349	352.0	6.41E-21	0.343
352.2	8.38E-21	0.337	352.4	1.55E-20	0.331	352.6	1.86E-20	0.326	352.8	1.94E-20	0.320	353.0	2.78E-20	0.314
353.2	1.96E-20	0.309	353.4	1.67E-20	0.303	353.6	1.75E-20	0.297	353.8	1.63E-20	0.291	354.0	1.36E-20	0.286
354.2	1.07E-20	0.280	354.4	9.82E-21	0.274	354.6	8.66E-21	0.269	354.8	6.44E-21	0.263	355.0	4.84E-21	0.257
355.2	3.49E-21	0.251	355.4	2.41E-21	0.246	355.6	1.74E-21	0.240	355.8	1.11E-21	0.234	356.0	7.37E-22	0.229
356.2	4.17E-22	0.223	356.4	1.95E-22	0.217	356.6	1.50E-22	0.211	356.8	8.14E-23	0.206	357.0	0.00E+00	0.200

Table 3. (continued)

WL (nm)	Abs (cm^2)	QY	WL (nm)	Abs (cm^2)	QY	WL (nm)	Abs (cm^2)	QY	WL (nm)	Abs (cm^2)	QY	WL (nm)	Abs (cm^2)	QY
Photolysis File = CCHOR														
260.0	2.00E-20	0.310	270.0	3.40E-20	0.390	280.0	4.50E-20	0.580	290.0	4.90E-20	0.530	295.0	4.50E-20	0.480
300.0	4.30E-20	0.430	305.0	3.40E-20	0.370	315.0	2.10E-20	0.170	320.0	1.80E-20	0.100	325.0	1.10E-20	0.040
330.0	6.90E-21	0.000												
Photolysis File = RCHO														
280.0	5.26E-20	0.960	290.0	5.77E-20	0.910	300.0	5.05E-20	0.860	310.0	3.68E-20	0.600	320.0	1.66E-20	0.360
330.0	6.49E-21	0.200	340.0	1.44E-21	0.080	345.0	0.00E+00	0.020						
Photolysis File = ACET-93C														
250.0	2.37E-20	0.760	260.0	3.66E-20	0.800	270.0	4.63E-20	0.640	280.0	5.05E-20	0.550	290.0	4.21E-20	0.300
300.0	2.78E-20	0.150	310.0	1.44E-20	0.050	320.0	4.80E-21	0.026	330.0	8.00E-22	0.017	340.0	1.00E-22	0.000
350.0	3.00E-23	0.000	360.0	0.00E+00	0.000									
Photolysis File = KETONE														
210.0	1.10E-21	1.000	220.0	1.20E-21	1.000	230.0	4.60E-21	1.000	240.0	1.30E-20	1.000	250.0	2.68E-20	1.000
260.0	4.21E-20	1.000	270.0	5.54E-20	1.000	280.0	5.92E-20	1.000	290.0	5.16E-20	1.000	300.0	3.44E-20	1.000
310.0	1.53E-20	1.000	320.0	4.60E-21	1.000	330.0	1.10E-21	1.000	340.0	0.00E+00	1.000			
Photolysis File = GLYOXAL1														
230.0	2.87E-21	1.000	235.0	2.87E-21	1.000	240.0	4.30E-21	1.000	245.0	5.73E-21	1.000	250.0	8.60E-21	1.000
255.0	1.15E-20	1.000	260.0	1.43E-20	1.000	265.0	1.86E-20	1.000	270.0	2.29E-20	1.000	275.0	2.58E-20	1.000
280.0	2.87E-20	1.000	285.0	3.30E-20	1.000	290.0	3.15E-20	1.000	295.0	3.30E-20	1.000	300.0	3.58E-20	1.000
305.0	2.72E-20	1.000	310.0	2.72E-20	1.000	312.5	2.87E-20	1.000	315.0	2.29E-20	1.000	320.0	1.43E-20	1.000
325.0	1.15E-20	1.000	327.5	1.43E-20	1.000	330.0	1.15E-20	1.000	335.0	2.87E-21	1.000	340.0	0.00E+00	1.000
Photolysis File = GLYOXAL2														
355.0	0.00E+00	1.000	360.0	2.29E-21	1.000	365.0	2.87E-21	1.000	370.0	8.03E-21	1.000	375.0	1.00E-20	1.000
380.0	1.72E-20	1.000	382.0	1.58E-20	1.000	384.0	1.49E-20	1.000	386.0	1.49E-20	1.000	388.0	2.87E-20	1.000
390.0	3.15E-20	1.000	391.0	3.24E-20	1.000	392.0	3.04E-20	1.000	393.0	2.23E-20	1.000	394.0	2.63E-20	1.000
395.0	3.04E-20	1.000	396.0	2.63E-20	1.000	397.0	2.43E-20	1.000	398.0	3.24E-20	1.000	399.0	3.04E-20	1.000
400.0	2.84E-20	1.000	401.0	3.24E-20	1.000	402.0	4.46E-20	1.000	403.0	5.27E-20	1.000	404.0	4.26E-20	1.000
405.0	3.04E-20	1.000	406.0	3.04E-20	1.000	407.0	2.84E-20	1.000	408.0	2.43E-20	1.000	409.0	2.84E-20	1.000
410.0	6.08E-20	1.000	411.0	5.07E-20	1.000	411.5	6.08E-20	1.000	412.0	4.86E-20	1.000	413.0	8.31E-20	1.000
413.5	6.48E-20	1.000	414.0	7.50E-20	1.000	414.5	8.11E-20	1.000	415.0	8.11E-20	1.000	415.5	6.89E-20	1.000
416.0	4.26E-20	1.000	417.0	4.86E-20	1.000	418.0	5.88E-20	1.000	419.0	6.69E-20	1.000	420.0	3.85E-20	1.000
421.0	5.67E-20	1.000	421.5	4.46E-20	1.000	422.0	5.27E-20	1.000	422.5	1.05E-19	1.000	423.0	8.51E-20	1.000
424.0	6.08E-20	1.000	425.0	7.29E-20	1.000	426.0	1.18E-19	1.000	426.5	1.30E-19	1.000	427.0	1.07E-19	1.000
428.0	1.66E-19	1.000	429.0	4.05E-20	1.000	430.0	5.07E-20	1.000	431.0	4.86E-20	1.000	432.0	4.05E-20	1.000
433.0	3.65E-20	1.000	434.0	4.05E-20	1.000	434.5	6.08E-20	1.000	435.0	5.07E-20	1.000	436.0	8.11E-20	1.000
436.5	1.13E-19	1.000	437.0	5.27E-20	1.000	438.0	1.01E-19	1.000	438.5	1.38E-19	1.000	439.0	7.70E-20	1.000
440.0	2.47E-19	1.000	441.0	8.11E-20	1.000	442.0	6.08E-20	1.000	443.0	7.50E-20	1.000	444.0	9.32E-20	1.000
445.0	1.13E-19	1.000	446.0	5.27E-20	1.000	447.0	2.43E-20	1.000	448.0	2.84E-20	1.000	449.0	3.85E-20	1.000
450.0	6.08E-20	1.000	451.0	1.09E-19	1.000	451.5	9.32E-20	1.000	452.0	1.22E-19	1.000	453.0	2.39E-19	1.000
454.0	1.70E-19	1.000	455.0	3.40E-19	1.000	455.5	4.05E-19	1.000	456.0	1.01E-19	1.000	457.0	1.62E-20	1.000
458.0	1.22E-20	1.000	458.5	1.42E-20	1.000	459.0	4.05E-21	1.000	460.0	4.05E-21	1.000	460.5	6.08E-21	1.000
461.0	2.03E-21	1.000	462.0	0.00E+00	1.000									
Photolysis File = MEGLYOX1														
220.0	2.10E-21	1.000	225.0	2.10E-21	1.000	230.0	4.21E-21	1.000	235.0	7.57E-21	1.000	240.0	9.25E-21	1.000
245.0	8.41E-21	1.000	250.0	9.25E-21	1.000	255.0	9.25E-21	1.000	260.0	9.67E-21	1.000	265.0	1.05E-20	1.000
270.0	1.26E-20	1.000	275.0	1.43E-20	1.000	280.0	1.51E-20	1.000	285.0	1.43E-20	1.000	290.0	1.47E-20	1.000
295.0	1.18E-20	1.000	300.0	1.14E-20	1.000	305.0	9.25E-21	1.000	310.0	6.31E-21	1.000	315.0	5.47E-21	1.000
320.0	3.36E-21	1.000	325.0	1.68E-21	1.000	330.0	8.41E-22	1.000	335.0	0.00E+00	1.000			
Photolysis File = MEGLYOX2														
350.0	0.00E+00	1.000	354.0	4.21E-22	1.000	358.0	1.26E-21	1.000	360.0	2.10E-21	1.000	362.0	2.10E-21	1.000
364.0	2.94E-21	1.000	366.0	3.36E-21	1.000	368.0	4.21E-21	1.000	370.0	5.47E-21	1.000	372.0	5.89E-21	1.000
374.0	7.57E-21	1.000	376.0	7.99E-21	1.000	378.0	8.83E-21	1.000	380.0	1.01E-20	1.000	382.0	1.09E-20	1.000
384.0	1.35E-20	1.000	386.0	1.51E-20	1.000	388.0	1.72E-20	1.000	390.0	2.06E-20	1.000	392.0	2.10E-20	1.000
394.0	2.31E-20	1.000	396.0	2.48E-20	1.000	398.0	2.61E-20	1.000	400.0	2.78E-20	1.000	402.0	2.99E-20	1.000
404.0	3.20E-20	1.000	406.0	3.79E-20	1.000	408.0	3.95E-20	1.000	410.0	4.33E-20	1.000	412.0	4.71E-20	1.000
414.0	4.79E-20	1.000	416.0	4.88E-20	1.000	418.0	5.05E-20	1.000	420.0	5.21E-20	1.000	422.0	5.30E-20	1.000
424.0	5.17E-20	1.000	426.0	5.30E-20	1.000	428.0	5.21E-20	1.000	430.0	5.55E-20	1.000	432.0	5.13E-20	1.000
434.0	5.68E-20	1.000	436.0	6.22E-20	1.000	438.0	6.06E-20	1.000	440.0	5.47E-20	1.000	441.0	6.14E-20	1.000
442.0	5.47E-20	1.000	443.0	5.55E-20	1.000	443.5	6.81E-20	1.000	444.0	5.97E-20	1.000	445.0	5.13E-20	1.000
446.0	4.88E-20	1.000	447.0	5.72E-20	1.000	448.0	5.47E-20	1.000	449.0	6.56E-20	1.000	450.0	5.05E-20	1.000
451.0	3.03E-20	1.000	452.0	4.29E-20	1.000	453.0	2.78E-20	1.000	454.0	2.27E-20	1.000	456.0	1.77E-20	1.000
458.0	8.41E-21	1.000	460.0	4.21E-21	1.000	464.0	1.68E-21	1.000	468.0	0.00E+00	1.000			
Photolysis File = BZCHO														
299.0	1.78E-19	1.000	304.0	7.40E-20	1.000	306.0	6.91E-20	1.000	309.0	6.41E-20	1.000	313.0	6.91E-20	1.000
314.0	6.91E-20	1.000	318.0	6.41E-20	1.000	325.0	8.39E-20	1.000	332.0	7.65E-20	1.000	338.0	8.88E-20	1.000
342.0	8.88E-20	1.000	346.0	7.89E-20	1.000	349.0	7.89E-20	1.000	354.0	9.13E-20	1.000	355.0	8.14E-20	1.000
364.0	5.67E-20	1.000	368.0	6.66E-20	1.000	369.0	8.39E-20	1.000	370.0	8.39E-20	1.000	372.0	3.45E-20	1.000
374.0	3.21E-20	1.000	376.0	2.47E-20	1.000	377.0	2.47E-20	1.000	380.0	3.58E-20	1.000	382.0	9.90E-21	1.000
386.0	0.00E+00	1.000												
Photolysis File = ACROLEIN														
250.0	1.80E-21	1.000	252.0	2.05E-21	1.000	253.0	2.20E-21	1.000	254.0	2.32E-21	1.000	255.0	2.45E-21	1.000
256.0	2.56E-21	1.000	257.0	2.65E-21	1.000	258.0	2.74E-21	1.000	259.0	2.83E-21	1.000	260.0	2.98E-21	1.000
261.0	3.24E-21	1.000	262.0	3.47E-21	1.000	263.0	3.58E-21	1.000	264.0	3.93E-21	1.000	265.0	4.67E-21	1.000
266.0	5.10E-21	1.000	267.0	5.38E-21	1.000	268.0	5.73E-21	1.000	269.0	6.13E-21	1.000	270.0	6.64E-21	1.000
271.0	7.20E-21	1.000	272.0	7.77E-21	1.000	273.0	8.37E-21	1.000	274.0	8.94E-21	1.000	275.0	9.55E-21	1.000
276.0	1.04E-20	1.000	277.0	1.12E-20	1.000	278.0	1.19E-20	1.000	279.0	1.27E-20	1.000	280.0	1.27E-20	1.000
281.0	1.26E-20	1.000	282.0	1.26E-20	1.000	283.0	1.28E-20	1.000	284.0	1.33E-20	1.000	285.0	1.38E-20	1.000
286.0	1.44E-20	1.000	287.0	1.50E-20	1.000	288.0	1.57E-20	1.000	289.0	1.63E-20	1.000	290.0	1.71E-20	1.000

Table 3. (continued)

WL (nm)	Abs (cm^2)	QY	WL (nm)	Abs (cm^2)	QY	WL (nm)	Abs (cm^2)	QY	WL (nm)	Abs (cm^2)	QY	WL (nm)	Abs (cm^2)	QY
291.0	1.78E-20	1.000	292.0	1.86E-20	1.000	293.0	1.95E-20	1.000	294.0	2.05E-20	1.000	295.0	2.15E-20	1.000
296.0	2.26E-20	1.000	297.0	2.37E-20	1.000	298.0	2.48E-20	1.000	299.0	2.60E-20	1.000	300.0	2.73E-20	1.000
301.0	2.85E-20	1.000	302.0	2.99E-20	1.000	303.0	3.13E-20	1.000	304.0	3.27E-20	1.000	305.0	3.39E-20	1.000
306.0	3.51E-20	1.000	307.0	3.63E-20	1.000	308.0	3.77E-20	1.000	309.0	3.91E-20	1.000	310.0	4.07E-20	1.000
311.0	4.25E-20	1.000	312.0	4.39E-20	1.000	313.0	4.44E-20	1.000	314.0	4.50E-20	1.000	315.0	4.59E-20	1.000
316.0	4.75E-20	1.000	317.0	4.90E-20	1.000	318.0	5.05E-20	1.000	319.0	5.19E-20	1.000	320.0	5.31E-20	1.000
321.0	5.43E-20	1.000	322.0	5.52E-20	1.000	323.0	5.60E-20	1.000	324.0	5.67E-20	1.000	325.0	5.67E-20	1.000
326.0	5.62E-20	1.000	327.0	5.63E-20	1.000	328.0	5.71E-20	1.000	329.0	5.76E-20	1.000	330.0	5.80E-20	1.000
331.0	5.95E-20	1.000	332.0	6.23E-20	1.000	333.0	6.39E-20	1.000	334.0	6.38E-20	1.000	335.0	6.24E-20	1.000
336.0	6.01E-20	1.000	337.0	5.79E-20	1.000	338.0	5.63E-20	1.000	339.0	5.56E-20	1.000	340.0	5.52E-20	1.000
341.0	5.54E-20	1.000	342.0	5.53E-20	1.000	343.0	5.47E-20	1.000	344.0	5.41E-20	1.000	345.0	5.40E-20	1.000
346.0	5.48E-20	1.000	347.0	5.90E-20	1.000	348.0	6.08E-20	1.000	349.0	6.00E-20	1.000	350.0	5.53E-20	1.000
351.0	5.03E-20	1.000	352.0	4.50E-20	1.000	353.0	4.03E-20	1.000	354.0	3.75E-20	1.000	355.0	3.55E-20	1.000
356.0	3.45E-20	1.000	357.0	3.46E-20	1.000	358.0	3.49E-20	1.000	359.0	3.41E-20	1.000	360.0	3.23E-20	1.000
361.0	2.95E-20	1.000	362.0	2.81E-20	1.000	363.0	2.91E-20	1.000	364.0	3.25E-20	1.000	365.0	3.54E-20	1.000
366.0	3.30E-20	1.000	367.0	2.78E-20	1.000	368.0	2.15E-20	1.000	369.0	1.59E-20	1.000	370.0	1.19E-20	1.000
371.0	8.99E-21	1.000	372.0	7.22E-21	1.000	373.0	5.86E-21	1.000	374.0	4.69E-21	1.000	375.0	3.72E-21	1.000
376.0	3.57E-21	1.000	377.0	3.55E-21	1.000	378.0	2.83E-21	1.000	379.0	1.69E-21	1.000	380.0	8.29E-24	1.000
381.0	0.00E+00	1.000												

0.37 and 0.75 to 1.55 and 0.51, and the AFG2 photolysis rate was reduced by a factor of 2, relative to those used by the 1993 version of the mechanism (Carter *et al.*, 1993a; Carter 1995). These updated aromatic mechanisms are still being developed, and a more detailed discussion of them are beyond the scope of this report. The reactions of the species of particular interest in this study are discussed in more detail below.

Atmospheric Reactions of t-Butyl Alcohol

The main atmospheric removal rate for TBA is expected to be reaction with hydroxyl radicals. As indicated above, the available data concerning the rate constant for this reaction are not in good agreement, with the rate constant of (1.43 ± 0.36) x 10^{-12} cm^3 $molec^{-1}$ s^{-1} measured in this work being significantly higher than the previously measured absolute rate constants of (1.07 ± 0.08) x 10^{-12} cm^3 $molec^{-1}$ s^{-1} (Wallington *et a*l., 1988) , (1.08±0.10) x 10^{-12} cm^3 $molec^{-1}$ s^{-1} (Teton *et al.*, 1996), and (8.1 ± 1.7) x 10^{-13} cm^3 $molec^{-1}$ s^{-1} (Saunders *et al*., 1994) and the relative rate measurement of Cox and Goldstone (1982) of 1.08 x 10^{-12} cm^3 $molec^{-1}$ s^{-1}, all for the 295-300°K temperature range. The lower rate constant of Saunders *et al.* (1994) is considered to be unreliable because they reported difficulties in handling TBA due to it's "stickiness". On the other hand, results of model simulations of the environmental chamber data were found to be inconsistent with the high rate constant measured in this work. For that reason, and based on the absolute rate measurements of Wallington *et al.* (1988) amd Teton *et al.* (1996), and the relative rate measurement of Cox and Goldstone (1982), we use

$$k(OH + TBA) = 1.08 \times 10^{-12}\ cm^3\ molec^{-1}\ s^{-1}$$

in our model simulations. The temperature dependence of this rate constant, which is small over temperature range in the lower atmosphere (Wallington *et al.*, 1988; Teton *et al*., 1996), is ignored.

Based on the group-adaptivity estimation methods of Atkinson (1987), The OH + TBA reaction is expected to proceed ~90% of the time by abstraction from the methyl groups, giving rise, after two NO to NO_2 conversions, to formation of formaldehyde and acetone, and regeneration of OH radicals.

$$OH + (CH_3)_3COH \rightarrow H_2O + \cdot CH_2C(OH)(CH_3)_2 \quad (4)$$
$$\cdot CH_2C(OH)(CH_3)_2 + O_2 \rightarrow \cdot OOCH_2C(OH)(CH_3)_2$$
$$\cdot OOCH_2C(OH)(CH_3)_2 + NO \rightarrow NO_2 + \cdot OCH_2C(OH)(CH_3)_2 \quad (5)$$
$$\cdot OOCH_2C(OH)(CH_3)_2 + NO \rightarrow O_2NOCH_2C(OH)(CH_3)_2 \quad (6)$$
$$\cdot OCH_2C(OH)(CH_3)_2 \rightarrow HCHO + \cdot C(OH)(CH_3)_2$$
$$\cdot C(OH)(CH_3)_2 + O_2 \rightarrow HO_2 + CH_3COCH_3$$
$$HO_2 + NO \rightarrow NO_2 + OH$$

(Peroxynitrate formation from peroxy radicals + NO_2 reactions are not shown because they is rapidly reversed by thermal decomposition of the peroxynitrates under the conditions of our experiments and atmospheric simulations.)

Alkyl nitrate formation from reaction (6) is expected to occur to some extent based on analogy to the observed formation of alkyl nitrates in the alkane photooxidation systems (Carter and Atkinson (1989b). Alkyl nitrate yields from OH substituted radicals such as these have not been measured directly. However, the same radical, $\cdot OOCH_2C(OH)(CH_3)_2$, is expected to be formed in the isobutene + OH reaction system, and from modeling isobutene - NO_x - air environmental chamber experiments, whose results are moderately sensitive to this reaction, we have derived $k_c/(k_b+k_c) = 0.1$. This is discussed further below.

The alternative initial reaction pathway, abstraction from the -OH group, is estimated to occur only ~10% of the time (Atkinson, 1987). However, it should be pointed out that this estimate is based on the rate constant for the reaction of OH with methanol, which may not be a good model for TBA. In addition, if reaction is assumed to occur primarily at the methyl groups, and the group adaptivity rate constants derived from OH + alkane rate constants are assumed (Atkinson, 1987), the OH + TBA rate constant is underestimated by over a factor of 2. This discrepancy could be accounted for if the OH abstraction from tertiary -OH groups were much faster than is the case for methanol, and occurred in TBA at a comparable rate as reaction at the methyl groups. In any case, the major expected reactions would be:

$$OH + (CH_3)_3COH \rightarrow H_2O + (CH_3)_3CO\cdot \quad (7)$$
$$(CH_3)_3CO\cdot \rightarrow (CH_3)_2CO + CH_3\cdot$$
$$(CH_3)_3CO\cdot + NO_2 \rightarrow (CH_3)_2CONO_2 \quad (8)$$
$$CH_3\cdot + O_2 \rightarrow CH_3OO\cdot$$
$$CH_3OO\cdot + NO \rightarrow CH_3O\rightarrow + NO_2$$

$$CH_3O\cdot + O_2 \rightarrow HCHO + HO_2$$
$$HO_2 + NO \rightarrow OH + NO_2$$

(Peroxynitrate and also alkyl nitrite formation reactions are not shown because they are rapidly reversed by thermal decomposition or by photolysis, respectively, under the conditions of our experiments or atmospheric simulations.) Note that except for the formation of t-butyl nitrate in reaction (8) following reaction (7), two reaction sequences have essentially the same net effect, formation of formaldehyde and acetone and two NO to NO_2 conversions. Reaction (8), which is relatively unimportant under most atmospheric conditions can be a non-negligible radical-termination process in some environmental chamber experiments where NO_x levels are relatively high. The possibility that reaction (7) occurs to a greater extent then estimated using the group-adaptivity methods of Atkinson (1987) was examined in the model simulations of the chamber experiments, but found not to be an important factor in affecting the results. For that reason, in the standard mechanism we did not modify the initial estimate that this pathway occurs ~10% of the time.

Atmospheric Reactions of N-Methyl Pyrrolidinone

The results of the laboratory studies discussed in the previous section indicated that, as expected, NMP reacts in the atmosphere to a significant extent with OH radicals, but not with ozone or by photolysis. The measured OH rate constant is 2.15 x 10^{-11} cm^3 $molec^{-1}$ s^{-1}, which is relatively high, being comparable to that for m-xylene. The laboratory data also indicated that NMP did not react to a significant extent with HNO_3, indicating that it is apparently not sufficiently basic for salt-forming reactions to be of concern. However, NMP also reacts at a significant rate with NO_3 radicals, with the rate constant being 1.26 x 10^{-13} cm^3 $molec^{-1}$ s^{-1}. Since NO_3 radicals are formed from the reaction of O_3 with NO_2, this means that NMP would be very rapidly removed by this reaction in polluted atmospheres at nighttime, when NO_3 levels are relatively high. Therefore, the NMP atmospheric photooxidation mechanism must include provision for both these reactions.

Although strictly speaking this was beyond the scope of this project, information was obtained concerning the products of NMP's reactions with OH and NO_3 radicals. The OH reaction was found to form two products, identified as N-methylsuccinimide (NMS), and 1-formyl-2-pyrrolidinone (1FP), in approximately the same yields (44% and 41%, respectively), which account for a substantial fraction of the reacting NMP. The same products are also seen in the NO_3 reaction, though in different relative yields, with N-methylsuccinimide being the major product with a ~60% yield, and the 1-formyl-2-pyrrolidinone being a minor product with an estimated ~4% yield. In both cases, the initial reactions are expected to be as follows:

$$\{OH \text{ or } NO_3\} + \begin{array}{l} CH_3 \\ H_2C\diagup N \diagdown C{=}O \\ CH_2CH_2 \end{array} \rightarrow \{H_2O + HNO_3\} + \begin{array}{l} CH_3 \\ HC\diagup N \diagdown C{=}O \\ CH_2CH_2 \end{array} \qquad (9)$$

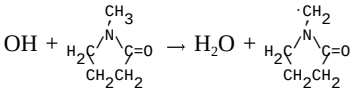

(10)

followed by

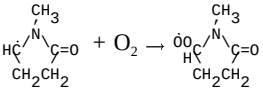

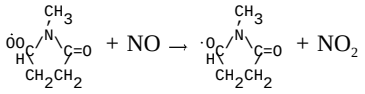

(11)

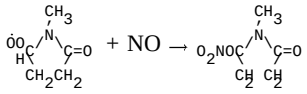

(12)

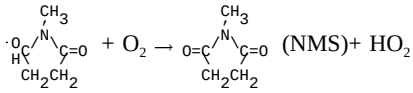

or

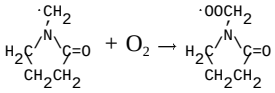

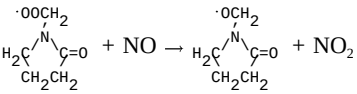

(13)

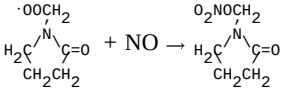

(14)

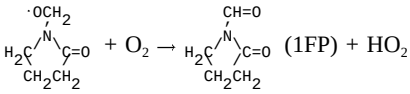

with apparently pathways (9) and (10) being about equally important in the OH reaction, but pathway (9) dominating in the NO_3 reaction.

Formation of organic nitrate products via pathways (12) and (14) is speculative, but is expected to occur at least to some extent based on the occurrence of analogous reactions in the photooxidations of n-alkanes (Atkinson, 1994, Carter and Atkinson, 1989b). The assumed alkyl nitrate formation yields, $k_{12}/(k_{11}+k_{12})$ or $k_{14}/(k_{13}+k_{14})$, in the reactions of OH with VOCs has been found to be an extremely sensitive parameter affecting model predictions of their ozone reactivity, because alkyl nitrate formation in this reaction represents both a radical and NO_x sink process. In the case of the n-alkanes, the nitrate yield increases with the size of the molecule (Atkinson, 1994; Carter and Atkinson, 1989b), and is a significant factor affecting reactivities of alkanes with five or more carbons (Carter and Atkinson, 1989a; Carter, 1994a, 1995). In C_{5+} VOCs where the nitrate yields are unknown, (which is the case for essentially all compounds except alkanes), it generally has to be derived by using it as an adjustable

parameter in model simulations of environmental chamber data (e.g., see Carter, 1995, and references therein). This is clearly the case for NMP as well.

Since the product species N-methylsuccinimide and 1-formyl-2-pyrrolidinone were found to react relatively rapidly, their subsequent reactions were also represented in the model simulations. Their mechanisms were derived based on analogy from the NMP reactions discussed above, noting that each has an analogue one of the two reacting sites in NMP. NMS was found to have a rate constant approximately half that of NMP, which is consistent with the product data indicating that approximately half the reaction for NMP is on the methyl group, which is assumed to be the most reactive site in NMS. The OH reaction at the methyl group is assumed to proceed to form N-formylsuccinimide (NFS) in a manner analogous to the formation of NMS from NMP. The NO_3 + NMS reaction is neglected, based on our laboratory results discussed above indicating that this reaction is slow.

1FP was found to have an OH rate constant approximately the same as that for NMP. This suggests that half of the reaction occurs at the -CH_2- group next to the nitrogen, since it would give it about the same rate constant as the analogous reaction for NMP, and the other half of the reaction occurs at the -CHO group, analogous to the (slightly faster) reaction of OH with other aldehydes. The product expected after reaction at the -CH_2- group is expected to be NSF, through a sequence of reactions analogous to the formation of NMS from NMP. The reaction at the -CHO group would be expected to yield an acyl peroxy (RCO-OO·) radical, and for simplicity we represent it in the model calculations with C2CO-O2, the lumped acyl peroxy radical formed from RCHO, the model species used to represent general aldehydes in the mechanism. The NO_3 reaction is expected to occur primarily at the -CH_2 group, as is apparently the case for NMP, and the same rate constant and an analogous mechanism is assumed as for NMP, except that in this case the product is NFS.

NFS is expected to react primarily at the -CHO group, and for simplicity in the model simulations it is represented by RCHO, the species used to represent general lumped higher aldehydes in the mechanism.

The specific reactions used for NMP and its products are shown on Table 2. Note that the alkyl nitrate yields, which are assumed to be the same in all the C_5 radicals in this system, is treated as an adjustable parameter in the model simulations, and the derivation of the value given on Table 2 is discussed later in this report.

Atmospheric Reactions of Propylene Carbonate

The laboratory studies discussed above indicate that propylene carbonate is consumed in the atmosphere primarily by reaction with the OH radical, with a rate constant of 6.9×10^{-13} cm^3 $molec^{-1}$ s^{-1}. Based on structure-reactivity estimates of Kwok and Atkinson (1995), reaction at the methyl group is estimated to occur with a rate constant of ~1.7×10^{-13} cm^3 $molec^{-1}$ s^{-1}, or ~25% of the time. As it turns

out, the relative rates of reaction at the other two positions does not affect our estimated overall reaction mechanism for PC. In particular, if the OH reaction occurred at the 2-position, the subsequent reactions are expected to be as follows:

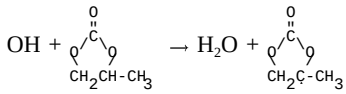

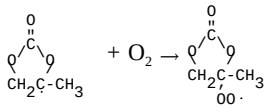

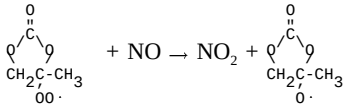

(15)

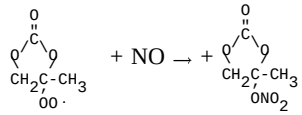

(16)

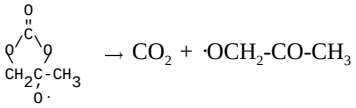

$$\cdot OCH_2\text{-}CO\text{-}CH_3 + O_2 \rightarrow HO_2 + HCO\text{-}CO\text{-}CH_3$$

resulting in the ultimate formation of either an organic nitrate or, after an NO to NO_2 conversion, methylglyoxal, CO_2, and HO_2. Reaction at the 1-position would be expected to be similar, with the only differences being that the nitrate substituent would be on the 1-position, and that the methylglyoxal would be formed from the reaction of O_2 with the $HCOCH(O\cdot)CH_3$ radical formed in the decomposition of the (II) radical. The representation in the model simulations would be the same in either case.

The above mechanism assumes that the initially formed peroxy radicals, such as (I), are consumed primarily by reaction with NO. However, the possibility that these radicals can decompose via,

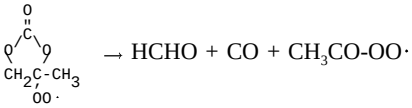

(17)

cannot be ruled out *a-priori*. This possibility was examined in the model simulations, but ruled out on the basis of being inconsistent with the observed formaldehyde yields.

The reactions subsequent to OH attack at the methyl group are expected to be similar, but somewhat more complex, and are shown below:

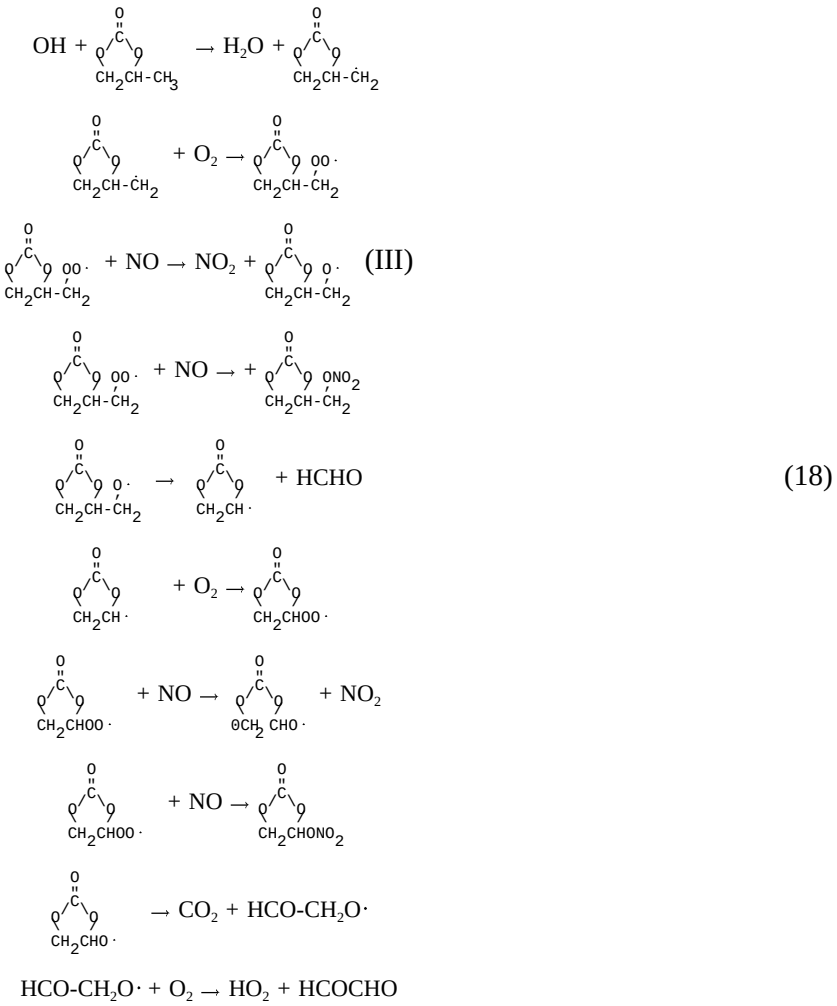

This is based on assuming that the decomposition of the (III) radical, reaction (18), is fast. This assumption is made because, as discussed later, it results in somewhat better fits to the formaldehyde yields observed in environmental chamber experiments with PC. However, if reaction (17) occurred to some extent, it might occur to the additional formaldehyde levels, rather than reaction (18).

The specific reactions used to represent the photooxidation mechanism for PC are shown on Table 2. As with the NMP mechanism, the nitrate yields in the reactions of NO with the various peroxy radicals are unknown and are adjusted based on model simulations of the environmental chamber experiments. For simplicity, the nitrate yields in the reactions of NO with all the C_3 peroxy radicals formed in the PC photooxidation system are assumed to be the same, but nitrate formation from the C_2 peroxy radical formed following reaction (a), above, is ignored.

Environmental Chamber Simulations

The ability of the chemical mechanisms to appropriately simulate the atmospheric impacts of the test compounds was evaluated by conducting model simulations of the environmental chamber experiments from this study. This requires including in the model appropriate representations of chamber-dependent effects such as wall reactions and characteristics of the light source. The methods used are based on those discussed in detail by Carter and Lurmann (1990, 1991), updated as discussed by Carter et al (1995b,d). The photolysis rates were derived from results of NO_2 actinometry experiments and direct measurements of the spectra of the light source. In the case of the blacklights used in the DTC, the spectrum was assumed to be constant and the blacklight spectrum given by Carter *et al*, (1995b,d) was employed. The thermal rate constants were calculated using the temperatures measured during the experiments, with the small variations of temperature with time during the experiment being taken into account. The computer programs and modeling methods employed are discussed in more detail elsewhere (Carter *et al.*, 1995b). The specific values of the chamber-dependent parameters used in the model simulations of the experiments for this study are given in Table 4.

Atmospheric Reactivity Simulations

To estimate its effects on ozone under conditions more representative of polluted urban atmospheres, incremental reactivities, defined as the change in O_3 caused by adding small amounts of a compound to the emissions, were calculated for TBA, NMP, PC, ethane, and several other representative compounds for various simulated atmospheric pollution scenarios. Carter (1994a) used a series of single-day EKMA box model scenarios (EPA, 1984) derived by the EPA to represent 39 different urban ozone exceedence areas around the United States (Baugues, 1990), to develop various reactivity scales to quantify impacts of VOCs on ozone formation in various environments. It was found NO_x levels is the most important factor affecting differences in relative ozone impacts among VOCs, and that the ranges of relative reactivities in the various scales can be reasonably well represented by ranges in relative reactivities in three "averaged conditions" scenarios representing three different NO_x conditions. These scenarios were derived by averaging the inputs to the 39 EPA scenarios, except for the NO_x emissions. In the "maximum reactivity" scenario, the NO_x inputs were adjusted such that the final O_3 level is most sensitive to changes in VOC emissions; in the "maximum ozone" scenario the NO_x inputs were adjusted to yield the highest maximum O_3 concentration; and in the "equal benefit" scenario the NO_x inputs were adjusted such that relative changes in VOC and NO_x emissions had equal effect on ozone formation. As discussed by Carter (1994a), there represent respectively the high, medium and range of NO_x conditions which are of relevance when assessing VOC control strategies for reducing ozone.

The chemical mechanisms used for these atmospheric simulations were the same as used to simulate the chamber experiments, except that the reactions representing chamber effects were removed,and the reactions for the full variety of VOCs emitted into the scenarios (Carter, 1994a) were represented (see Table 2). Most of the emitted VOCs (other than the test compound whose reactivity is being calculated) are not represented in the model explicitly, but are represented using lumped model

Table 4. Values of chamber-dependent parameters used in the model simulations of the experiments for this study. [a]

Parm.	Value(s)	Discussion
k(1)	0.222 → 0.220 min^{-1}	Derived by fitting results of quartz tube NO_2 actinometry measurements to curve similar to that derived for other blacklight chambers by Carter *et al.* (1995b). The results of the actinometry measurements during this study were within the uncertainty range of this extrapolation.
k(O3W)	$1.5x10^{-4}$ min^{-1}	The results of the O_3 dark decay experiments in this chamber are consistent with the recommended default of Carter *et al.* (1995b) for Teflon bag chambers in general.
k(N25I) k(N25S)	$2.8\ x10^{-3}$ min^{-1}, $1.5x10^{-6}$ - k_g ppm^{-1} min^{-1}	Based on the N_2O_5 decay rate measurements in a similar chamber (Tuazon et al. 1983). Although we previously estimated their rate constants were lower in the larger Teflon bag chambers (Carter and Lurmann, 1990, 1991), we now consider it more reasonable to use the same rate constants for all such chambers (Carter et al., 1995b).
k(NO2W) yHONO	$1.6x10^{-4}$ min^{-1} 0.2	Based on dark NO_2 decay and HONO formation measured in a similar chamber by Pitts et al. (1984). Assumed to be the same in all Teflon bag chambers (Carter et al, 1995b).
k(XSHC)	250 min^{-1}	Estimated by modeling pure air irradiations. Not an important parameter affecting model predictions except for pure air or NO_x-air runs.
RS/K1	$3.27x10^{6}$ $e^{-7297/T}$ ppm	Based on model simulations of n-butane - NO_x experiments. The temperature dependence is derived from simulating outdoor experiments as discussed by Carter et al. (1995b).
E-NO2/K1	0.03 ppb	Based on model simulations of pure air experiments.

[a] See Table 2 for definition of parameters.

species whose rate constants and product yield parameters are derived based on the mixture of compounds they represent. The rate constants and mechanistic parameters for the emitted species in the scenarios were the same as those used previously (Carter, 1994a; Carter *et al.*, 1993a), except for the aromatics, whose unknown photoreactive product yields were re-optimized in a manner analogous to that discussed above for toluene and m-xylene (unpublished results from this laboratory). The listing on Table 2 gives the lumped model species used to represent the emissions into the scenarios, and Table 1 indicates the types of species each is used to represent, and gives the rate constants and product yield parameters used.

ENVIRONMENTAL CHAMBER AND MECHANISM EVALUATION RESULTS

Summary of Experiments

Table 5 give chronological listings of all the environmental chamber experiments carried out for this program. These consisted primarily of incremental reactivity experiments, whose conditions and selected results are summarized in more detail on Table 6. In addition, several of characterization runs were carried out to determine chamber-dependent inputs needed for the model simulations of the experiments, control experiments were conducted to assure consistency with previous results, and side equivalency tests were conducted to assure that essentially equivalent results are obtained when equal mixtures are simultaneously irradiated in each of the dual reaction bags. Comments on Table 5 summarize relevant results from these characterization and control runs.

The results of the characterization and control runs generally as expected based on our previous experience with these and similar chambers in our laboratories (Carter *et al.*, 1995b and references therein). Good side equivalency was observed when equivalent surrogate - NO_x (under both high and low NO_x conditions), propene - NO_x, CO - NO_x (not shown), or n-butane - NO_x mixtures were simultaneously irradiated in the dual reactors. The results of the n-butane - NO_x experiments, which are highly sensitive to the magnitude of the chamber radical source assumed in the model (see Table 4), were well simulated by the model, indicating that the model is appropriately representing this effect for these runs. The acetaldehyde - air run suggested that the chamber model may be slightly underestimating the NO_x offgasing rates during the period of these experiments, but this effect is relatively unimportant in the simulations of the experiments of interest in this study. The actinometry results agreed with the extrapolated values based on results of previous determinations (see Table 4), to within the variability of these determinations.

T-Butyl Alcohol Experiments and Mechanism Evaluation

Summaries of the conditions and results of the incremental reactivity experiments for t-butyl alcohol are included in Table 6, and Figures 8 - 13 give time series plots for relevant measurements used for mechanism evaluation. These include concentrations of d(O_3-NO) and m-xylene in the base case and test experiments, concentrations of the test compound in the test experiment, and the d(O_3-NO) and IntOH incremental reactivities derived from the differences between the two. Results of model calculations, discussed below, are also shown on these figures.

Table 6 and Figures 8-13 show that the addition of TBA has positive effects on ozone formation and NO oxidation, as indicated by its positive d(O_3-NO) incremental reactivities. However, the magnitudes of their reactivities are relatively low, being around 0.02 molecules of NO oxidized or O_3 formed per molecule of TBA added to the experiments. This is due to a large part to it's relatively low

Table 5. Chronolological listing of the environmental chamber experiments carried out for this program.

RunID	Date	Title	Comments
DTC-227	7/13/95	Propene - NOx	Control run for comparison with other propene runs in this chamber. Run could not be modeled because of lack of temperature data, but results were consistent with results of other propene runs in this chamber.
DTC-228	7/14/95	n-Butane - NOx	Characterization run to determine chamber radical source parameter. Observed NO consumption rate consistent with predictions of chamber effects model.
DTC-235	7/25/95	Mini-Surrogate + PC	Improper PC injection method; only part of it injected. Effect of PC injection was found to be minor, essentially same NO consumption, O3 formation, and m-xylene consumption rates on PC side as control side.
DTC-236	7/26/95	n-Butane - NOx	Characterization run to determine chamber radical source parameter. Observed NO consumption rate consistent with predictions of chamber effects model.
DTC-239	8/3/95	Mini-Surrogate + PC (B)	Improper PC injection method; only part of it injected. Effect of PC injection was found to be minor, essentially same NO consumption, O3 formation, and m-xylene consumption rates on PC side as control side.
DTC-240	8/4/95	Mini-Surrogate + NMP (A)	
DTC-241	8/8/95	Mini-Surrogate + TBA (B)	Effect of TBA Addition was relatively small
DTC-244	8/11/95	Mini-Surrogate + NMP (B)	
DTC-246	8/15/95	Propene + NOx	Control run for comparison with other propene runs in this chamber. Experimental O3 formation rate was somewhat slower than model prediction, but results were within the normal range for propene runs in this chamber.
DTC-247	8/16/95	Acetaldehyde - Air	Characterization run used to measure the NOx offgasing rate in the chamber. Approximately 16 ppb of O3 was formed in both sides of the chamber after 6 hours, slightly more than the 12 ppb predicted by the chamber model, but in the normal range.
DTC-248	8/17/95	Full Surrogate + NOx	Side equivalency control run. Excellent side equivalency observed.
DTC-249	8/18/95	Full Surrogate + TBA (A)	
DTC-250	8/22/95	Full Surrogate + PC (B)	
DTC-251	8/23/95	Full Surrogate - NOx	Side equivalency control run to test for possible effects of PC contamination. Excellent side equivalency observed.
DTC-252	8/24/95	Full Surrogate + NMP (A)	
DTC-253	8/25/95	n-Butane - NOx	Characterization run to determine chamber radical source parameter. Observed NO consumption rates were in excellent agreement with predictions of chamber effects model.
DTC-254	8/28/95	NO2 Actinometry	Measured NO_2 photolysis rate was 0.227 min^{-1}, in good agreement with the curve fit to the full set of actinometry results for this chamber, which gave 0.221 min^{-1}.
DTC-255	8/29/95	Full Surrogate + NMP (B)	No formaldehyde data. Initial formaldehyde for modeling were estimated based on amount injected and averages for the other full surrogate runs.

Table 5. (continued)

RunID	Date	Title	Comments
DTC-256	8/30/95	Full Surrogate + TBA (A)	
DTC-257	8/31/95	Full Surrogate + PC (B)	
DTC-258	9/1/95	Low NOx Full Surrogate	Side equivalency control run. Excellent side equivalency observed.
DTC-259	9/6/95	Low NOx Full Surrogate + TBA (A)	
DTC-260	9/7/95	LOW NOx Full Surrogate + PC (B)	
DTC-261	9/8/95	Low NOx Full Surrogate + NMP (A)	Small amount of PC contamination observed.
DTC-264	9/14/95	Mini-Surrogate + PC (B)	Effect of PC addition was found to be small.
DTC-266	9/19/95	Low NOx Full Surrogate + PC (A)	
DTC-267	9/20/95	Low NOx Full Surrogate + NMP (B)	
DTC-268	9/21/95	Low NOx Full Surrogate + TBA	TBA accidently injected on both sides.
DTC-269	9/22/95	Low NOx Full Surrogate + TBA (A)	
DTC-270	9/26/95	Formaldehyde - NOx	Control run. Model slightly underpredicts rate of O3 formation and formaldehyde consumption, but results within the normal range.
DTC-285	10/26/95	n-Butane + NOx	Characterization run to determine chamber radical source parameter. Observed NO consumption rates were in excellent agreement with predictions of chamber effects model.
DTC-286	10/27/95	Pure Air Irriadiation	Characterizaton run to test model for wall offgasing effects. Approximately 35 ppb of O3 observed on both sides after 6 hours irriadiation, in excellent agreement with predictions of the chamber effects model.
DTC-287	10/30/95	NO2 Actinometry	Measured NO_2 photolysis rate was 0.220 min^{-1}, in good agreement with the curve fit to the full set of actinometry results for this chamber, which gave 0.219 min^{-1}.

Table 5. (continued)

rate of reaction. Despite having a positive effect on O_3 formation and NO oxidation, it has a negative effect on OH radical levels, as indicated by its negative IntOH reactivities in all the experiments. It is not unusual for VOCs to have negative IntOH reactivities while having positive d(O_3-NO) reactivities; in fact all but the very most reactive VOCs — on an O_3 formed per molecule reacted basis — tend to have moderately negative effects on integrated OH radical levels (Carter *et al.*, 1993b; 1995a). For such compounds, the positive effects on O_3 formation and NO oxidation caused by the direct reactions of the radicals formed in their oxidation are more than enough to offset the negative effects of slightly suppressing radical levels, causing less O_3 formation from the other VOCs present.

In the initially estimated TBA mechanism, the nitrate yield in the NO + $(CH_3)_2C(OH)CH_2OO\cdot$ reaction, $k_6/(k_5+k_6)$, was assumed to be the same as derived in model simulations of isobutene - NO_x experiments carried out previously (unpublished results from this laboratory.) The results of these calculations are shown on the figures with the curves labeled "Same Nitrate as Isobutene". This model gave reasonably good simulations of the d(O_3-NO) and IntOH reactivity results in the full surrogate

Table 6. Summary of conditions and results of the incremental reactivity experiments.

Run	Initial Reactants (ppm)			t=6 d(O_3-NO) (ppm)			t=5 IntOH (10^{-6} min)		
	NOx	Surg [a]	Me.Acet.	Base	Test	IR [b]	Base	Test	IR
t-Butyl Alcohol									
Mini-Surrogate									
DTC-241 (B)	0.33	5.3	11.4	0.54	0.68	0.0119	17	13	-0.4
DTC-233 (A)	0.30	5.4	6.4	0.58	0.69	0.0178	15	15	-0.1
Full Surrogate - High NOx									
DTC-249 (A)	0.25	3.7	10.8	0.46	0.72	0.024	23	21	-0.2
DTC-256 (A)	0.26	3.6	6.3	0.46	0.55	0.0138	26	23	-0.4
Full Surrogate - Low NOx									
DTC-269 (A)	0.17	3.8	9.0	0.45	0.59	0.0156	29	22	-0.8
DTC-259 (A)	0.16	3.6	8.6	0.41	0.54	0.0151	30	21	-1.0
N-Methyl Pyrrolidinone									
Mini-Surrogate									
DTC-244 (B)	0.33	5.2	4.2	0.48	0.61	0.030	13	5	-1.9
DTC-240 (A)	0.31	5.4	2.1	0.56	0.63	0.034	17	6	-5.3
Full Surrogate - High NOx									
DTC-252 (A)	0.26	3.8	2.9	0.48	0.55	0.024	27	7	-6.8
DTC-255 (B)	0.26	3.3	0.62	0.42	0.56	0.22	24	16	-12.2
Full Surrogate - Low NOx									
DTC-267 (B)	0.16	3.7	0.80	0.43	0.44	0.012	31	13	-22
DTC-261 (A)	0.16	3.5	0.45	0.39	0.40	0.025	29	16	-30
Propylene Carbonate									
Mini-Surrogate									
DTC-243 (A)	0.32	5.1	24.16	0.52	0.59	0.0026	14	6	-0.4
DTC-264 (B)	0.30	5.1	8.62	0.53	0.54	0.0012	16	9	-0.9
DTC-239 (B)	0.31	5.2	8.22	0.59	0.56	-0.0037	15	15	-0.1
DTC-235 (B)	0.30	5.0	1.84	0.59	0.57	-0.0092	16	12	-1.9
Full Surrogate - High NOx									
DTC-250 (B)	0.26	3.4	14.12	0.45	0.67	0.0157	23	13	-0.7
DTC-257 (B)	0.26	3.5	7.23	0.45	0.61	0.0213	25	18	-1.0
Full Surrogate - Low NOx									
DTC-266 (A)	0.16	3.3	11.78	0.39	0.51	0.0094	30	14	-1.3
DTC-260 (B)	0.17	3.5	7.50	0.42	0.53	0.0139	29	19	-1.3

Notes

[a] Total base ROG surrogate in ppmC.

[b] Incremental reactivity

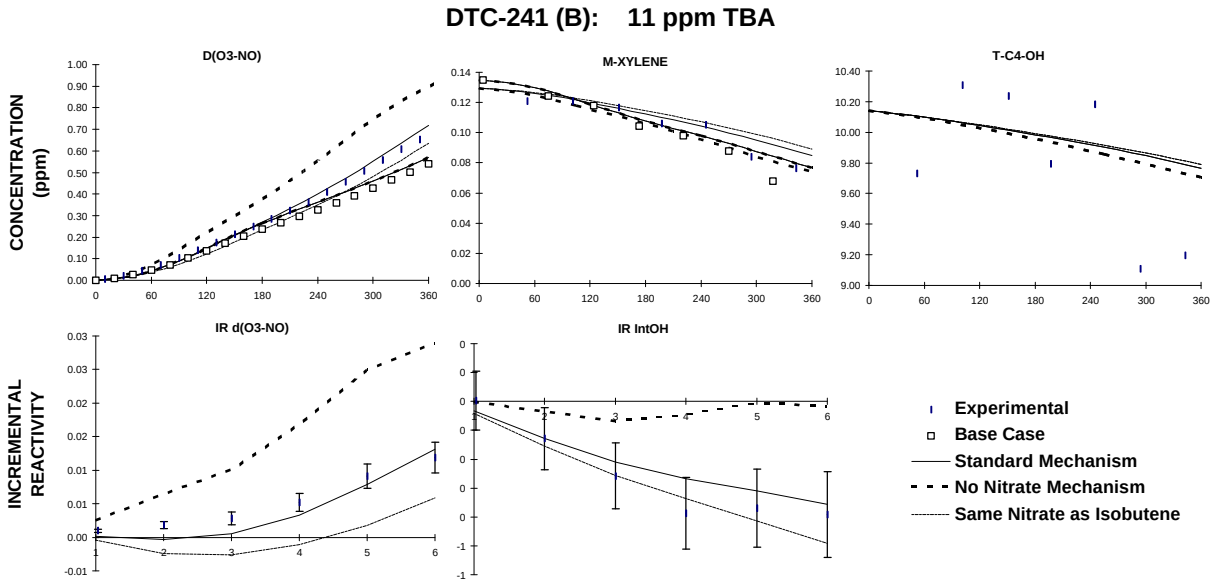

Figure 8. Plots of selected results of the mini-surrogate + t-butyl alcohol run DTC-241.

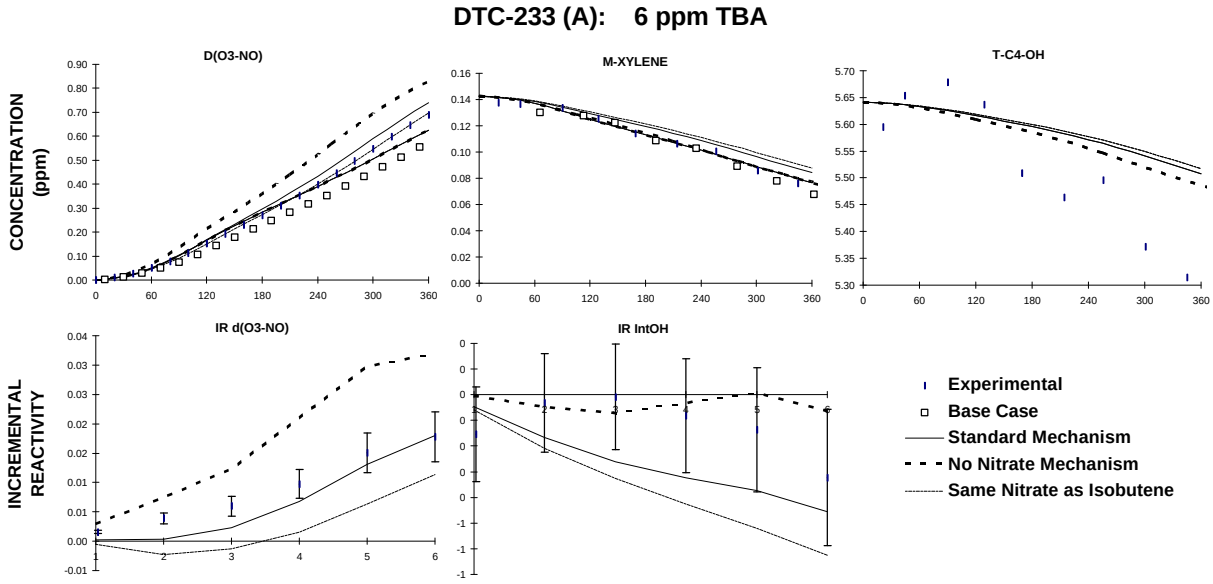

Figure 9. Plots of selected results of the mini-surrogate + t-butyl alcohol run DTC-233.

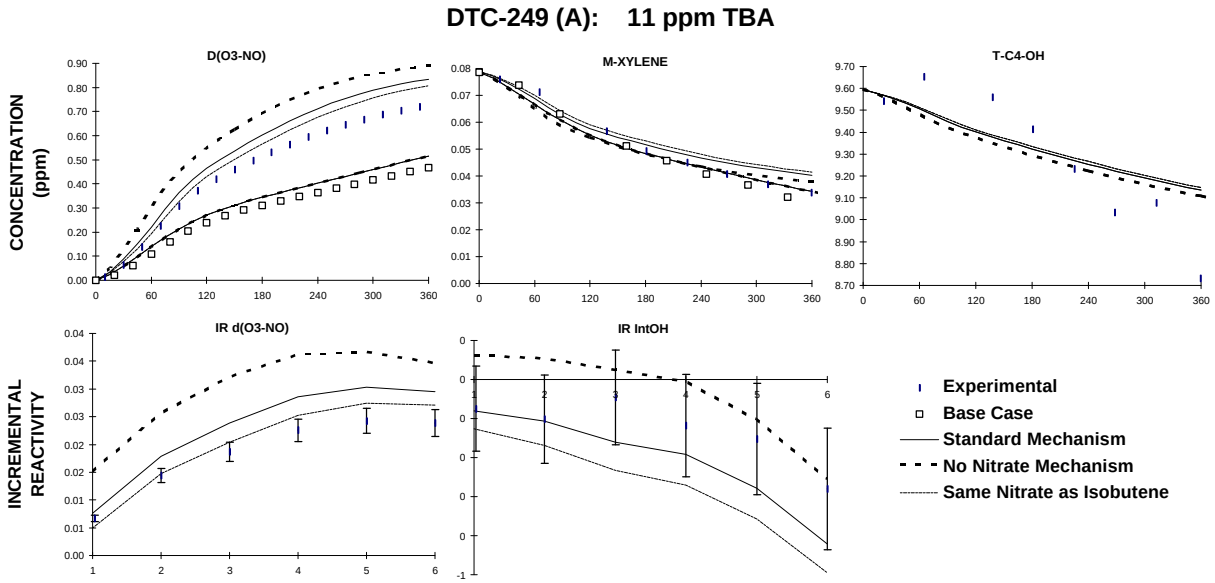

Figure 10. Plots of selected results of the full surrogate + t-butyl alcohol run DTC-249.

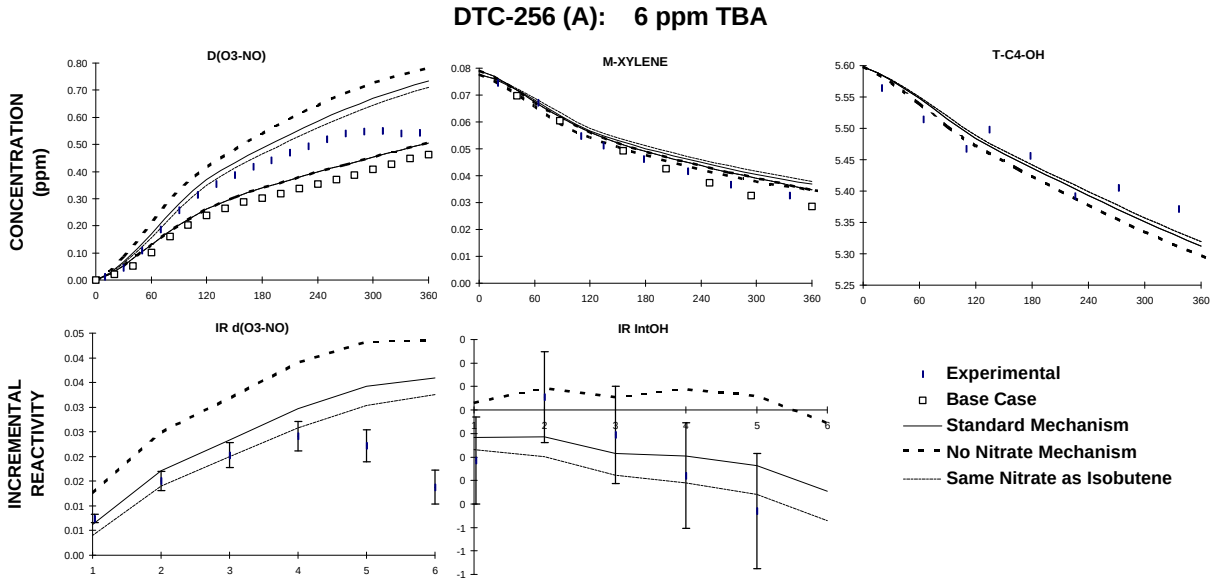

Figure 11. Plots of selected results of the full surrogate + t-butyl alcohol run DTC-256.

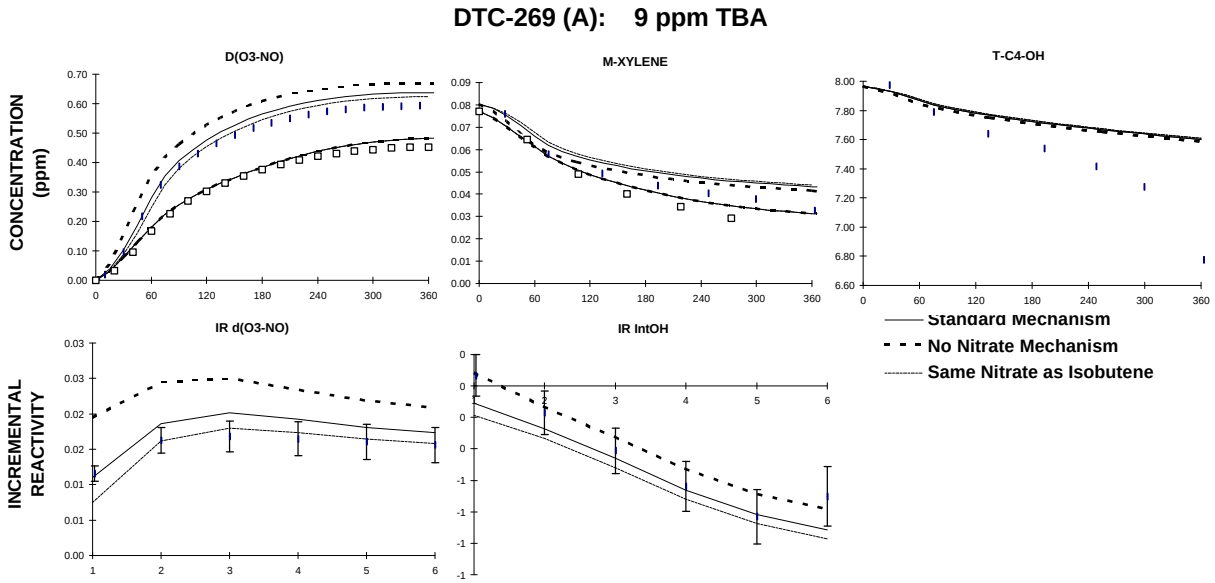

Figure 12. Plots of selected results of the low NOx full surrogate + t-butyl alcohol run DTC-269

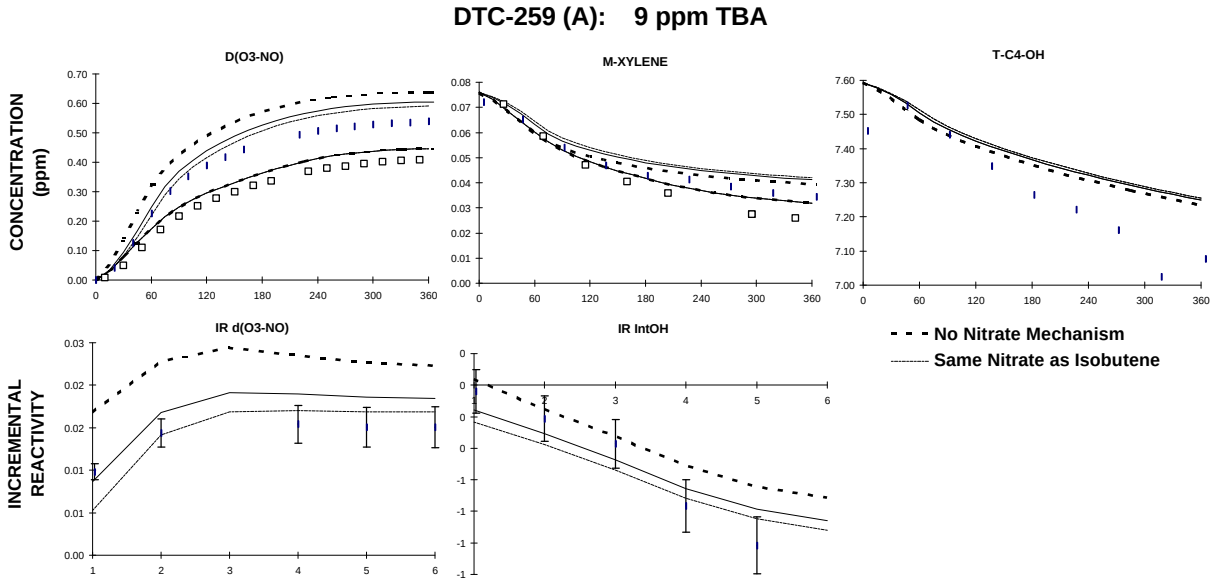

Figure 13. Plots of selected results of the low NOx full surrogate + t-butyl alcohol run DTC-259

experiments, but tended to underpredict the d(O_3-NO) reactivities in the mini-surrogate runs, which were more sensitive to this parameter. On the other hand, as shown on the figures, model simulations assuming no nitrate formation in this reaction, i.e. k_6=0, significantly overpredicts reactivities in these experiments. Best results are obtained with a slight downward adjustment of $k_6/(k_5+k_6)$ from 0.1 to 0.07, as is shown on the figures with the curves labeled "Standard Mechanism". This mechanism is slightly biased towards overpredicting d(O_3-NO) reactivities in the full surrogate experiments, but the results can be considered to be within the uncertainty of the determination. This mechanism was used in the atmospheric reactivity simulations.

The addition of TBA in the reactivity experiments resulted in enhanced yields of formaldehyde and the observed formation of acetone, which is formed significantly in the base case runs. This is consistent with the expected reactions of TBA discussed above. The experimental and calculated yields of formaldehyde and acetone in these experiments are shown on Figures 14 and 15, respectively. It can be seen that the standard mechanism gives quite good simulations of these data, with the possible exception of the formaldehyde yields in run DTC-249, which was underpredicted in the base case as well as the added TBA side. However, even for that case the incremental effect of the TBA addition was well predicted.

As discussed above, the OH + TBA rate constant used in the model simulations was based on the measurements of Cox and Goldstone (1982), Wallington *et al*. (1988) and Teton *et al.* (1996), and not the value measured in this study, which is ~30% higher. Use of the higher rate constant was found to cause the slight bias of the model towards overpredicting the d(O_3-NO) reactivities in the full surrogate runs to increase beyond the uncertainty of the determination, and also caused a bias in the model towards overpredicting the incremental effect of TBA on formaldehyde formation and the TBA yields. The latter result is shown on Figures 14 and 15 with the curves labeled "higher kOH". This tended to support our use of the lower rate constants as determined by Cox and Goldstone (1982), Wallington *et al.* (1988) and Teton *et al.* (1996) in the standard mechanism.

N-Methyl Pyrrolidinone Experiments and Mechanism Evaluation

Summaries of the conditions and results of the incremental reactivity experiments for NMP are included in Table 6, and Figures 16 - 21 give time series plots for relevant measurements used for mechanism evaluation. Results of model calculations are also shown. Table 6 shows that NMP has the highest positive d(O_3-NO) reactivities of the three compounds studied, though it's IntOH reactivities are significantly negative. Thus, although this compound has a net negative effect on OH radical levels, it still has a positive effect on ozone formation, at least by the end of the experiments reported here. However, NMP has somewhat unusual reactivity characteristics in that its d(O_3-NO) reactivities are either negative or close to zero at the initial stages of the experiments, but increase relatively rapidly once ozone formation begins.

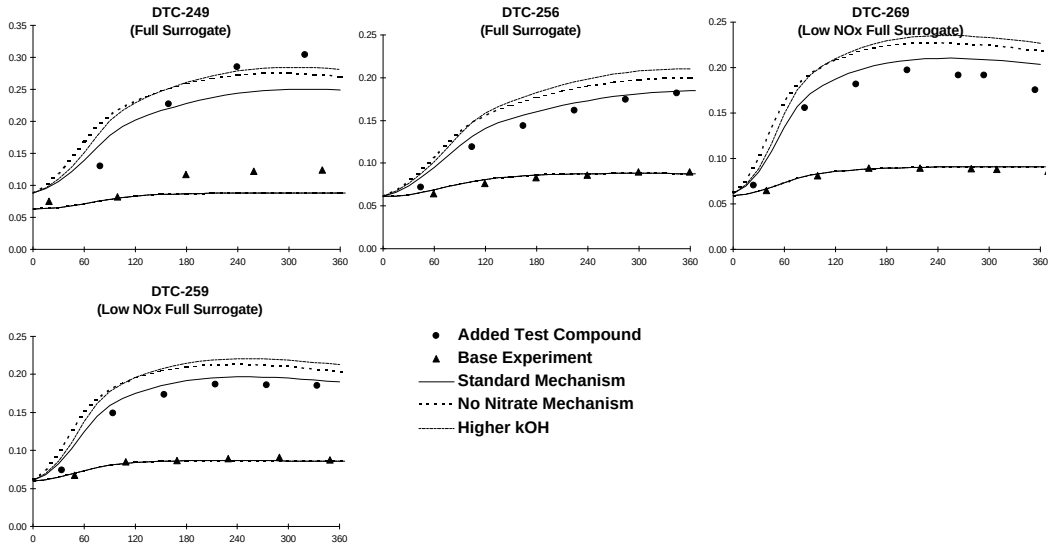

Figure 14. Experimental and calculated concentration-time plots for formaldehyde for the t-butyl alcohol reactivity experiments where such data were available.

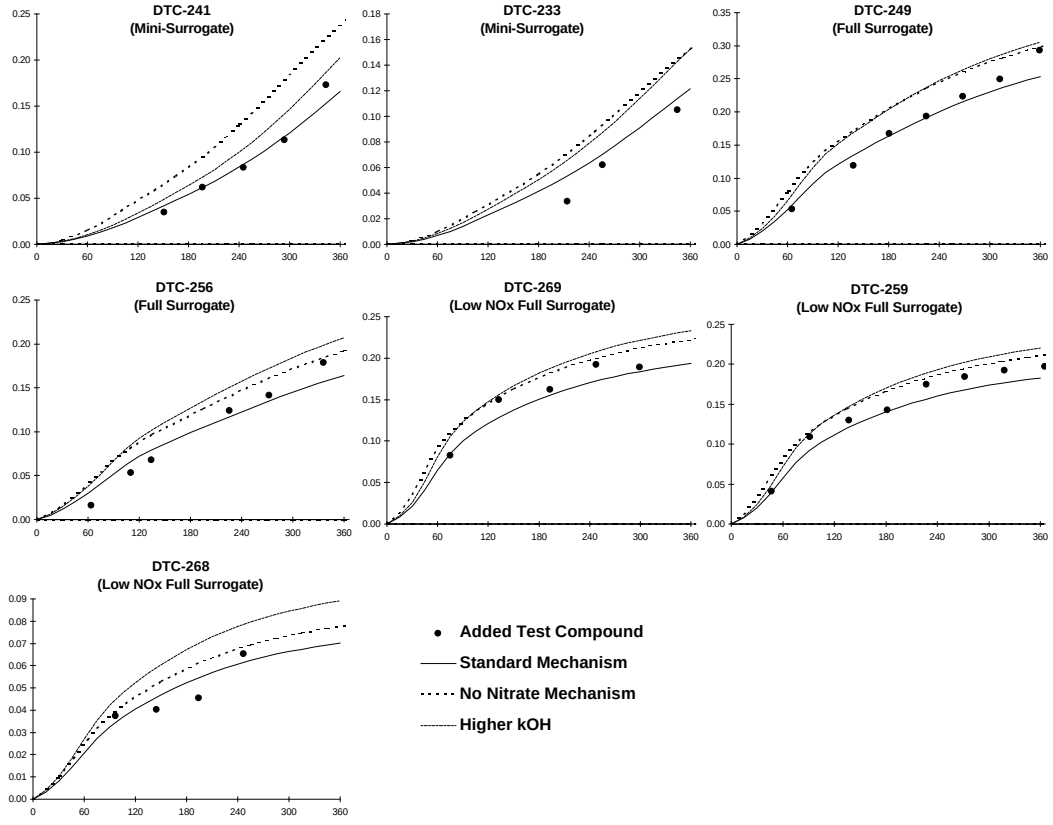

Figure 15. Experimental and calculated concentration-time plots for acetone for the t-butyl alcohol reactivity experiments where such data were available.

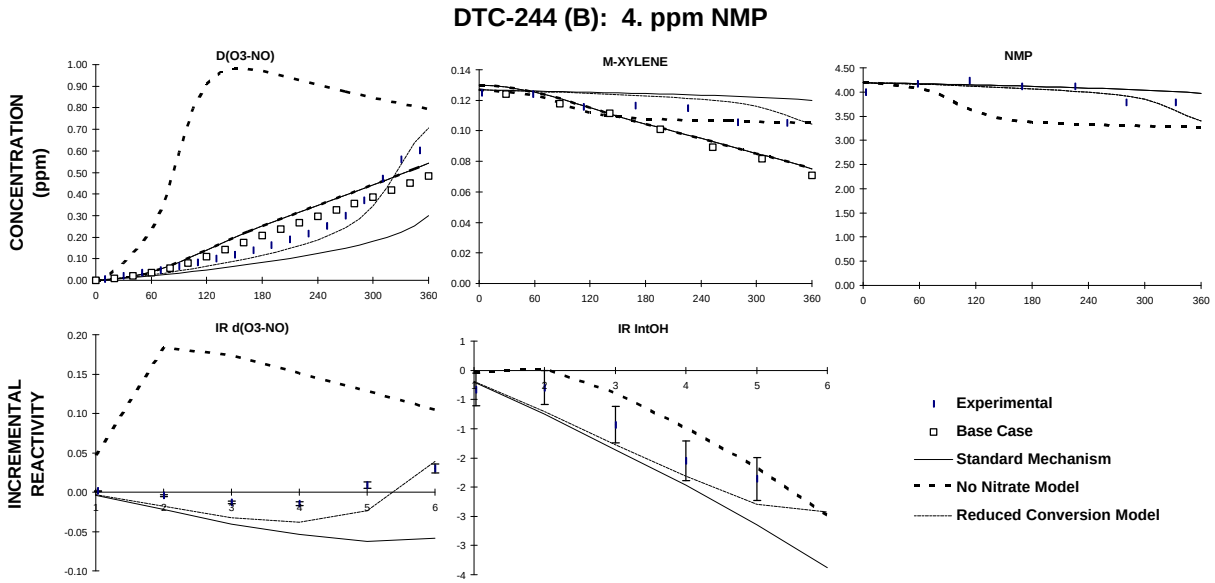

Figure 16. Plots of selected results of the mini-surrogate + N-methyl pyrrolidone run DTC-244.

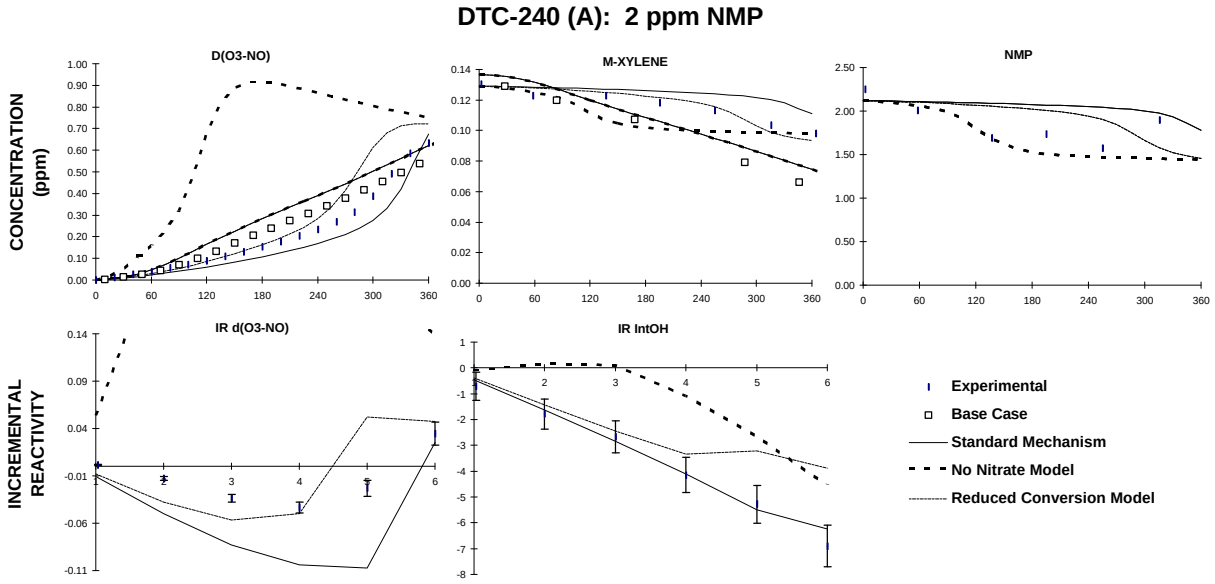

Figure 17. Plots of selected results of the mini-surrogate + N-methyl pyrrolidone run DTC-240.

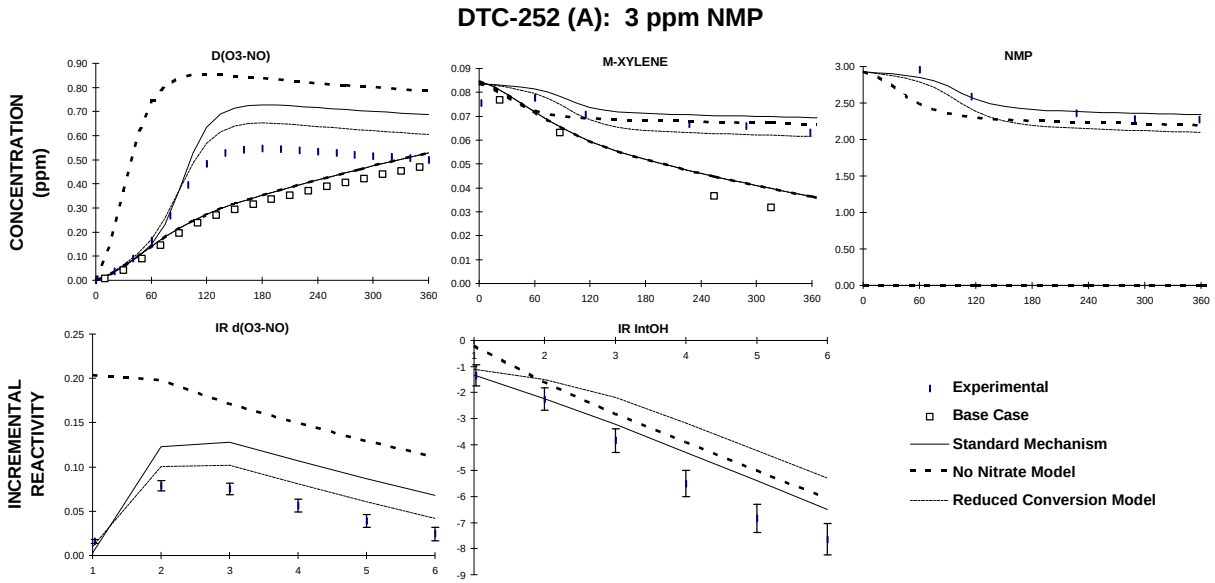

Figure 18. Plots of selected results of the full surrogate + N-methyl pyrrolidone run DTC-252

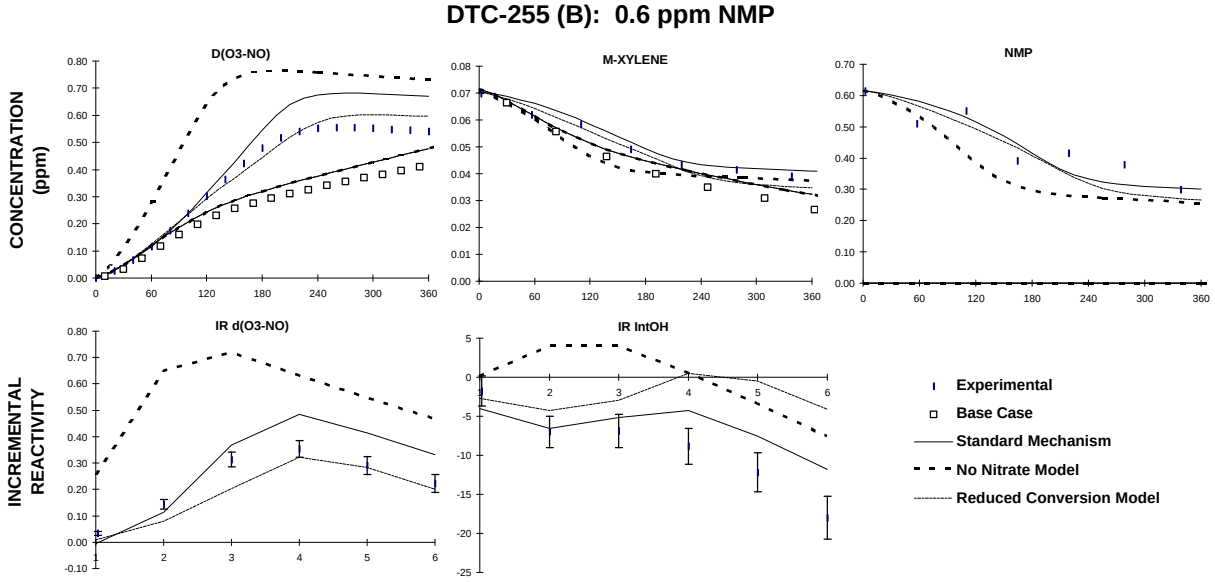

Figure 19. Plots of selected results of the full surrogate + N-methyl pyrrolidone run DTC-255

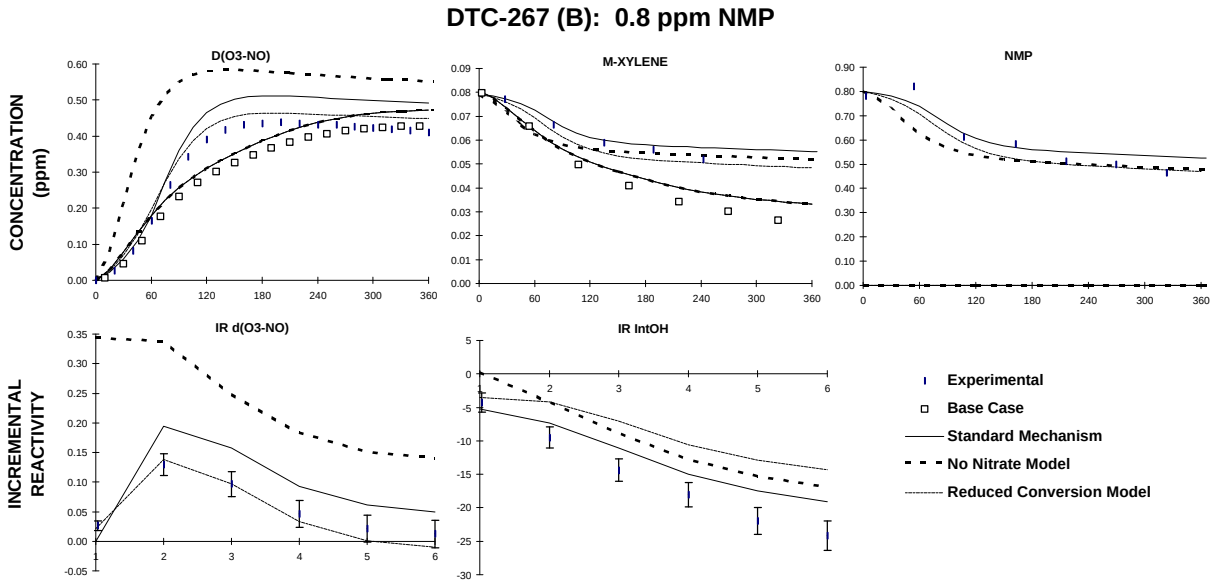

Figure 20. Plots of selected results of the low NOx full surrogate + N-methyl pyrrolidone run DTC-267.

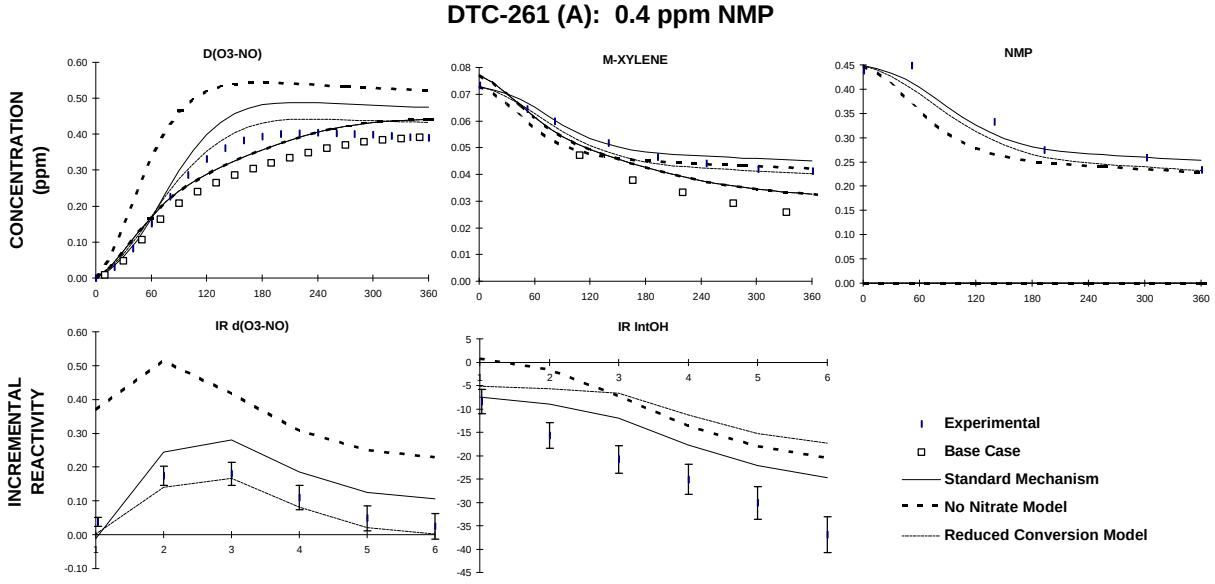

Figure 21. Plots of selected results of the low NOx full surrogate + N-methyl pyrrolidone run DTC-261.

The unusual reactivity characteristics of NMP are most evident in the mini-surrogate experiments shown in Figures 17 and 18, and also in Figure 22, which shows the experimental O_3 and NO data for one such run. In these runs, the addition of NMP initially causes the rate of NO oxidation to slow significantly, but once the ozone starts forming, the O_3 formation rate in the NMP side accelerates and eventually surpasses the ozone on the base case side. This effect is also occurring in the full surrogate runs, but is less noticeable because ozone formation begins much earlier in these runs. In those experiments, the rate of consumption of NMP can also be seen to increase once significant ozone formation begins, being relatively slow initially.

Similar reactivity characteristics have been observed in terpene - NO_x environmental chamber experiments, where they tend to have inhibiting characteristics initially, but then rapidly enhance ozone formation, and their own rates of consumption, once ozone formation begins (unpublished results from this laboratory). In the case of these terpenes, this is due to their relatively rapid direct reaction with O_3, which not only enhances their rate of consumption, but introduces radicals into the system which cause net O_3 formation (overwhelming the direct O_3 loss due to the direct reaction) and increased consumption of other VOCs (unpublished results from this laboratory). However, this cannot be the explanation for NMP, since it was found not to react significantly with O_3.

In the case of NMP, this enhancement of reactivity is due to its relatively rapid rate of reaction with NO_3 radicals. NO_3 radicals are formed from the reaction of O_3 with NO_2, and are rapidly removed by reaction with NO. Thus, they are not present at significant levels until O_3 formation begins. Once O_3 formation begins, it reacts with NO_3 to form NO_3, which introduce radicals into the system which enhance O_3 formation, to a greater extent than its loss due to reaction with NO_2. Thus the net effect is that the reactivity characteristics of NMP are somewhat like the terpenes, though the reasons are somewhat different. NMP is the first VOC we studied where the NO_3 reaction was such an important factor affecting its reactivity.

The model calculations were able to duplicate, at least qualitatively, NMP's reactivity characteristics, provided that it was assumed that alkyl nitrate formation from the peroxy + NO reactions (Reactions 12 and 14, above) was occurring to some extent. The dotted lines on Figures 16-21 show results of model calculations based on assuming that nitrate formation in these reactions are negligible, and clearly these calculations significantly overpredict NMP's reactivity. The best fits to the full surrogate experiments are obtained if it is assumed that the nitrate yields $[k_{12}/(k_{11}+k_{12)} = k_{14}/(k_{13}+k_{14})]$ are 0.15, and the results of calculations based on this are shown on those figures. This model tends to overestimate the initial inhibiting effects in the mini-surrogate experiments and overpredict final O_3 yields in the full surrogate runs, but overall gives the best performance of all the alternative mechanisms we examined. (Somewhat higher priority was given to optimizing performance in the simulations of the full surrogate runs, since these are more closely representative of atmospheric conditions.) As discussed above, the nitrate yields, at least for the alkanes (Carter and Atkinson, 1989b; Atkinson, 1996) tend to

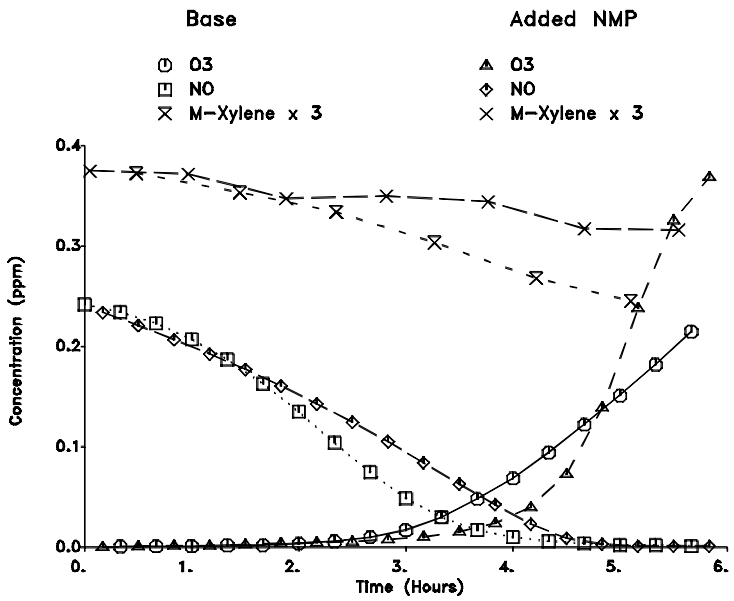

Figure 22. Experimental concentration-time plots for ozone, NO, and m-xylene in the added NMP mini-surrogate experiment DTC-244.

increase with the size of the molecule, being in the ~15% range for n-pentane to n-hexane. Therefore, ~15% nitrate yields for peroxy radicals of the size formed in the NMP system are not unreasonable.

Although the best fit model standard mechanism correctly simulates the O_3 initiation effects on NMP reactivity, its performance is not totally satisfactory in that it consistently overpredicts final O_3 yields. No chemically justifiable adjustment to the mechanism could be found to cause improved performance in this respect, without significantly degrading model performance in other unacceptable ways. For example, using increased nitrate yields would cause lower final O_3 predictions, but only at the expense of significantly overestimating the initial inhibition and length of time before the ozone formation begins to accelerate. Making reasonable changes to the mechanisms for NMP's major oxidation products, NMS and 1FP, do not significantly affect results of the simulations. This tendency of the model to overpredict final O_3 yields in the added NMP experiments means that the mechanism can be expected to be biased towards overestimating NMP's incremental reactivity in simulation of low NO_x scenarios.

The only adjustment to the mechanism which we found would improve the ability of the model to predict effects of NMP on final O_3 yields was to assume that fewer NO to NO_2 conversions are involved in the NMP + OH and NMP + NO_3 photooxidation reactions. Unfortunately, there is no reasonable mechanistic justification for such an assumption, so we cannot recommend use of this mechanism for atmospheric reactivity modeling. However, for assessing the effect that the bias in the standard mechanism may have in its predictions of reactivity under atmospheric conditions, it is useful

to have an alternative mechanism which does not have this bias, or at least whose biases or errors may be different. For this purpose, we derived an alternative NMP photooxidation mechanism where the same products are formed, but where one fewer NO to NO_2 conversion is involved for each molecule reacting. (As shown on Table 2, this is done by replacing the model species "RO2-R.", which represents an NO to NO_2 conversions and HO_2 formation, with simply HO_2.) For this mechanism to fit the mini-surrogate chamber data, we needed to re-adjust the nitrate yields from the reaction of NO with the peroxy radicals downwards to ~7%. The results of the calculations with this adjusted model are shown on Figures 16-21 with the curves labeled "Reduced conversion model". It can be seen that this adjusted mechanism performs considerably better in simulating the d(O_3-NO) reactivities, though it does not perform as well as the standard mechanism in predicting the effect of NMP in inhibiting IntOH. We should stress that we do not consider this to be a chemically reasonable mechanism because we do not have reasonable rationalization for reducing the NO to NO_2 conversions, and that we are using its calculations for sensitivity analysis purposes only.

Propylene Carbonate Experiments and Mechanism Evaluation

Summaries of the conditions and results of the incremental reactivity experiments for PC are included in Table 6, and Figures 23 - 30 give time series plots for relevant measurements used for mechanism evaluation. Results of model calculations are also shown. Table 6 shows that PC was found to have the lowest incremental reactivity of all the three compounds studied, though it generally had a positive effect on O_3 formation, at least in the experiments using the full surrogate. As with the other VOCs studied, it tended to have an inhibiting effect on overall OH radicals, being intermediate in this regard between t-butyl alcohol and NMP.

It should be pointed out that PC was a fairly difficult compound to handle experimentally because of its relatively low volatility, and the measurements of its concentration are somewhat less precise than for other VOCs. In the first experiment conducted with this compound, DTC-235, the amount of PC intended to be injected into the chamber was significantly less than the amount measured in the gas phase. The slight increase in measured gas-phase PC concentrations during this experiment suggests that some may have been absorbed on the walls, and desorbed as time went on. After this run, a modified injection procedure designed to improve the injection efficiency (see experimental section) was employed. However, the results of these experiments appear to be reasonably consistent with expected based on model calculations, as discussed below.

PC is unusual in that its incremental reactivities were found to be much lower in the mini-surrogate experiments than in the experiments with the full surrogate. For example, the mini-surrogate runs DTC-264 and DTC-269 had slightly more PC added than the high NO_x full surrogate run DTC-257 and the low NO_x run DTC-260, but the effect on NO oxidation and O_3 formation was almost undetectable in the mini-surrogate runs, while it had a definite, positive, effect on O_3 in the full surrogate runs. This

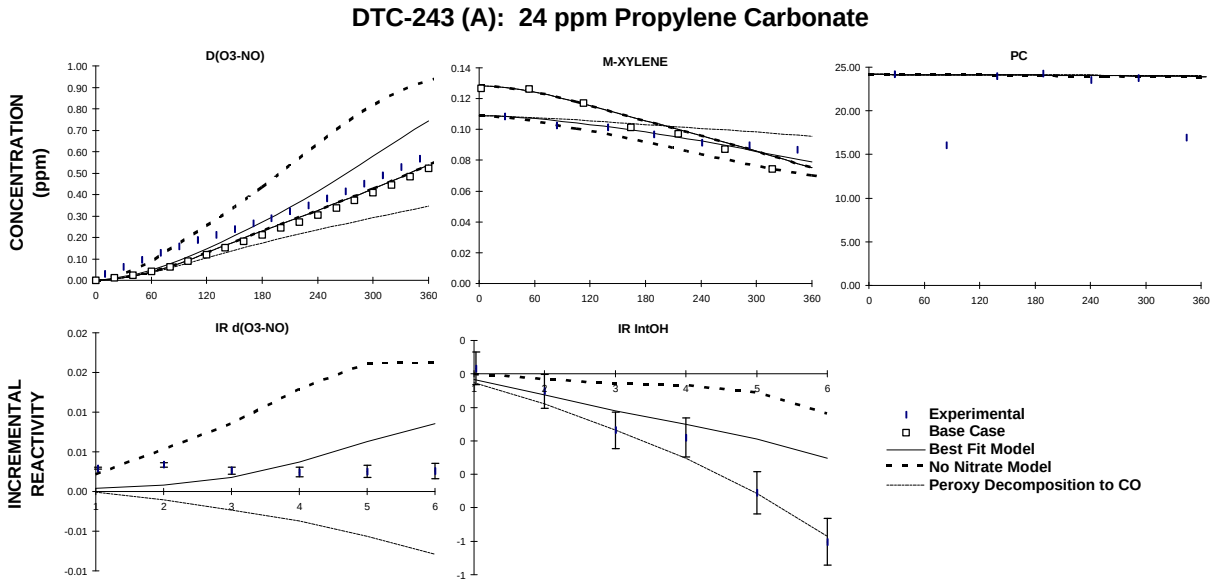

Figure 23. Plots of selected results of the mini-surrogate + propylene carbonate run DTC-243.

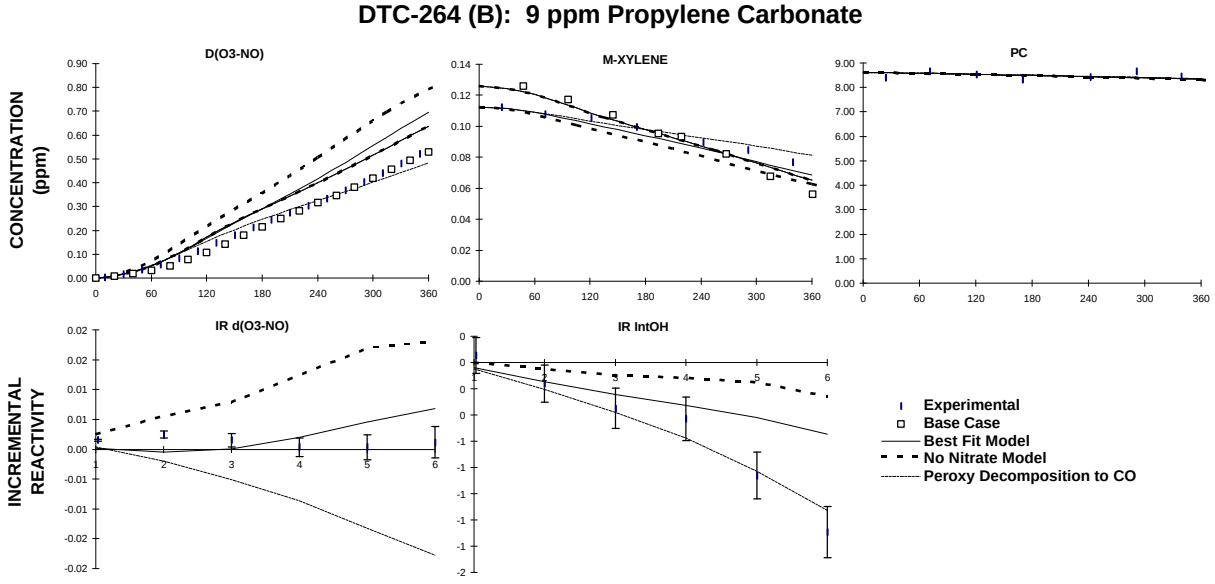

Figure 24. Plots of selected results of the mini-surrogate + propylene carbonate run DTC-264.

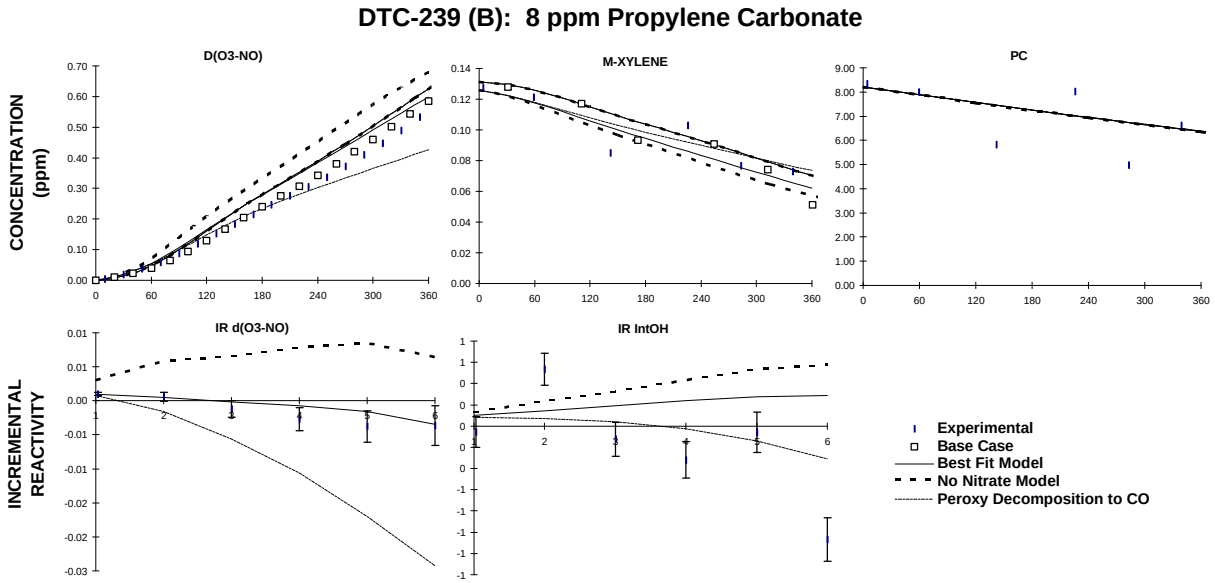

Figure 25. Plots of selected results of the mini-surrogate + propylene carbonate run DTC-239.

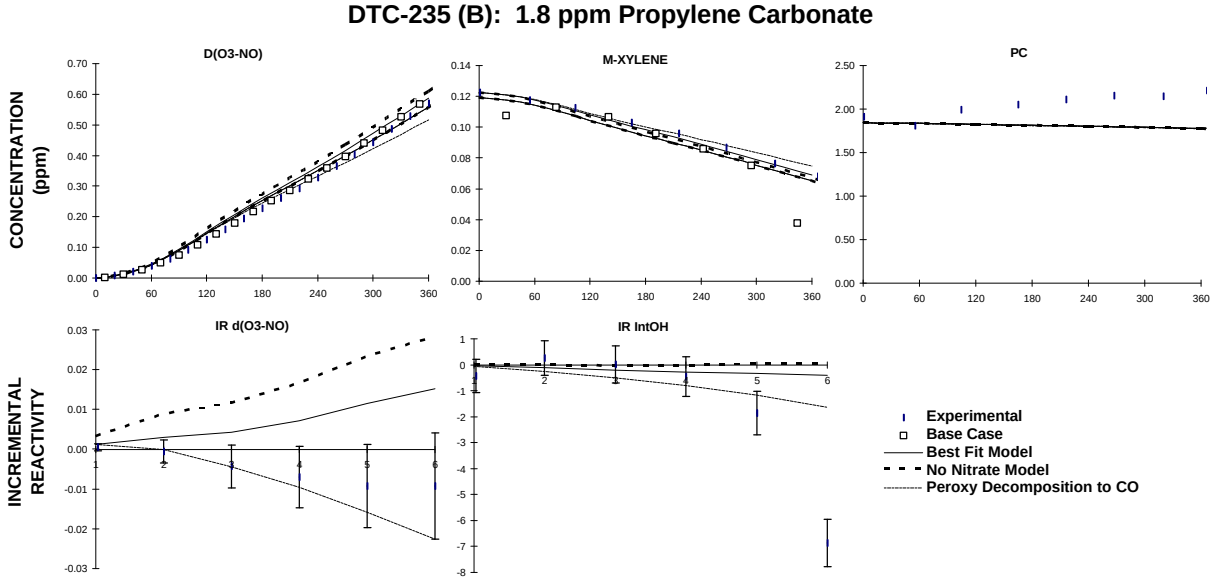

Figure 26. Plots of selected results of the mini-surrogate + propylene carbonate run DTC-235.

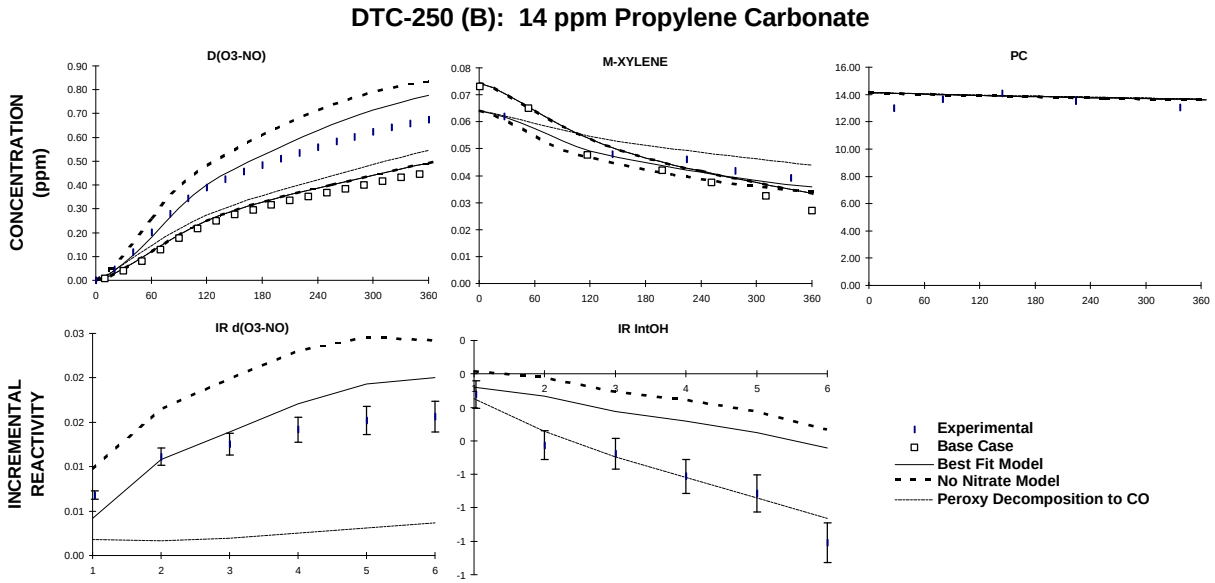

Figure 27. Plots of selected results of the full surrogate + propylene carbonate run DTC-250.

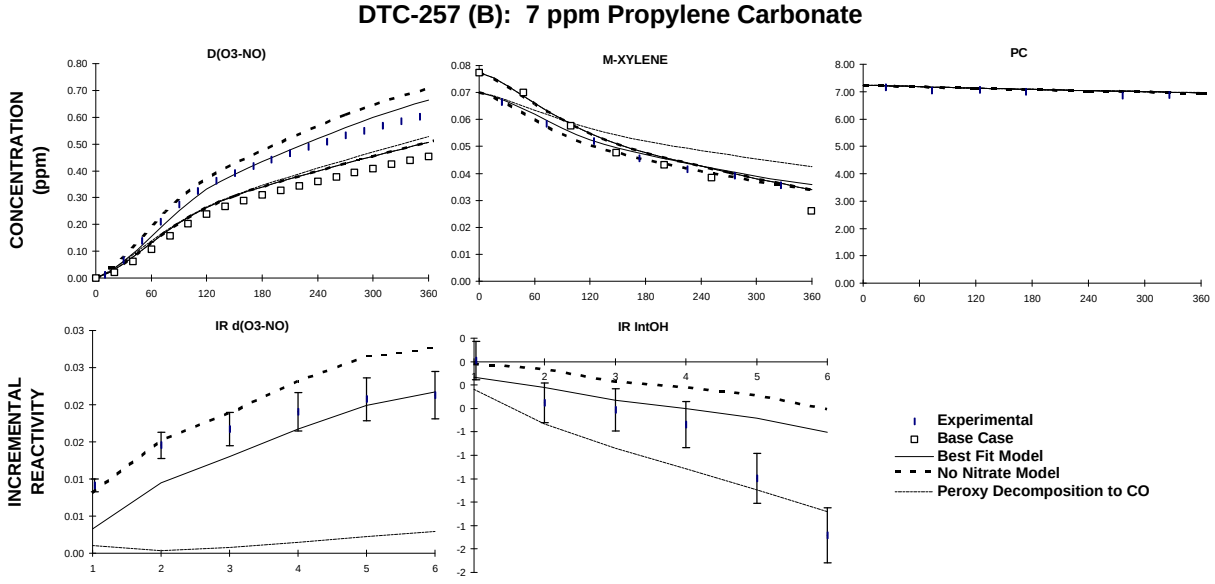

Figure 28. Plots of selected results of the full surrogate + propylene carbonate run DTC-257.

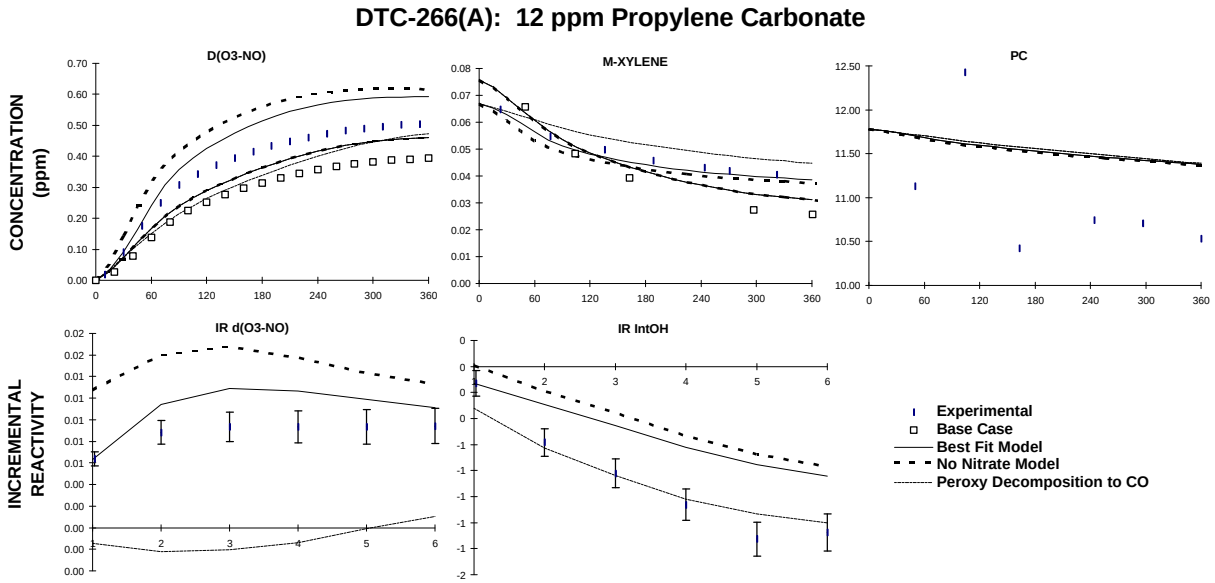

Figure 29. Plots of selected results of the low NOx full surrogate + propylene carbonate run DTC-266.

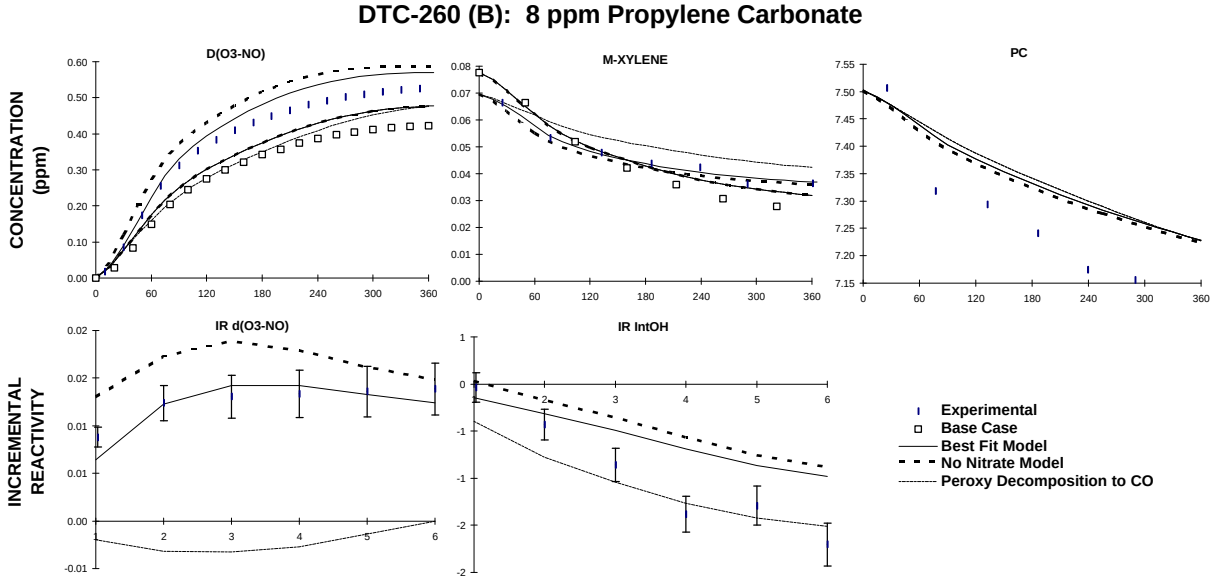

Figure 30. Plots of selected results of the low NOx full surrogate + propylene carbonate run DTC-260.

is in contrast with many other VOCs, for which the mini-surrogate experiments tend to be more sensitive (Carter *et al.*, 1993b). This is attributed to the fact that for compounds, such as PC, which are radical inhibitors, there is a balance between the negative effects on reactivity due to the radical inhibition effects and the positive effects due to NO to NO_2 conversions from the radicals formed in the compound's reactions. These two opposing effects appear to be closely in balance for PC in the mini-surrogate experiments, while in the full surrogate experiments the positive effect is clearly much more important. This is consistent with the fact that mini-surrogate experiments tend to be much more sensitive to radical inhibition effects than the runs with the full surrogate (Carter *et al.*, 1995a).

The model simulations carried out assuming there is no significant alkyl nitrate formation in PC's mechanisms (e.g., via Reaction 16, above) tended to overpredict the reactivity of PC, though to a much lesser extent than was the case with NMP. The sensitivity to nitrate formation was much greater in the mini-surrogate experiments than in the full surrogate runs, consistent with the greater sensitivity of the mini-surrogate runs to radical inhibition effects as noted above. The best fits are obtained with an assumed nitrate yield, $k_{16}/(k_{15}+k_{16})$, of 8%.

As indicated above, the possibility needs to be considered that the initially formed peroxy radical may decompose via Reaction (17) to form formaldehyde, CO, and acetyl peroxy radicals. However, if this is assumed, then the model significantly underpredicts the d(O_3-NO) reactivity of PC, though it does perform slightly better in predicting PC's effects on IntOH. This is shown on Figures 23-30 with the calculations designated "Peroxy decomposition to CO". These calculations assume no nitrate formation, so any adjustments of this parameter could only make these fits worse. However, the formaldehyde data give even more definitive evidence against this decomposition, since the model using this assumption significantly overpredicts the formaldehyde yield. This is shown on Figure 31, which shows experimental and calculated formaldehyde yields in the three full surrogate experiments which had usable formaldehyde data.

While the formaldehyde yield from PC is clearly not as high as would be predicted if reaction (17) were assumed, Figure 31 shows that PC addition does cause some increase in formaldehyde formation. This can be accounted for by Reaction (18), the decomposition of the alkoxy radical formed after OH reacts at the CH_3 position. If this decomposition is assumed to be slow, then the radical would be expected to react with O_2 to form HO_2 and the corresponding aldehyde. Model calculations where this is assumed predict approximately the same d(O_3-NO) and IntOH reactivities as our standard, best fit, mechanism, but predict that PC will have essentially no effect on formaldehyde yields. This is shown on Figure 31 for the calculations labeled "k(18) = 0". Therefore, we assume that this decomposition is fast in the standard mechanism used in the atmospheric reactivity simulations.

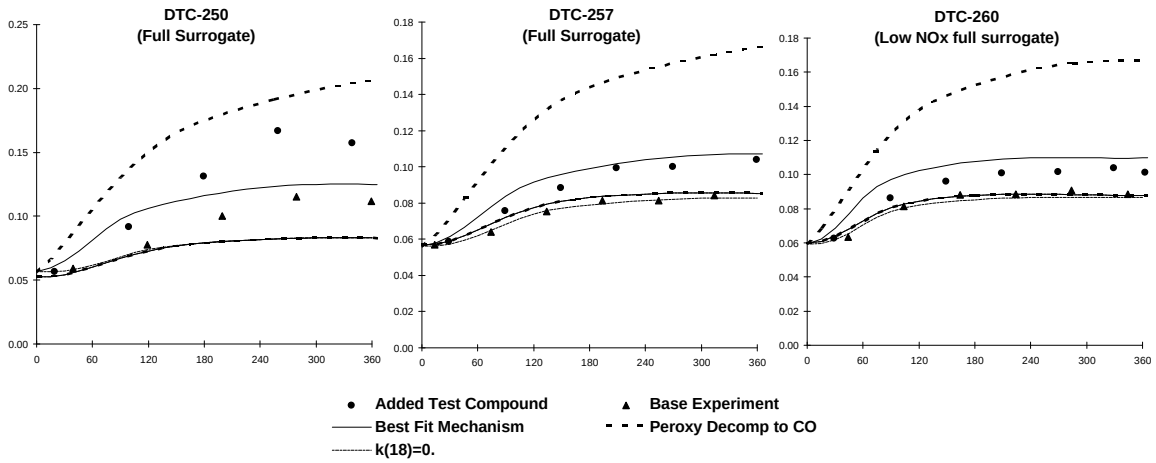

Figure 31. Plots of experimental and calculated formaldehyde data for those propylene carbonate reactivity experiments for which such data were available.

ATMOSPHERIC REACTIVITY CALCULATIONS

Incremental reactivities of VOCs have been shown to be highly dependent on environmental conditions, so reactivities measured in environmental chamber experiments cannot necessarily be assumed to be exactly the same as those in the atmosphere (Carter and Atkinson, 1989a; Carter *et al.*, 1995a). The only method available to obtain quantitative estimates of incremental reactivities of VOCs in ambient air pollution episodes is to conduct airshed model simulations of the episodes. Since these simulations cannot be any more reliable than the chemical mechanisms used, the major objective of this program was to provide experimental data necessary to develop and evaluate mechanisms for the compounds of interest for use in such simulations. This was discussed in the previous sections. In this section, we discuss the results of model simulations of its incremental reactivities in a variety of model scenarios representing ozone exceedence episodes in various areas in the United States (Baugues, 1990), and compare the results to incremental reactivities calculated for ethane, the compound used by the EPA as the criterion for determining "negligible" reactivity, and for the base ROG, the mixture representing total ROG emissions from all sources.

Scenarios Used for Reactivity Assessment

The set of airshed scenarios employed to assess the test compounds' reactivities for this study is the same as those used for calculating the MIR and other reactivity scales, which were also used in our previous assessment of acetone reactivity (Carter, 1994a; Carter *et al.*, 1993a). The objective is to use a set of scenarios which represents, as much as possible, a comprehensive distribution of the environmental conditions where unacceptable levels of ozone is formed. Although a set of scenarios has not been developed for the specific purpose of VOC reactivity assessment, the EPA developed an extensive set of scenarios for conducting analyses of effects of ROG and NO_x controls on ozone formation using the EKMA modeling approach (Gipson *et al.*, 1981; Gipson and Freas, 1983; EPA, 1984; Gery *et al.*, 1987; Baugues, 1990). The EKMA approach involves use of single-cell box models to simulate how ozone formation in one day episodes is affected by changes in ROG and NO_x inputs. Although single-cell models cannot represent realistic pollution episodes in great detail, they can represent dynamic injection of pollutants, time-varying changes of inversion heights with entrainment of pollutants from aloft as the inversion height increases throughout the day, and time-varying photolysis rates, temperatures, and humidities (Gipson and Freas, 1981; EPA, 1984; Gipson, 1984; Hogo and Gery, 1988). Thus, they can be used to simulate a wide range of the chemical conditions which affect ozone formation from ROG and NO_x. These are the same as those affecting VOC reactivity. Therefore, at least to the extent they are suitable for their intended purpose, an appropriate set of EKMA scenarios should also be suitable for assessing methods to develop reactivity scales encompassing a wide range of conditions.

Base Case Scenarios. The set of EKMA scenarios used in this study were developed by the United States EPA for assessing how various ROG and NO_x control strategies would affect ozone nonattainment in various areas of the country (Baugues, 1990). The characteristics of these scenarios and the methods used to derive their input data are described in more detail elsewhere (Baugues, 1990; Carter, 1993, 1994b). Briefly, 39 urban areas in the United States were selected based on geographical representativeness of ozone nonattainment areas and data availability, and a representative high ozone episode was selected for each. The initial NMOC and NO_x concentrations, the aloft O_3 concentrations, and the mixing height inputs were based on measurement data for the various areas, the hourly emissions in the scenarios were obtained from the National Acid Precipitation Assessment Program emissions inventory (Baugues, 1990), and biogenic emissions were also included. Table 7 gives a summary of the urban areas represented and other selected characteristics of the scenarios.

Several changes to the scenario inputs were made based on discussions with the California ARB staff and others (Carter, 1993). Two percent of the initial NO_x and 0.1% of the emitted NO_x in all the scenarios was assumed to be in the form of HONO. The photolysis rates were calculated using solar light intensities and spectra calculated by Jeffries (1991) for 640 meters, the approximate mid-point of the mixed layer during daylight hours. The composition of the NMOCs entrained from aloft was based on the analysis of Jeffries *et al.* (1989). The composition of the initial and emitted reactive organics was derived as discussed below. Complete listings of the input data for the scenarios are given elsewhere (Carter, 1993, 1994b).

This set of 39 EKMA scenarios are referred to as "base case" to distinguish them from the scenarios derived from them by adjusting NO_x inputs to yield standard conditions of NO_x availability as discussed below. No claim is made as to the accuracy of these scenarios in representing any real episode, but they are a result of an effort to represent, as accurately as possible given the available data and the limitations of the formulation of the EKMA model, the range of conditions occurring in urban areas throughout the United States. When developing general reactivity scales it is more important that the scenarios employed represent a realistic distribution of chemical conditions than any accurately representing the details of any one particular episode.

The Base ROG mixture is the mixture of reactive organic gases used to represent the chemical composition of the initial and emitted anthropogenic reactive organic gases from all sources in the scenarios. Consistent with the approach used in the original EPA scenarios, the same mixture was used for all scenarios. The speciation for this mixture was derived by Croes (1991) based on an analysis of the EPA database (Jeffries *et al.* 1989) for the hydrocarbons and the 1987 Southern California Air Quality Study (SCAQS) database for the oxygenates (Croes *et al.*, 1994; Lurmann *et al.*, 1992). This mixture consists of 52% (by carbon) alkanes, 15% alkenes, 27% aromatics, 1% formaldehyde, 2% higher aldehydes, 1% ketones, and 2% acetylene. The detailed composition of this mixture is given elsewhere (Carter, 1993, 1994b).

Table 7. Summary of conditions of base case scenarios used for atmospheric reactivity assessment.

City, State	Calc. Max O_3 (ppb)	ROG /NO_x	NO_x /NO_x^{MOR}	Final Height (km)	Init.+Emit Base ROG (mmol m^{-2})	Aloft O_3 (ppb)
Atlanta, GA	178	7.3	0.7	2.1	12	63
Austin, TX	174	9.3	0.5	2.1	11	85
Baltimore, MD	323	5.2	1.1	1.2	17	84
Baton Rouge, LA	245	6.8	1.0	1.0	11	62
Birmingham, AL	237	6.9	0.6	1.8	13	81
Boston, MA	194	6.5	0.6	2.6	14	105
Charlotte, NC	143	7.8	0.3	3.0	7	92
Chicago, IL	280	11.6	0.5	1.4	25	40
Cincinnati, OH	197	6.4	0.8	2.8	17	70
Cleveland, OH	250	6.6	1.0	1.7	16	89
Dallas, TX	210	4.7	1.3	2.3	18	75
Denver, CO	209	6.3	1.2	3.4	29	57
Detroit, MI	236	6.8	0.8	1.8	17	68
El Paso, TX	186	6.6	1.1	2.0	12	65
Hartford, CT	169	8.4	0.5	2.3	11	78
Houston, TX	305	6.1	1.0	1.7	25	65
Indianapolis, IN	210	6.6	0.9	1.7	12	52
Jacksonville, FL	156	7.6	0.7	1.5	8	40
Kansas City, MO	154	7.1	0.6	2.2	9	65
Lake Charles, LA	290	7.4	0.7	0.5	7	40
Los Angeles, CA	576	7.6	1.0	0.5	23	100
Louisville, KY	209	5.5	0.9	2.5	14	75
Memphis, TN	224	6.8	0.7	1.8	15	58
Miami, FL	133	9.6	0.4	2.7	9	57
Nashville, TN	165	8.1	0.5	1.6	7	50
New York, NY	361	8.1	0.8	1.5	39	103
Philadelphia, PA	240	6.2	1.0	1.8	19	53
Phoenix, AZ	273	7.6	1.0	3.3	40	60
Portland, OR	164	6.5	0.7	1.6	6	66
Richmond, VA	232	6.2	0.8	1.9	16	64
Sacramento, CA	201	6.6	0.9	1.1	7	60
St Louis, MO	319	6.1	1.1	1.6	26	82
Salt Lake City, UT	183	8.5	0.6	2.2	11	85
San Antonio, TX	131	3.9	1.1	2.3	6	60
San Diego, CA	195	7.1	1.0	0.9	8	90
San Francisco, CA	308	4.8	1.8	0.7	25	70
Tampa, FL	230	4.4	1.1	1.0	8	68
Tulsa, OK	224	5.3	0.9	1.8	15	70
Washington, DC	275	5.3	0.9	1.4	13	99

Adjusted NO_x scenarios. Incremental reactivities in the base case scenarios would be expected to vary widely, since incremental reactivities depend on the ROG/NO_x ratio, and that ratio varies widely among the base case scenarios. To obtain reactivity scales for specified NO_x conditions, separate sets of scenarios, designated MIR (for maximum incremental reactivity), MOR (for maximum ozone reactivity), and Equal Benefit Incremental Reactivity (EBIR) were developed (Carter, 1994a). In the MIR scenarios, the NO_x inputs were adjusted so the base ROG mixture (and most other VOCs) have their highest incremental reactivity. This is representative of the highest NO_x conditions of relevance to VOC reactivity assessment because at higher NO_x levels O_3 yields become significantly suppressed, but is also the condition where O_3 is most sensitive to VOC emissions. In the MOR scenarios, the NO_x inputs were adjusted to yield the highest ozone concentration. In the EBIR scenarios, the NO_x inputs were adjusted so that the relative effects of NO_x reductions and total ROG reductions on peak ozone levels were equal. This represents the lowest NO_x condition of relevance for VOC reactivity assessment, because O_3 formation becomes more sensitive to NO_x emissions than VOC emissions at lower NO_x levels. As discussed by Carter (1994a) the MIR and EBIR ROG/NO_x ratios are respectively ~1.5 and ~0.7 times those for the MOR scenarios in all cases.

For this study, the MIR, MOIR, and EBIR reactivities were approximated by reactivities calculated for the "averaged conditions" scenarios with the corresponding adjusted NO_x conditions. As discussed by Carter (1994a), the averaged conditions scenario consists of a set of scenarios where all inputs (except NO_x) are averages of those for the base case scenarios, and where the NO_x inputs are adjusted as described above to yield the specified NO_x conditions. Reactivities calculated using these adjusted NO_x averaged conditions scenarios were found to give very good approximations to those of the corresponding adjusted NO_x base case scenarios (Carter, 1993), and thus give a good indication of how the relative reactivities of compounds vary with varying NO_x conditions.

NO_x Conditions in the Base Case Scenarios. The variability of ROG/NO_x ratios in the base case scenarios suggest a variability of reactivity characteristics in the base case scenarios. However, as discussed previously (Carter, 1994a), the ROG/NO_x ratio is also variable in the MIR or MOR scenarios, despite the fact that the NO_x inputs in these scenarios are adjusted to yield a specified reactivity characteristic. Thus, the ROG/NO_x ratio, by itself, is not necessarily a good predictor of reactivity characteristics of a particular scenario. The NO_x/NO_x^{MOR} ratio is a much better predictor of this, with values greater than 1 indicating relatively high NO_x conditions where ozone formation is more sensitive to VOCs, and values less than 1 indicating NO_x-limited conditions. NO_x/NO_x^{MOR} ratios less than 0.7 represent conditions where NO_x control is a more effective ozone control strategy than ROG control (Carter, 1994a). This ratio is shown for the various base case scenarios on Table 7. Note that more than half of the base case scenarios represent NO_x-limited conditions, and ~25% of them represent conditions where NO_x control is more beneficial than VOC control. A relatively small number of scenarios represent MIR or near MIR conditions. However, as discussed elsewhere (Carter, 1994a), this set of scenarios is

based on near-worst-case conditions for ozone formation in each of the airsheds. Had scenarios representing less-than-worst-case conditions been included, one might expect a larger number of MIR or near MIR scenarios. This is because NO_x is consumed more slowly on days with lower light intensity or temperature, and thus the scenario is less likely to become NO_x-limited.

Incremental and Relative Reactivities

The incremental reactivity of a VOC in an airshed scenario is the change in ozone caused by adding the VOC to the emissions, divided by the amount of VOC added, calculated for sufficiently small amounts of added VOC that the incremental reactivity is independent of the amount added. The procedure used to calculate incremental reactivities in a scenario was as discussed in detail elsewhere (Carter, 1993, 1994a,b). The incremental reactivities depend on how the amount of VOC added are quantified. In this work, the added VOC was quantified on a mass basis, since this is how VOCs are regulated. In addition, the incremental reactivities also depend on how ozone impacts are quantified (Carter, 1994a). In this work, two different ozone quantifications were used, resulting in two different incremental reactivities being calculated for a VOC in a scenario. These are discussed below.

The "Ozone Yield" incremental reactivities measure the effect of the VOC on the total amount of ozone formed in the scenario at the time of its maximum concentration. In this work, this is quantified as grams O_3 formed per gram VOC added. This gives the same ratios of incremental reactivities as reactivities calculated from peak ozone concentrations, but is preferred because it permits magnitudes of reactivities in scenarios with differing dilutions to be compared on the same basis. Most previous recent studies of incremental reactivity (Dodge, 1984; Carter and Atkinson, 1987, 1989a, Chang and Rudy, 1990; Jeffries and Crouse, 1991) have all been based on ozone yield or peak ozone concentration reactivities.

The ozone yield incremental reactivities do not necessarily measure the effect of the VOC on exposure of unacceptable levels of ozone because it does not measure how long high levels of ozone is present. A quantification which reflects this is integrated ozone over the standard, which is defined as the sum of the hourly ozone concentrations for the hours when ozone exceeds the standard in the base case scenarios (Carter 1994a). In the previous work (Carter, 1994a), we used the California ozone standard of 90 ppb, but in this work we will use the national standard of 0.12 ppm. Reactivities relative to this quantification of ozone are referred to by the designation "IntO_3>0.12" reactivities.

Relative reactivities are ratios of incremental reactivities to incremental reactivities of some standard VOC or mixture. Since these are the quantities which usually are the most relevant to control strategy applications, the results in this work will be given in terms of relative reactivities. In our previous work (Carter 1991, 1994a), we used the incremental reactivity of the base ROG mixture, i.e., the mixture representing ROG pollutants from all sources, as the standard to define relative reactivities. However, because of the tendency within the EPA to consider ethane as the standard to define exempt vs controlled VOCs, in this work we will present reactivity ratios where ethane is used as the standard.

Reactivity Scales

A reactivity scale is a set of incremental or relative reactivities for a particular scenario or group of scenarios. Two types of reactivity scales will be discussed here, "base case" scales and adjusted NO_x scales. Base case scales are simply the set of incremental or relative reactivities in the 39 base case scenarios. Two sets of base case scales are derived — those based ozone yield reactivities and those based on $IntO_3$>0.12 reactivities. In the previous work (Carter, 1991, 1994a) we derived various multi-scenario scales from the individual base case scales by averaging or other procedures, to evaluate alternative approaches for developing single reactivity scales for applications requiring single scales. However, the decision of whether to exempt a VOC, or classify it as "highly reactive", should not be made based on relative reactivities of a single scale, but on a knowledge of the range of relative reactivities for a variety of conditions. Thus in this work we present the distribution of base case relative reactivities for the 39 individual scenarios rather than developing aggregated or optimum scales which represent the distribution by single numbers.

The adjusted NO_x incremental reactivity scales refer to the MIR (maximum incremental reactivity), MOIR (maximum ozone incremental reactivity), or the EBIR (Equal Benefit Incremental Reactivity) scales. In this work, these consist of ozone yield incremental reactivities in averaged conditions scenarios where NO_x inputs were adjusted to yield MIR, MOR or EBIR conditions, respectively. Relative reactivities in these scales are ratios of incremental reactivities in these scales. Reactivities in the MIR scale are of interest because the California Air Resources Board utilized an MIR scale to calculate reactivity adjustment factors in its clean fuels/low emissions vehicle regulations (CARB, 1993). The justification for using this scale in applications requiring a single scale (such as the CARB vehicle regulations) is that it reflects conditions where ozone is most sensitive to changes in VOC emissions, and complements NO_x control, which is most effective for reducing ozone under conditions where the MIR scale is least applicable (Carter, 1994a). The MOIR scale is preferred by many as an alternative for such applications because it reflects conditions which are most favorable for ozone, and is more representative of the distribution of conditions in the base case scenarios (Carter 1994a). Most other alternative reactivity scales which might be appropriate for assessing VOC control strategies (i.e., excluding scales representing highly NO_x-limited conditions where ozone is more sensitive to NO_x than VOCs) tend to fall in the range defined by the MIR and MOIR scales. Since the EBIR scale represents lower NO_x conditions where O_3 is less sensitive to VOCs, its use in applications requiring a single scale has not been considered. However, it is useful for assessing how reactivities depend on NO_x conditions.

Note that the MIR, MOIR, EBIR and base case scales derived in this work are somewhat different from those calculated previously (Carter, 1994a; Carter *et al.*, 1993a) because an updated chemical mechanism was used. The updates to the mechanism were discussed in the previous section. In addition, as indicated above, the MIR, MOIR and EBIR scales were calculated using a single averaged conditions

scenario, rather than the average of the adjusted NO_x base case scenarios as done previously (Carter, 1994a).

Calculated Relative Reactivities of the Test Compounds

Table 8 lists the ozone yield and $IntO_3$>0.12 reactivities, relative to ethane, for t-butyl alcohol, N-methyl pyrrolidinone, and propylene carbonate for the base case and the adjusted NO_x averaged conditions scenarios. Two sets of calculations are shown for NMP, one using the best fit standard mechanism which may be biased towards overpredicting NMP's effect on maximum ozone, and one using the mechanism adjusted (without chemical rationalization) to remove this bias. For comparison purposes, the reactivities relative to ethane for toluene and the average of all emissions (the base ROG) are also shown. Toluene is shown because it has been proposed that it's reactivity serve as the borderline between "reactive" and "highly reactive" for regulatory purposes (Dimitriades, private communication, 1995). The base ROG is shown because it indicates the relative impacts of regulating emissions of these compounds compared to regulating emissions of all VOCs equally. The results for the three test compounds are discussed below, in order of their reactivity.

Propylene Carbonate. PC is calculated to be the least reactive, on a gram basis, of the three compounds studied. Its average reactivities in the base case scenarios are very close to that of ethane. It has a slightly higher MIR value than ethane, but its reactivity relative to ethane decreases with decreasing NO_x availability, though to a much lesser extent than is the case for aromatics such as toluene. In this regard, it is similar to acetone, which was also found to have a slightly higher MIR reactivity than ethane, but where the full distribution of reactivities overlapped that of ethane, with it also being less reactive than ethane in most of the base case scenarios (Carter *et al.*, 1993a). However, PC's reactivity relative to ethane is calculated to be much less variable from scenario to scenario than was found to be the case for acetone. PC's reactivity relative to ethane is somewhat higher when O_3 impacts are quantified by integrated O_3 over the standard then when they are quantified by ozone yields, though the difference is relatively small. This is consistent with reactivities calculated for other VOCs (Carter, 1994a), where O_3 yield and integrated O_3 reactivities tended to be about the same under MIR conditions, but where integrated O_3 reactivities changed less as NO_x was reduced than was the case for reactivities quantified by peak O_3 yields.

T-Butyl Alcohol. TBA is calculated to be only slightly more reactive than PC on a per-gram basis (by about 10%, on the average), which is an insignificant difference given the uncertainties of the mechanisms and the model. The MIR reactivities of the two compounds (both ozone yield and integrated O_3) are essentially the same, both being ~40% higher than that of ethane. Like PC, TBA's reactivity relative to ethane is somewhat higher when O_3 is quantified by integrated O_3 over the standard rather than by O_3 yield, and is somewhat higher under MIR conditions than in scenarios where NO_x is more limited. In the base case scenarios, its average ozone yield reactivity is essentially the same as that of ethane,

Table 8. Summary of calculated incremental reactivities (gram basis) relative to ethane for t-butyl alcohol, N-methyl pyrrolodinone, propylene carbonate, and the total of all emitted VOCs.

Scenario	O_3 Yield Reactivity relative to Ethane						$IntO_3$ >0.12 Reactivity relative to Ethane					
	PC	TBA	NMP (std.)	NMP (adj.)	Toluene	Base ROG	PC	TBA	NMP (std.)	NMP (adj.)	Toluene	Base ROG
Averaged Conditions												
MIR	1.43	1.36	7.0	6.2	15.4	12.4	1.46	1.41	7.3	6.3	16.1	13.5
MOIR	0.95	1.02	6.0	5.2	5.2	6.8	1.15	1.22	6.5	5.4	9.6	10.2
EBIR	0.79	0.93	5.2	4.5	0.7	5.3	0.95	1.19	5.5	4.3	4.1	8.1
Base Case												
Average	**0.89**	**1.00**	**5.5**	**4.7**	**3.0**	**6.3**	**1.05**	**1.20**	**5.9**	**4.8**	**6.7**	**9.2**
St.Dev	**21%**	**21%**	**16%**	**17%**	**149%**	**38%**	**19%**	**17%**	**17%**	**18%**	**63%**	**30%**
ATL GA	0.87	1.00	5.2	4.5	3.7	6.0	1.00	1.24	5.6	4.4	6.3	8.4
AUS TX	0.78	0.86	4.8	4.3	1.0	5.2	0.86	1.14	5.2	3.9	2.7	7.3
BAL MD	0.89	1.01	6.5	5.5	3.7	6.6	1.18	1.23	7.0	5.8	10.2	11.5
BAT LA	1.01	1.21	5.1	4.2	4.6	6.6	1.19	1.50	5.5	4.1	8.4	9.8
BIR AL	0.73	0.75	5.3	4.8	-1.6	4.3	0.90	1.00	5.6	4.7	2.4	7.6
BOS MA	0.77	0.92	5.5	4.5	1.6	4.9	0.92	1.14	6.2	4.7	5.0	8.0
CHA NC	0.70	0.80	4.7	4.2	0.8	4.8	0.74	0.95	4.8	3.9	1.9	6.0
CHI IL	0.75	1.02	3.3	2.8	-7.1	3.8	0.86	1.35	3.7	2.4	-4.1	6.0
CIN OH	0.77	0.83	6.1	5.3	2.0	5.3	0.94	1.01	6.5	5.4	5.8	8.2
CLE OH	0.92	1.07	6.1	5.1	3.5	6.8	1.18	1.30	6.7	5.3	9.4	11.3
DAL TX	1.18	1.10	6.0	5.3	10.1	8.6	1.29	1.22	6.3	5.4	12.4	10.9
DEN CO	1.12	1.32	6.4	5.2	7.4	9.4	1.40	1.52	6.9	5.4	13.4	13.8
DET MI	0.78	0.84	5.9	5.1	1.5	5.1	0.95	1.03	6.3	5.2	5.5	7.9
ELP TX	1.13	1.14	6.0	5.1	7.6	8.9	1.35	1.40	6.3	5.1	12.2	12.7
HAR CT	0.71	0.74	5.3	4.8	0.9	4.9	0.83	0.96	5.4	4.6	3.4	7.0
HOU TX	0.86	0.94	5.5	4.7	2.7	5.4	1.05	1.16	6.2	5.0	7.0	9.0
IND IN	0.89	0.97	5.6	5.0	4.2	6.4	1.11	1.19	5.8	4.9	8.6	9.5
JAC FL	0.88	1.07	4.8	4.1	3.8	6.2	0.92	1.20	4.7	3.9	4.7	7.1
KAN MO	0.74	0.75	5.8	5.2	2.6	5.1	0.86	0.94	6.0	5.1	5.0	7.1
LAK LA	0.86	1.22	4.0	3.3	-0.3	4.6	1.03	1.53	3.9	2.7	2.8	7.6
LOS CA	0.94	1.19	5.3	3.6	-1.0	6.7	1.22	1.40	6.4	4.5	6.8	11.9
LOU KY	0.85	0.92	5.2	4.5	3.8	5.4	0.99	1.12	5.6	4.6	6.5	7.6
MEM TN	0.79	0.94	5.3	4.5	1.2	4.9	0.93	1.17	5.6	4.5	4.4	7.5
MIA FL	0.73	0.86	4.0	3.8	1.3	5.5	0.74	0.91	3.8	3.6	1.5	5.9
NAS TN	0.73	0.76	4.4	4.3	1.0	4.3	0.75	0.86	4.2	4.0	1.9	5.2
NEW NY	0.81	1.68	5.2	2.8	-8.5	5.8	1.11	1.82	7.0	3.9	1.6	11.4
PHI PA	0.86	0.99	5.8	4.9	3.4	6.0	1.04	1.20	6.3	5.1	7.4	9.0
PHO AZ	0.90	0.88	6.3	5.6	2.5	6.2	1.15	1.10	6.6	5.7	8.6	10.6
POR OR	0.81	0.89	5.3	4.6	3.7	5.7	0.91	1.07	5.4	4.4	5.4	7.1
RIC VA	0.77	0.88	6.2	5.4	1.5	5.4	0.97	1.11	6.5	5.4	6.1	8.7
SAC CA	0.89	0.85	5.5	5.0	4.4	5.9	1.06	1.05	5.5	5.0	8.0	8.5
SAI MO	0.94	1.08	6.4	5.3	3.4	7.1	1.21	1.31	7.1	5.6	10.1	12.3
SAL UT	0.79	0.79	5.6	5.0	1.2	5.4	0.98	1.01	5.8	4.9	5.3	8.6
SAN TX	1.10	0.99	5.9	5.3	8.9	8.0	1.12	1.05	6.0	5.4	9.7	8.6
SDO CA	1.05	1.24	6.1	4.7	5.6	8.5	1.18	1.39	6.3	4.6	8.9	11.0
SFO CA	1.72	1.51	8.8	7.5	19.8	18.3	1.73	1.55	8.7	7.2	20.5	20.1
TAM FL	1.07	1.18	5.5	4.7	7.2	7.5	1.26	1.38	6.0	4.9	11.2	10.9
TUL OK	0.84	1.01	5.8	4.9	3.4	5.6	1.03	1.18	6.4	5.2	7.7	9.0
WAS DC	0.81	0.92	5.7	4.8	1.7	5.2	1.00	1.13	6.3	5.1	6.2	8.9

while its average integrated ozone reactivity is about 20% higher than that of ethane, slightly over the standard deviation of being the same.

N-Methyl Pyrrolidinone. NMP is by far the most reactive of the three compounds studied, being around six times more reactive than ethane under most conditions. However, it is not an unusually reactive compound compared to most emissions, since has somewhat lower average reactivity than the mixture representing the total of all emissions. It also has a lower MIR and lower integrated ozone reactivities than does toluene, whose reactivity indicates the proposed dividing line between "reactive" and "highly reactive". [The MOIR, EBIR and base case ozone reactivities of toluene are not particularly useful for a classification scheme, because its strong NO_x sinks significant suppress its effect on peak ozone (Carter, 1994a) in low NO_x scenarios. For this reason, toluene is not a particularly good choice as a reference compound for reactivity comparisons.] As with the other VOCs studied, its reactivities relative to ethane are slightly higher when O_3 impacts is quantified by integrated O_3 over the standard compared to when they are quantified by peak O_3 yields. On the other hand, compared to the base ROG (probably a more meaningful comparison for this compound) NMP's relative reactivities when quantified by integrated ozone are lower than those when quantified by ozone yields. This is because of the effect of the quantification method on the reactivity of ethane relative to the base ROG.

As discussed above, the modeling of the chamber experiments suggests that the standard NMP mechanism may be biased towards overpredicting its reactvity, and an adjusted mechanism was derived to remove this bias. The adjustment reduces NMP's predicted atmospheric reactivity by ~15-20%, depending on scenario or ozone quantification method. This is not a large difference considering the overall uncertaities and variabilities of atmospheric reactivity modeling.

CONCLUSIONS

The decision whether it is appropriate to regulate a compound as an ozone precursor requires a qualitative assessment of its ozone impacts under a variety of environmental conditions. This in turn requires developing and experimentally validating a chemical mechanism for the compounds relevant atmospheric reactions, which can then be used in airshed models to predict its atmospheric reactivity. Until this study, there was no experimental information concerning the atmospheric ozone impacts of any of the three compounds studied, and only for t-butyl alcohol were kinetic data and estimated mechanisms available. Thus, models for predicting atmospheric reactivities for N-methyl pyrrolidinone and propylene carbonate did not exist, and those for TBA were highly uncertain. The objective of this study was to provide the data needed to verify the predictive capabilities of an atmospheric reaction mechanism for TBA, and to derive and verify mechanisms for NMP and PC, thus allowing for improved estimates of their relative ozone impacts under atmospheric conditions. We believe this program succeeded in addressing this objective. The conclusions drawn from the studies of the three compounds are summarized below.

T-Butyl Alcohol

Based on reactions of similar compounds, the OH radical reaction was already known to be the only significant loss process for t-butyl alcohol in the atmosphere. Although the OH radical rate constant was measured in this work, the value obtained, $(1.43 \pm 0.36) \times 10^{-12}$ cm^3 $molecule^{-1}$ s^{-1}, is considered to be high, and the value of 1.08×10^{-12} cm^3 $molecule^{-1}$ s^{-1}, derived previously from three different studies (Cox and Goldstone, 1982; Wallington *et al.*, 1988; Teton *et al.*, 1996), is still preferred for use in atmospheric reactivity modeling. This is because both absolute and relative measurements gave good agreement, and because a model using the higher rate constant did not perform as well in simulating the results of our environmental chamber experiments. Good fits to the chamber data are obtained in a model using the lower rate constant and current estimates of the reaction pathways, and an adjusted organic nitrate yield in the NO + $(CH_3)_2C(OH)CH_2OO\cdot$ reaction of ~7%. This adjusted nitrate yield is reasonably consistent with the nitrate yield of 10% previously derived from model simulations of isobutene - NO_x environmental chamber experiments, where formation of the same radical is expected. Thus we conclude that this mechanism is chemically reasonable as well as being consistent with the chamber data and results of previous kinetic studies.

Using this mechanism, the atmospheric reactivity of TBA was calculated to be quite similar to that of ethane, average slightly higher using some quantificaion methods, and about the same using others. In particular its MIR reactivity was ~40% higher than that of ethane, and its average integrated ozone reactivity was about 20% higher than that of ethane, slightly over the standard deviation of being the same. On the other hand, TBA's average ozone yield reactivity is essentially the same as that of ethane.

While the reactivity of TBA relative to ethane varied somewhat from scenario to scenario, this variation was less than was previously observed to be the case with acetone.

This relatively low reactivity is despite the fact that TBA's rate of reaction in the atmosphere ~4 times that of ethane. This is attributed to the fact that TBA's reactions form somewhat less reactive products, on a per gram basis, and also to the fact that to fit the chamber data the model assumed that ~7% of the reaction proceeded via nitrate formation, a radical termination process which is assumed to be negligible in the photooxidation of ethane.

N-Methyl Pyrrolidinone

The atmospheric reactions of N-methyl pyrrolidinone have not been studied prior to this work. It reacts relatively rapidly with OH radicals, having a measured rate constant of $(2.15 \pm 0.36) \times 10^{-11}$ cm^3 $molecule^{-1}$ s^{-1} at 296 K. It also has a relatively high rate constant for reaction with NO_3 radicals, which was found to be $(1.26 \pm 0.40) \times 10^{-13}$ cm^3 $molecule^{-1}$ s^{-1}, also at 296 K. This is high enough that the NO_3 reaction could be a significant loss process for NMP even in the daytime. On the other hand, it is not consumed to a measurable extent by reaction with O_3 or direct photolysis, nor does it undergo significant gas-phase reaction with N_2O_5 or HNO_3.

When NMP reacts with OH radicals, it forms *N*-methylsuccinimide and 1-formyl-2-pyrrolidinone in approximately equal yields (44% and 41%, respectively). This suggests that the OH reaction occurs approximately half the time on the methyl group, and approximately the other half of the time on the CH_2 group next to the nitrogen, since these are the products expected to be formed in those cases. On the other hand, in the NO_3 reaction N-methylsuccinimide appears to be be the dominant product with a 59% yield. Although 1-formyl-2-pyrrolidinone is also formed in the NO_3 reaction, it is only a minor product with an estimated ~4% yield. Apparently, the NO_3 is more selective in its reaction site, and preferentially reacts at the CH_2 by the nitrogen rather than at the CH_3 group.

The environmental chamber experiments showed somewhat unusual reactivity characteristics for NMP. In particular, NMP addition was found to slow down the rate of NO oxidation in the early stages of the experiments, when its consumption is dominated by the OH radical reaction. This inhibition is accounted for by organic nitrate formation in the reactions of NO with the organic peroxy radicals formed, with best fits to the chamber data being obtained if relatively high nitrate yields of 15% are assumed. However, once NO was mostly consumed and O_3 formation began, NMP switches over from being inhibitor to have an accelerating effect on O_3 formation, and the O_3 formation in the experiment with the added NMP quickly overtakes the O_3 formed in the base case (control) run where NMP is absent. The rate of consumption of NMP also accelerates. This behavior is attributed to the NMP + NO_3 reaction, which is expected to become important once NO_3 begins to be formed from the reaction of O_3 with NO_2. This behavior is reasonably well duplicated by the model simulations using the OH and NO_3 radical rate constants measured in this work. This behavior is qualitatively similar to behavior we observed previously

for terpenes, though in the case of those compounds, the acceleration once O_3 formation begins is attributed to their direct reaction with O_3, rather than the NO_3 reaction which is the case of NMP.

Although with an appropriately adjusted nitrate yield and the estimated mechanism could reasonably well simulate the effects of NMP on initial NO oxidation and O_3 formation rates and on integrated OH radicals observed in the NMP environmental chamber experiments, the initially estimated mechanism was found to overpredict, by up to ~50%, the effects of NMP on the final O_3 yields in runs where significant ozone formation occurred. Acceptable simulations in this regard could only be obtained if we assumed there was one fewer NO to NO_2 conversion in NMP's photooxidation reactions than expected, though this assumption could not be rationalized with any reasonable mechanistic explanation.

As expected because of its relatively high rate constants, and the enhanced effect on O_3 formation apparently caused by its NO_3 reaction, NMP was calculated have the highest reactivities of the compounds studied under atmospheric conditions, being 5-6 times more reactive than ethane, depending on the model scenario or the mechanism assumed. Thus exempting NMP from regulation as an ozone precursor on the basis of negligible reactivity is clearly not an option. However, NMP should also not be considered to be a "highly reactive" compound, since its reactivity is less than that of the average of all emissions, and its MIR is less than half that of toluene, the compound proposed as representing the dividing line between reactive and highly reactive. The uncertainties concerning the possible bias of the standard mechanism towards overpredicitng the effect of NMP's on maximum ozone do not significantly affect conclusions about whether it is negligibly or highly reactive, since adjusting the mechanism to remove this bias causes the atmospheric reactivity predictions to be reduced by only 15-20%.

Propylene Carbonate

It is not consumed to a measurable extent by reaction with NO_3 radicals, ozone, or direct photolysis, so OH radical reaction should be its only significant loss process. It's OH radical rate constant of $(6.9 \pm 1.5) \times 10^{-13}$ cm^3 $molecule^{-1}$ s^{-1} at 298 K makes it a relatively slowly reacting compound, but clearly not uncreative, since it is ~2.5 times that of ethane. Although product studies were not performed, the model simulations of the chamber experiments were consistent with an estimated mechanism which predicted that the major products in the OH radical reaction would be methylglyoxal and CO_2. An alternative mechanism predicting formation of formaldehyde and peroxyacetyl radicals was found to be inconsistent with the formaldehyde yields observed in the experiments, as well as with the ozone reactivity results. In order to fit the chamber data it was also necessary to also assume that the organic nitrate formation in the reactions of NO with the peroxy radical intermediates occurred ~8% of the time. This is a reasonable organic nitrate yield for a molecule of this size, being similar to that which was derived for TBA based on model simulations of the experiments with that compound. However, it would be of interest to determine whether the prediction of methylglyoxal formation is confirmed by product studies.

The mechanism derived for propylene carbonate, and adjusted to fit the chamber data, predicted that reactivity of this compound was very close to that of ethane. Like TBA, it was calculated to have a MIR reactivity about 40% higher than that of ethane, but in most of the base case and lower NO_x scenarios, it had reactivities less than ethane when O_3 was quantified by peak ozone yields, and comparable reactivities as ethane when ozone was quantified by integrated O_3 over the standard. This is despite the fact that the methylglyoxal predicted to be formed in PC's photooxidation is a highly reactive product which contributes significantly to the high reactivities observed for aromatics. The relatively low OH + PC rate constant (~2.5 times that of ethane), the relatively high molecular weight, and the ~8% termination due to nitrate formation are apparently sufficient to overcome this, and account for PC's relatively low reactivity on a per gram basis.

REFERENCES

Atkinson, R. (1987): "A Structure-Activity Relationship for the Estimation of Rate Constants for the Gas-Phase Reactions of OH Radicals with Organic Compounds," Int. J. Chem. Kinet., 19, 799-828.

Atkinson, R. (1989): "Kinetics and Mechanisms of the Gas-Phase Reactions of the Hydroxyl Radical with Organic Compounds," J. Phys. Chem. Ref. Data, Monograph no 1.

Atkinson, R. (1991): "Kinetics and Mechanisms of the Gas-Phase Reactions of the NO_3 Radical with Organic Compounds," J. Phys. Chem. Ref. Data, 20, 459-507.

Atkinson, R. and W. P. L. Carter (1984): "Kinetics and Mechanisms of the Gas-Phase Reactions of Ozone with Organic Compounds under Atmospheric Conditions," Chem. Rev. 1984, 437-470.

Baugues, K. (1990): "Preliminary Planning Information for Updating the Ozone Regulatory Impact Analysis Version of EKMA," Draft Document, Source Receptor Analysis Branch, Technical Support Division, U. S. Environmental Protection Agency, Research Triangle Park, NC, January.

Campbell, I. M. and P. E. Parkinson (1978): Chem. Phys. Lett. 53, 385.

CARB (1993): "Proposed Regulations for Low-Emission Vehicles and Clean Fuels — Staff Report and Technical Support Document," California Air Resources Board, Sacramento, CA, August 13, 1990. See also Appendix VIII of "California Exhaust Emission Standards and Test Procedures for 1988 and Subsequent Model Passenger Cars, Light Duty Trucks and Medium Duty Vehicles," as last amended September 22, 1993. Incorporated by reference in Section 1960.1 (k) of Title 13, California Code of Regulations.

Calvert, J. G., and J. N. Pitts, Jr. (1966): Photochemistry, John Wiley and Sons, New York.

Carter, W. P. L. (1990): "A Detailed Mechanism for the Gas-Phase Atmospheric Reactions of Organic Compounds," Atmos. Environ., 24A, 481-518.

Carter, W. P. L. (1991): "Development of Ozone Reactivity Scales for Volatile Organic Compounds", EPA-600/3-91/050, August.

Carter, W. P. L. (1993): "Development and Application of an Up-To-Date Photochemical Mechanism for Airshed Modeling and Reactivity Assessment," Draft final report for California Air Resources Board Contract No. A934-094, April 26.

Carter, W. P. L. (1994a): "Development of Ozone Reactivity Scales for Volatile Organic Compounds," J. Air & Waste Manage. Assoc., 44, 881-899.

Carter, W. P. L. (1994b): "Calculation of Reactivity Scales Using an Updated Carbon Bond IV Mechanism," Draft Report Prepared for Systems Applications International Under Funding from the Auto/Oil Air Quality Improvement Research Program, April 12.

Carter, W. P. L. (1995): "Computer Modeling of Environmental Chamber Measurements of Maximum Incremental Reactivities of Volatile Organic Compounds," Atmos. Environ., 29, 2513-2517.

Carter, W. P. L. and R. Atkinson (1987): "An Experimental Study of Incremental Hydrocarbon Reactivity," Environ. Sci. Technol., 21, 670-679

Carter, W. P. L. and R. Atkinson (1989a): "A Computer Modeling Study of Incremental Hydrocarbon Reactivity", Environ. Sci. Technol., 23, 864.

Carter, W. P. L. and R. Atkinson (1989b): "Alkyl Nitrate Formation from the Atmospheric Photooxidation of Alkanes; a Revised Estimation Method," J. Atm. Chem. 8, 165-173.

Carter, W. P. L., and F. W. Lurmann (1990): "Evaluation of the RADM Gas-Phase Chemical Mechanism," Final Report, EPA-600/3-90-001.

Carter, W. P. L. and F. W. Lurmann (1991): "Evaluation of a Detailed Gas-Phase Atmospheric Reaction Mechanism using Environmental Chamber Data," Atm. Environ. 25A, 2771-2806.

Carter, W. P. L, D. Luo, I. L. Malkina, and J. A. Pierce (1993a): "An Experimental and Modeling Study of the Photochemical Ozone Reactivity of Acetone," Final Report to Chemical Manufacturers Association Contract No. KET-ACE-CRC-2.0. December 10.

Carter, W. P. L., J. A. Pierce, I. L. Malkina, D. Luo and W. D. Long (1993b): "Environmental Chamber Studies of Maximum Incremental Reactivities of Volatile Organic Compounds," Report to Coordinating Research Council, Project No. ME-9, California Air Resources Board Contract No. A032-0692; South Coast Air Quality Management District Contract No. C91323, United States Environmental Protection Agency Cooperative Agreement No. CR-814396-01-0, University Corporation for Atmospheric Research Contract No. 59166, and Dow Corning Corporation. April 1.

Carter, W. P. L., D. Luo, I. L. Malkina, and J. A. Pierce (1995a): "Environmental Chamber Studies of Atmospheric Reactivities of Volatile Organic Compounds. Effects of Varying ROG Surrogate and NO_x," Final report to Coordinating Research Council, Inc., Project ME-9, California Air Resources Board, Contract A032-0692, and South Coast Air Quality Management District, Contract C91323. March 24.

Carter, W. P. L., D. Luo, I. L. Malkina, and D. Fitz (1995b): "The University of California, Riverside Environmental Chamber Data Base for Evaluating Oxidant Mechanism. Indoor Chamber Experiments through 1993," Report submitted to the U. S. Environmental Protection Agency, EPA/AREAL, Research Triangle Park, NC., March 20..

Carter, W. P. L., J. A. Pierce, D. Luo, and I. L. Malkina (1995c): "Environmental Chamber Study of Maximum Incremental Reactivities of Volatile Organic Compounds," Atmos. Environ. 29, 2499-2511.

Carter, W. P. L., D. Luo, I. L. Malkina, and J. A. Pierce (1995d): "Environmental Chamber Studies of Atmospheric Reactivities of Volatile Organic Compounds. Effects of Varying Chamber and Light Source," Final report to National Renewable Energy Laboratory, Contract XZ-2-12075, Coordinating Research Council, Inc., Project M-9, California Air Resources Board, Contract A032-0692, and South Coast Air Quality Management District, Contract C91323, March 26.

Chang, T. Y. and S. J. Rudy (1990): "Ozone-Forming Potential of Organic Emissions from Alternative-Fueled Vehicles," Atmos. Environ., 24A, 2421-2430.

Cox, R. A. and A. Goldstone (1982): Atmospheric reactivity of oxygenated motor fuel additives, "*Physico-Chemical Behaviour of Atmospheric Pollutants*", Proc. 2nd European Symposium, D. Reidle Publishing Compamy, Dordrecht, The Netherlands, pp. 112-119.

Croes, B. E., Technical Support Division, California Air Resources Board, personal communication (1991).

Croes, B. E., *et al.* (1994): "Southern California Air Quality Study Data Archive," Research Division, California Air Resources Board.

Dodge, M. C. (1984): "Combined effects of organic reactivity and NMHC/Nox ratio on photochemical oxidant formation -- a modeling study," Atmos. Environ., 18, 1657.

EPA (1984): "Guideline for Using the Carbon Bond Mechanism in City-Specific EKMA," EPA-450/4-84-005, February.

Gery, M. W., R. D. Edmond and G. Z. Whitten (1987): "Tropospheric Ultraviolet Radiation. Assessment of Existing Data and Effects on Ozone Formation," Final Report, EPA-600/3-87-047, October.

Gipson, G. L., W. P. Freas, R. A. Kelly and E. L. Meyer, "Guideline for Use of City-Specific EKMA in Preparing Ozone SIPs, EPA-450/4-80-027, March, 1981.

Gipson, G. L. and W. P. Freas (1983): "Use of City-Specific EKMA in the Ozone RIA," U. S. Environmental Protection Agency, July.

Gipson, G. L. (1984): "Users Manual for OZIPM-2: Ozone Isopleth Plotting Package With Optional Mechanism/Version 2," EPA-450/4-84-024, August.

Hogo, H. and M. W. Gery (1988): "Guidelines for Using OZIPM-4 with CBM-IV or Optional Mechanisms. Volume 1. Description of the Ozone Isopleth Plotting Package Version 4", Final Report for EPA Contract No. 68-02-4136, Atmospheric Sciences Research Laboratory, Research Triangle Park, NC. January.

Jeffries, H. E., K. G. Sexton, J. R. Arnold, and T. L. Kale (1989): "Validation Testing of New Mechanisms with Outdoor Chamber Data. Volume 2: Analysis of VOC Data for the CB4 and CAL Photochemical Mechanisms," Final Report, EPA-600/3-89-010b.

Jeffries, H. E. and R. Crouse (1991): "Scientific and Technical Issues Related to the Application of Incremental Reactivity. Part II: Explaining Mechanism Differences," Report prepared for Western States Petroleum Association, Glendale, CA, October.

Jeffries, H. E. (1991): "UNC Solar Radiation Models," unpublished draft report for EPA Cooperative Agreements CR813107, CR813964 and CR815779". Undated.

Johnson, G. M. (1983): "Factors Affecting Oxidant Formation in Sydney Air," in "The Urban Atmosphere -- Sydney, a Case Study." Eds. J. N. Carras and G. M. Johnson (CSIRO, Melbourne), pp. 393-408.

Lurmann, F. W. and H. H. Main (1992): "Analysis of the Ambient VOC Data Collected in the Southern California Air Quality Study," Final Report to California Air Resources Board Contract No. A832-130, February.

Pitts, J. N., Jr., E. Sanhueza, R. Atkinson, W. P. L. Carter, A. M. Winer, G. W. Harris, and C. N. Plum (1984): "An Investigation of the Dark Formation of Nitrous Acid in Environmental Chambers," Int. J. Chem. Kinet., 16, 919-939.

Saunders, S. M., D. L. Baulch, K. M. Cooke, M. J. Pilling, and P. I. Smurthwaite (1994): "Kinetics and mechanisms of the reactions of OH with some oxygenated compounds of importance in tropospheric chemistry," Int. J. Chem. Kinet., 26, 113-130.

Teton, S., A. Mellouki, G. Le Bras, and H. Sidebottom (1996): "Rate Constants for Reactions of OH Radicals with a Series of Asymmetrical Ethers and tert-butyl alcohol," Int. J. Chem. Kinet. 28, 291-297.

Tuazon, E. C., R. Atkinson, C. N. Plum, A. M. Winer, and J. N. Pitts, Jr. (1983): "The Reaction of Gas-Phase N_2O_5 with Water Vapor," Geophys. Res. Lett. 10, 953-956.

Wallington, T. J., P. Dagaut, R. Liu, and M. J. Kurylo (1988): Gas-phase reactions of hydroxyl radicals with the fuel additives methyl *tert*-butyl ether and *tert*-butyl alcohol over the temperature range 240-440 K, *Environ. Sci. Technol., 22,* 842-844.

Zafonte, L., P. L. Rieger, and J. R. Holmes (1977): "Nitrogen Dioxide Photolysis in the Los Angeles Atmosphere," Environ. Sci. Technol. 11, 483-487.